SHEAR TRANSFER IN EXPOSED COLUMN BASE PLATES

by

Ivan Gomez
Amit Kanvinde

University of California, Davis

Chris Smith
Gregory Deierlein

Stanford University

Report Presented to the

American Institute of Steel Construction

March 2009

Executive Summary

This report presents the results of an experimental study investigating shear transfer mechanisms of column base plate details. This investigation is the first phase of a broader study whose aim is to develop improved design guidelines for column base plates. A review of existing design guidelines and published research reveals that shear transfer mechanisms in exposed base plates are not well understood, and methods to characterize strength capacities in shear are not adequately supported by experimental data.

To investigate shear transfer in exposed column base plates, seven large scale specimens were subjected to a combination of axial compression, axial tension and lateral shear deformations. The tests investigated three mechanisms commonly used for shear transfer in base plates, including (1) friction between the base plate and the grouted footing, with and without steel shim stacks (2) anchor rod bearing and (3) shear key bearing. The base plate tests are complemented by ancillary tests to characterize material properties.

Three tests which investigate surface friction indicate that the coefficient of friction between a steel base plate with mill scale and a grouted surface, with or without shim stacks, is 0.45. This value is lower than the design value of 0.55 recommended by the Steel Design Guide One, published by the American Institute of Steel Construction.

Two tests that address anchor rod bearing indicate that without the consideration of rod bending, the estimated strength of the anchor rod mechanism is significantly higher (i.e. unconservative) as compared to the observed strength. The tests indicate that the anchor rods initially bend in reverse curvature over a distance measured from the top of the grout layer to the center of the plate washer welded to the top surface of the base plate. However, this bending length increases as the grout sustains damage due to cyclic inelastic loading. At larger lateral base plate slip, the anchor rods exhibit increased strength due to second order geometric effects. In addition, the rods may come into contact within the base plate holes, thus decreasing the bending length.

Two tests which investigate shear key bearing indicate that the current design method used in the AISC Steel Design Guide One (based on the consideration of a uniform tensile stress acting of a 45 degree failure cone) for calculating the side blowout strength of a shear key loaded toward a free edge of an unreinforced concrete footing may be unconservative for large foundation sizes (mean test-to-predicted ratios equal to 0.51 with a coefficient of variation of 0.14). This unconservatism is attributed to the size effect in concrete, which predicts that failure is controlled by the initiation of cracking, rather than the development of concrete tensile strength over the failure surface. The concrete capacity design (CCD) method, which incorporates this size effect from fracture mechanics theory, is presented to characterize the concrete blowout strength. The strength estimates determined as per this method agree closely with experimental capacities (mean test-to-predicted ratio of 1.07 with a coefficient of variation of 0.19).

On-going work, as well as design strategies based on the experimental findings, is briefly outlined.

Acknowledgments

Table of Contents

List of Tables

List of Figures

xi

List of Symbols

A   -   Nominal unthreaded area of the anchor rod

A_{35} -   Effective area of the concrete failure surface based on a 35 degree projected plane from the bearing edges of the shear lug to the free surface, excluding the bearing area of the shear lug, inches^2

A_{45} -   Effective area of the concrete failure surface based on a 45 degree projected plane from the bearing edges of the shear lug to the free surface, excluding the bearing area of the shear lug, inches^2

A_{no} -   Projected area of the concrete failure surface for one anchor at the concrete surface unlimited by edge influences or neighboring anchors, idealizing the failure cone as a pyramid with a base length of three times the embedment depth

c -   Free edge distance from the shear key, inches

COV   -   Coefficient of variation

d   -   Shear key embedment depth; or nominal (unthreaded) diameter of anchor rod

d_u -   Threaded diameter of anchor rod

E	-	Young's modulus
e	-	Concrete footing corner distance
f_c'	-	Concrete compression strength, psi
f_t, f_v	-	Required tensile and shear stress, respectively
f_{ta}	-	Required axial stress from axial loading
f_{tb}	-	Required axial stress from bending
F_{nt}, F_{nv}	-	Nominal tensile strength and shear strength, respectively
F_u	-	Ultimate tensile strength of rod
$F_{u,rod}$	-	Mean ultimate strength of rod
$F_{y,rod}$	-	Mean yield strength of rod
h	-	Foundation height
h_{ef}	-	Effective concrete embedment depth, inches
I_t	-	Second moment of area of threaded anchor rod
k_{nc}	-	Calibration factor; equal to 40 for cast-in situ headed studs and headed anchor bolts

k	-	Effective length factor of the anchor rod (i.e. lever arm factor)
k_{35}	-	Calibration constant; equal to $40/9 = 4.\overline{4}$
l	-	Length of anchor rod in bending
$L_{effective}$	-	Effective bending length of anchor rod
$L_{initial}$	-	Effective bending length of the undeformed anchor rod
M_l	-	Resisting moment of anchor rod
n	-	Number of anchor rods
N_{no}	-	Concrete cone failure load of a single anchor in uncracked concrete unaffected by edge influences or overlapping cones of neighboring anchors loaded in tension based on the concrete capacity design (CCD) approach
P	-	Applied axial load
P_1	-	Resultant axial force on deformed anchor rod
R	-	Correlation coefficient
$R_{measured,eliptical}^{PV}$	-	Predicted anchor rod capacity assuming rod tension and shear; considering measured rod dimensions and an elliptical stress interaction equation

$R^{PVM}_{measured,eliptical}$ -   Predicted anchor rod capacity assuming rod tension, shear and bending (bending length equal to the thickness of the base plate plus half the thickness of the welded plate washer); considering measured rod dimensions and an elliptical stress interaction equation

$R^{PVM*}_{measured,eliptical}$ -   Predicted anchor rod capacity assuming rod tension, shear and bending (bending length equal to the thickness of the base plate and grout pad plus half the thickness of the welded plate washer) considering measured rod dimensions and an elliptical stress interaction equation

$R^{PV}_{measured,trilinear}$ -   Predicted anchor rod capacity assuming rod tension and shear; considering measured rod dimensions and a trilinear stress interaction equation

$R^{PVM}_{measured,trilinear}$ -   Predicted anchor rod capacity assuming rod tension, shear and bending (bending length equal to the thickness of the base plate plus half the thickness of the welded plate washer); considering measured rod dimensions and a trilinear stress interaction equation

$R^{PVM*}_{measured,trilinear}$ -   Predicted anchor rod capacity assuming rod tension, shear and bending (bending length equal to the thickness of the base plate and grout pad plus half the thickness of the welded plate washer) considering measured rod dimensions and a trilinear stress interaction equation

$R^{PV}_{no\min al,eliptical}$ — Predicted anchor rod capacity assuming rod tension and shear; considering nominal rod dimensions and an elliptical stress interaction equation

$R^{PVM}_{no\min al,eliptical}$ — Predicted anchor rod capacity assuming rod tension, shear and bending (bending length equal to the thickness of the base plate plus half the thickness of the welded plate washer); considering nominal rod dimensions and an elliptical stress interaction equation

$R^{PVM*}_{no\min al,eliptical}$ — Predicted anchor rod capacity assuming rod tension, shear and bending (bending length equal to the thickness of the base plate and grout pad plus half the thickness of the welded plate washer) considering measured rod dimensions and an elliptical stress interaction equation

$R^{PV}_{no\min al,trilinear}$ — Predicted anchor rod capacity assuming rod tension and shear; considering nominal rod dimensions and a trilinear stress interaction equation

$R^{PVM}_{no\min al,trilinear}$ — Predicted anchor rod capacity assuming rod tension, shear and bending (bending length equal to the thickness of the base plate plus half the thickness of the welded plate washer); considering nominal rod dimensions and a trilinear stress interaction equation

$R_{no\,min\,al,trilinear}^{PVM*}$ - Predicted anchor rod capacity assuming rod tension, shear and bending (bending length equal to the thickness of the base plate and grout pad plus half the thickness of the welded plate washer) considering measured rod dimensions and a trilinear stress interaction equation

R_{peak}, $R_{peak}^{reversed}$ - Peak lateral load observed for the anchor rod bearing tests for each slip direction

t_{grout} - Thickness of the grout pad

t_{plate} - Thickness of the base plate

t_{waher} - Thickness of the welded plate washer

V - Applied shear load

V_1 - Resultant shear force on deformed anchor rod

$V_{peak}^{effective}$ - Peak load observed during the second (i.e. final) load drop minus the resistance offered by friction observed in the shear key bearing tests

$V_{peak}^{initial}$ - Peak shear load prior to the first load drop observed in the shear key bearing tests

$V_{peak}^{ultimate}$ - Peak shear load prior to the second load drop (i.e. ultimate load) observed in the shear key bearing tests

w - Shear key width

Z -   Plastic section modulus of unthreaded anchor rod

Z_t -   Plastic section modulus of threaded anchor rod

Δ -   Lateral displacement of anchor rod bolted end

θ -   Effective angle of rod rotation

μ -   Coefficient of friction

μ_{min} -   Minimum coefficient of friction value extracted from test observation

$\sigma_{failure}$ -   Nominal failure stress for CCD method

ϕ -   Resistance factor

ϕ_{45} -   Strength reduction factor of the 45 degree cone method = 0.85

ϕ_{CCD} -   Strength reduction factor of the CCD method = 0.75

Chapter 1

Introduction

1.1 INTRODUCTION

This report describes the first phase of large scale testing conducted as part of a comprehensive project whose aim is to characterize the performance of column base plates under various loading conditions. The project proposal was initiated in response to a request for proposal for proposal by the American Institute of Steel Construction (AISC RFP 6807, 2006). At the time of writing this report, the project is ongoing, and future reports will focus on other aspects of base plate response, including flexural loading. This report focuses on completed work, which addresses shear-dominated loading.

1.2 GENERAL

Column base connections are critical components in steel structures because they transfer axial forces, shear forces and moments to the foundation. Laboratory testing has demonstrated the susceptibility of column base plate connections to various failure modes, including weld fracture (e.g. Astaneh-Asl & Bergsma, 1993; Fahmy *et al.*, 1999; Burda & Itani, 1999), base plate yielding, anchor rod fracture and concrete crushing (DeWolf & Sarisley, 1980). Recent studies by Grauvilardell *et al.* (2005) indicate that in structural systems such as braced frames, a base plate connection may experience extremely large shear-to-moment ratios, such that failure of the connection is dominated by shear. However, experimental investigations of shear transfer in base plates are highly limited, and most current design guidelines are based on adaptations of experimental data from component testing in different contexts. For example, several studies investigate the frictional behavior between steel and concrete/grout material interfaces. However, no documented studies examine common detailing practice used for column erection, such as the use of steel shim stacks for base plate construction. Similarly, most studies which investigate anchor rods in base plates focus on concrete failure modes, rather than the failure of anchor rods from axial tension, shear and bending. Thus, there is a lack of

experimental research which investigates structural details and modes of failure that may be unique to the entire column base plate component. An investigation of these issues is the primary motivation for the research program presented in this report.

Seven large scale experiments focusing on shear transfer in column base plates form the main scientific basis of this study. These tests are supported by a set of analyses, as well as ancillary tests of the materials used. The large scale tests were conducted at the state-of-the-art Network for Earthquake Engineering Simulation (NEES) Structures Laboratory at the University of California at Berkeley in Richmond, California. The experiments were conducted using an elaborate testing apparatus which enabled the application of combined tensile/compressive axial loading and cyclic lateral (shear) loading.

The large scale tests investigate three load transfer mechanisms which are commonly used to resist shear in exposed column base plates, including surface friction, anchor rod bearing and shear key bearing (see Figure 1.1). Three tests were conducted to investigate surface friction, two tests investigated anchor rod bearing and two tests examined a shear key detail.

Chapter 2 presents a detailed literature review and documents recent and past research on column base plates, with a focus on shear transfer mechanisms. Chapter 2 evaluates this research in the context of current design guidelines and common construction practice, and presents the specific objectives of this study. Chapter 3 presents the experimental data in detail, including the ancillary tests and the large scale base plate tests. The results are analyzed and improved guidelines are presented to characterize the strength capacity of various failure modes. Chapter 4 summarizes the findings of the study and presents design implications, while outlining future work. Appendix A provides an inventory of the ancillary tests, along with material descriptions. Detailed experimental data is archived in Appendix B. The last three Appendices (C, D & E) outline proposed capacity equations and provide calculation examples for the anchor rod bearing mechanism (Appendix C and D) and the shear key bearing mechanism (Appendix E).
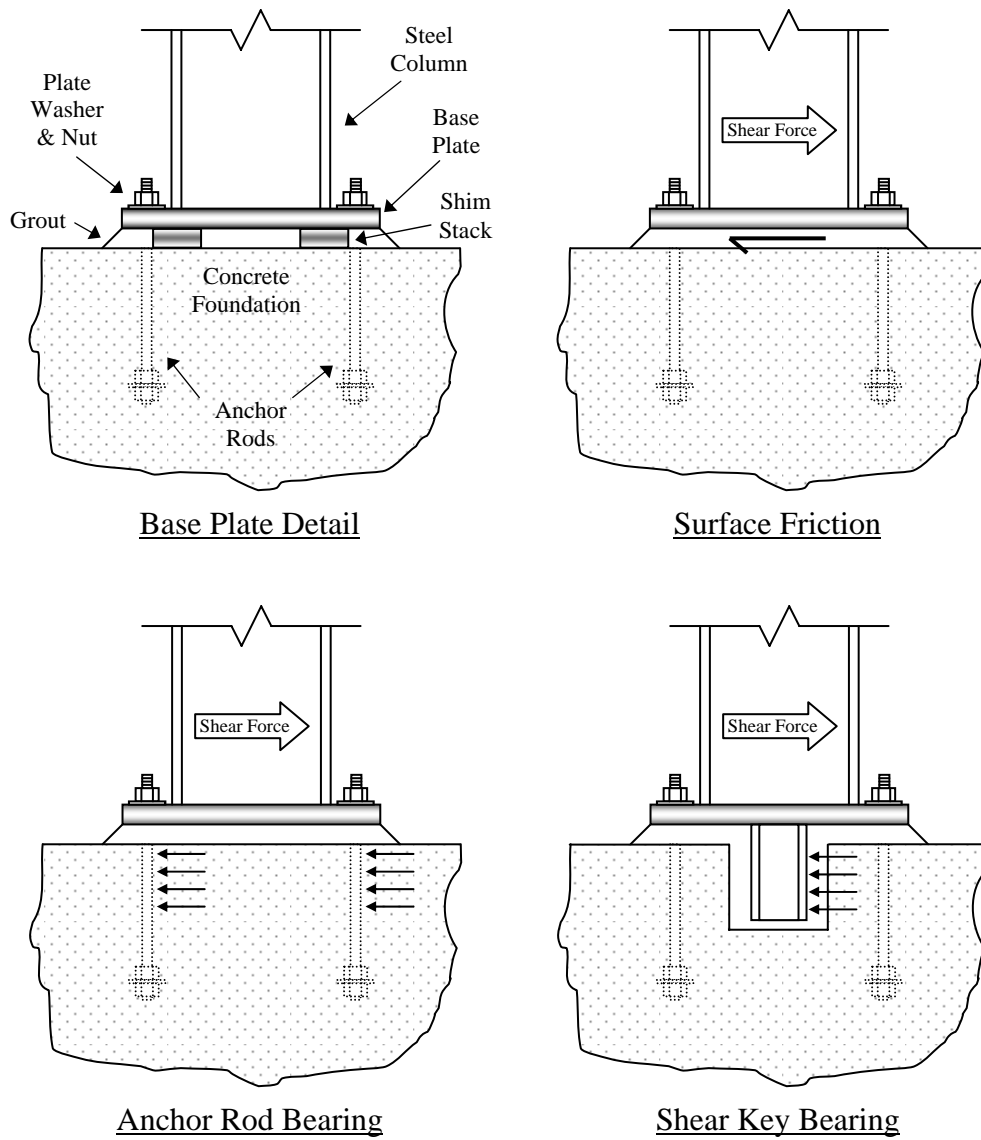
Figure 1.1 – Schematic of typical exposed column base plate and associated shear transfer mechanisms (adapted from AISC Seismic Provisions, 2005)

Chapter 2

Background and Objectives

2.1 INTRODUCTION

To provide background for the current investigation, this chapter presents a review of literature relevant to shear transfer in exposed column base plates. Specifically, the literature review addresses the three shear transfer mechanisms examined in this study, i.e. surface friction, anchor rod bearing and shear key bearing. The chapter summarizes currently used design strategies that incorporate these mechanisms, while outlining state-of-the-art research relevant to improving these design guidelines. The chapter concludes by describing the objectives of the current study in the context of the presented literature review.

2.2 CURRENT DESIGN PROVISIONS

In 1990, the American Institute of Steel Construction (AISC) released a report authored by DeWolf & Ricker (1990) which presented a compilation of existing information on the design of base plates of steel columns. This report, part of the AISC's *Steel Design Guide Series 1 – Column Base Plates*, provides methods and suggestions for base plate design, including bases subjected to axial compression and flexure. However, the report cites the lack of design provisions for bases subjected to shear loading, in part due to limited availability of test data. The report lists a limited number of publications regarding shear transfer in base plates, such as Ballio & Mazzolani (1983), Goldman (1983), Shipp & Haninger (1983) and Tronzo (1984), but recognizes that a large majority of these are analytical studies.

The second edition of the AISC base plate design guide (Fisher & Kloiber, 2006) was released partly in response to new significant research and a new Occupational Safety and Health Administration (OSHA) provision requiring four anchor rods for most base plate connections (OSHA, 2001). This new edition of the AISC *Steel Design Guide 1*

includes some additional information on shear transfer, such as providing a more exhaustive treatment of anchor rod and shear key design for shear loading. However, not all the additional information was supported by experimental verification of large scale base plate prototypes. The *Steel Design Guide 1 - Base Plate and Anchor Rod Design* (Fisher & Kloiber, 2006) relies on specifications from several organizations, including the AISC Steel Construction Manual (2005), the American Concrete Institute (ACI) Committee 318 (2002), and OSHA (2001). The *Steel Design Guide 1*, along with its referenced codes and standards, form the basis of typical steel column base plate design considerations in the United States.

Additionally, special design provisions have been developed for column base plates of structures subjected to special loadings. For example, both the AISC Seismic Provisions (AISC Seismic Design Manual, 2005) and the ACI code requirements for concrete structures for nuclear facilities (ACI 349, 2006) provide guidelines for the design of column base plates. In the context of shear transfer, the ACI 349 specifications provide the most exhaustive and detailed design requirements. On the other hand, the Commentary to the AISC Seismic Provisions addresses shear transfer in a more qualitative sense while emphasizing that future experimental research on column base plates should investigate seismic loading and larger prototypes subjected to shear loading.

2.3 CURRENT STATE OF RESEARCH

A recently published AISC sponsored synthesis of research on column base connections (Grauvilardell *et al.*, 2005) reveals that shear transfer in exposed column base plates are not as well understood as flexural or axial load transfer. In fact, only two references listed in this exhaustive synthesis, Goldman (1983) and Tronzo (1984), specifically address shear transfer. These studies focus on design examples and design methods without a detailed description of supporting experimental data. The authors of these two publications express their concern for the lack of building code provisions and the general lack of experimental research on base plate shear transfer, especially in the context of column bases attached to braced frames, where the shear-to-moment ratio is typically large.

An independent review of literature by the authors of the current study reveals that experimental research of shear transfer in base plates has not been explicitly addressed, although the associated mechanisms (e.g. surface friction or certain modes of concrete or anchor rod failure) have been researched in separate contexts. Thus, current design provisions for base plates typically adapt and combine findings from several of these studies, which rely on small-scale component tests of specific failure mechanisms (e.g. pullout or shear tests of individual anchor rods). Therefore, there is a lack of data involving large scale base plate components, where various mechanisms may interact with each other or may be influenced by the construction procedures or geometry of the base connection itself. Moreover, few studies examine the effect of cyclic loading on base plate shear transfer details, which is important from the perspective of seismic design.

This section summarizes research relevant to the development of design considerations for shear transfer in exposed column base plates. Specifically, this section outlines studies that address three common shear transfer mechanisms, which are featured in the AISC *Steel Design Guide 1* (Fisher & Kloiber, 2006) and subsequently examined experimentally in this study. These mechanisms include (1) surface friction (2) anchor rod bearing and (3) shear lug (shear key) bearing. Other details have been proposed for shear transfer in base plates. For example, the column and base plate can be embedded directly into the concrete foundation or attached to a grade beam (Grauvilardell *et al.*, 2005).

For a more extensive literature review regarding column base plates, the authors refer the reader to the first edition of the AISC *Steel Design Guide 1* (DeWolf & Ricker, 1990) and the aforementioned research synthesis (Grauvilardell *et al.*, 2005).

2.3.1 Surface Friction

Under situations of low column base shear (e.g. in low-rise buildings subjected to modest wind forces), shear loading in column base plates may be adequately resisted by surface friction between the steel plate and grout/concrete interface due to the axial compressive

gravity load in the column. However, large lateral loads sustained by the structure (especially in braced frames) may result in uplift of the base connection such that the frictional resistance is reduced (or eliminated) and the shear force must be transferred to the foundation by other means (e.g. through anchor rods or a shear key). In addition, under seismic loading, high shear loads and other issues such as foundation rocking, vibrations and tension uplift render surface friction an impractical choice for shear transfer. Astaneh-Asl (2008) points outs that most seismic codes do not allow the surface friction mechanism for base plates. Nevertheless, surface friction will always be active when a compressive axial load is present and may be adequate to transfer low shear forces.

The AISC *Steel Design Guide 1* (unless otherwise noted, this reference henceforth indicates the *second edition* of the AISC *Steel Design Guide 1*; i.e. Fisher & Kloiber, 2006) provides design coefficient of friction values for steel on grout and steel on concrete (listed as 0.55 and 0.70, respectively). These values are adapted from ACI 349 criteria (ACI, 1985) and are based on historical test programs which have investigated steel on grout/concrete surface friction under monotonic loading. Examples of such studies investigating steel on grout friction include Cannon *et al.* (1975), Rabbat & Russell (1985) and more recently Nagae *et al.* (2006). These studies report average coefficient of friction values in the range of 0.52 - 0.65. Of these studies, only the most recent (Nagae *et al.*, 2006) examines frictional behavior between grout and steel under reversed cyclic loading. This study provides a theoretical analysis of the surface friction mechanism and, from small scale experiments, concludes that a friction coefficient of 0.50 is appropriate for design.

Although base plates typically rest on a grouted surface, surface friction between *concrete* and steel has been studied by various researchers including Burdette *et al.* (1987), Cook & Klingner (1991) and Baltay & Gjelsvik (1990). These studies examine frictional behavior under monotonic loading and report average friction coefficient values in the range 0.43 - 0.65. However, grout, rather than concrete, is typically installed at the base plate interface, especially for large bases and those with shear keys.

It is important to note that none of the surface friction studies mentioned in this section specifically investigate the interaction of column erection procedures, such as the use of shim stacks, on the frictional response of base plates. In addition, while past tests investigate a large range of surface pressures (e.g. 1-10,000 psi for Baltay & Gjelsvik [1990]; 460-1,400 psi for Nagae *et al.* [2006]), most experimental programs investigate relatively small scale base plates. For example, the base plates used in the study of Nagae *et al.* (2006) are only 10 inches square. Nevertheless, the study publication by Nagae *et al.* (2006) provides a detailed theoretical analysis of surface friction between steel and grout. A combined theory of adhesion and plowing, originally used for friction between steels, is applied to interpret the friction behavior and indicates reasonable agreement with test results.

In summary, coefficient of friction values for the design of column base plate shear transfer are, in general, based on studies that may not incorporate all the effects observed in actual column base plate details. In addition to the limited large scale experimental data of friction between steel and grout (especially under cyclic loading), other issues not addressed by these studies include the effect of column erection procedures (e.g. the use of shim stacks) and the associated evolution of frictional response.

2.3.2 Anchor Rod Bearing

Shear forces in column bases may be resisted by the base plate bearing against anchor rods embedded in the concrete foundation. This mechanism may be practical under low compressive axial loads or under axial tension (i.e. uplift) at the column base, when sufficient frictional resistance cannot be developed. Fisher & Kloiber (2006) note that the use of anchor rods to transfer shear forces must be carefully examined due to several assumptions regarding the force transfer to the rods. A primary concern is the uncertainty of uniform transfer of shear loads to all the anchor rods due to lateral displacement (or slip) of the base plate. Highly oversized anchor rod holes (larger than standard oversize holes – refer Fisher & Kloiber, 2006) are typically used in base plates in order to compensate for construction tolerances. To reduce the extent of slip before engagement

of all anchor rods, plate washers (installed around the rods, with a minimal clearance) may be fillet welded to the top surface of base plate.

As discussed above, anchor rods may be used to resist axial tension and shear loads, or a combination thereof. Consequently, the AISC *Steel Design Guide 1* provides guidelines and design examples to assist in the design of anchor rods to resist shear and tension. Transfer of shear through anchor rod bearing involves several issues. Summarized briefly, these include (1) failure of either the grout or the concrete in the immediate vicinity of the anchor rod either due to pullout, localized crushing or free edge blowout (under shear), (2) the effects associated with eccentric placement of anchor rods within the holes of the base plate, which may result in nonuniform load distribution amongst the anchor rods and (3) failure of the anchor rod itself due to a combination of axial and shear loading, which may also produce flexure (i.e. bending) in the rods. An additional consideration, not addressed by the *Steel Design Guide 1*, is the response related to second order effects due to large lateral base plate displacements, which may increase the shear strength and stiffness of the connection due to increased tension forces in the anchor rods.

With respect to issue (1) above, various researchers have examined the strength of steel embedments and anchors in concrete, mainly in the context of the design of concrete systems. These include the studies of Conrad (1969), Cannon *et al.* (1975), Bailey & Burdette (1977) and Cannon *et al.* (1981), which all consider anchor rods embedded in concrete loaded in monotonic shear or tension. Klinger *et al.* (1982) investigated anchor bolts subject to monotonic and reversed cyclic shear loads and provided design equations and design recommendations. However, it is important to note that these studies primarily investigate concrete failure modes. Thus, the design considerations from these studies focus on issues such as providing adequate anchor embedment lengths, edge distances and reinforcement details. Several of these considerations have been adopted into concrete design codes (e.g. ACI 318 and ACI 349). Building on these experimental programs, Fuchs *et al.* (1995) developed the concrete capacity design (CCD) method

which is currently the preferred approach for the concrete design of embedded fasteners under shear or tensile loading (ACI 349, 2006).

With respect to issue (2) above, the installation of welded plate washers typically ensures that all anchor rods are engaged by the base plate almost simultaneously. However, the eccentric placement of anchor rods may have other consequences. For example, anchor rods that are close to the edge of the base plate hole in the direction of loading may exhibit restrained bending (due to interaction with the base plate), thereby influencing their strength and mode of failure. This issue is discussed later in Chapter 3.

With respect to issue (3) above, the AISC *Steel Design Guide 1* suggests that anchor rods in base plates be designed with adequate consideration of the interaction of axial tension, flexural and shear stresses. The *Design Guide* refers to an equation listed in the AISC Steel Construction Manual (section J3.7 in the commentary; AISC, 2005) for a description of the interaction relationship between axial (normal) stresses and shear stresses. This interaction relationship is based on extensive studies by Kulak *et al.* (1987). The *Design Guide* suggests that for the calculation of flexural stresses in the anchor rods, it is assumed that the anchor rods bend freely in double curvature over a certain length, which is measured from the top of the grout pad to the center of welded plate washer (i.e. the base plate thickness plus half the plate washer thickness).

Response of anchor rods in grouted base plates subjected to combined monotonic lateral and tensile loading was studied experimentally by Adihardjo and Soltis (1979). This study determined that existing shear/tension interaction equations based on bolts embedded directly into concrete (from PCI, 1971) may not be applicable in grouted base plate details. While it was determined that the shear capacity of bolts for grouted plates is reduced as compared with ungrouted plates (partly due to the localized damage of the grout), no design recommendations were given. Analytical design aids of bolts subjected to tension plus shear loading are presented by Scacco (1992), Fisher (1981) and Shipp & Haninger (1983). More recently, Nakashima (1998) examined the mechanical properties of steel column base anchor bolts under combined tension and shear. In addition to

examining the effects of anchor rod threads, Nakashima determined that, due to grout separation, the ultimate capacity of anchor bolts placed through a grout layer is lower as compared with typical structural bolts. Kawano *et al.* (2003) experimentally studied anchor bolts in exposed steel column bases, focusing on bolts which are subjected to tensile and shearing forces with relatively short concrete edge distances.

Current experimental and theoretical research on column bases loaded with a combination of shear and tension forces by Gresnigt *et al.* (2008) specifically investigates anchor rod bearing. Gresnigt *et al.'s* results are consistent with past studies which show that the shear strength of anchor bolts is considerably lower than the shear strength of bolts in bolted connections between steel plates. Two analytical capacity models are reported to describe the anchor rod load-deformation behavior. One model gives very conservative results, especially with "large" tensile axial forces and/or "large" grout thicknesses. Another proposed model, which does not take into account bending moments in the bolts, gives results that are consistent with test results.

In summary, studies on the behavior of anchor rods have focused mainly on concrete failure modes, and on the axial-shear interaction of the anchor bolts. The behavior of anchor rods in grouted base plates has received limited attention by way of experimental studies. Moreover, additional studies are required to appropriately characterize the effects of bending on the capacity of anchor rods.

2.3.3 Shear Key Bearing

To resist moderate to high column base shear loads, such as induced by seismic loading in low- to mid-rise structures, one or multiple shear lugs (also known as a shear key) may be attached to the base plate. The shear key is often provided in the form of a plate welded to the underside of the base plate. In some cases, a stub W-section is used to provide the required lug strength. The shear lug detail requires additional welding and the need for a grout pocket in the concrete foundation, which may lead to more costly and difficult construction.

Guidelines and examples for shear key design are provided in the AISC *Steel Design Guide 1*. Transfer of shear through shear key bearing may be accompanied by three failure modes including: (1) failure of the grout/concrete directly in front of the load path of the shear key, (2) failure of the steel shear key itself, including the welded connection to the base plate and (3) distortion (e.g. bending) of the base plate due the loading of the connected shear key.

With respect to issue (1) described above, three typical failure modes of the concrete/grout are associated with the shear key mechanism: (a) concrete/grout bearing failure directly in front of the shear key bearing surface load path, (b) concrete shear-friction failure and (c) concrete free edge side blowout failure. Failure modes (a) and (b) are common for foundations with large areas surrounding the shear key while failure mode (c) is common for foundations with short edge distances from the shear key such as in pier footings. Provisions for failure modes (a) and (b) are provided in ACI 349 and are based on tests by Rotz & Reifschneider (1989). Regarding concrete side blowout, a literature search did not reveal any experimental data for base plate shear lugs. ACI 349 provides two methods to predict the blowout shear capacity of concrete embedments toward a free edge: the 45 degree cone method and the concrete capacity design (CCD) method.

The 45 degree cone method for concrete embedments was developed by the ACI Committee 349 (ACI 349, 1985). As per this method, the concrete blowout capacity of a fastening/embedment subjected to tension or shear is calculated by assuming a constant tensile stress acting on the projected area of a failure cone, assuming the inclination between the failure surface and the concrete surface as 45 degrees. This method was adapted by ACI 349 (ACI 349, 2006) for the shear capacity of shear lugs loaded towards a free edge, assuming a 45 degree failure plane from the bearing edges of the shear key. However, no experimental tests were conducted to verify this method in the context of shear keys attached to base plates.

The CCD method (Fuchs *et al.*, 1995) was developed in response to the limitations of the 45 degree cone method and is currently the standard design method for concrete anchors under shear and tensile loading (ACI 349, 2006). The CCD method is based on the principle that for large concrete members, the blowout strength is associated with fracture initiation, rather than the development of concrete tensile strength over a large failure surface, such as assumed by the 45 degree cone method. Thus, for large foundation sizes, the 45 degree cone method may overestimate the available strength. To address this issue, the CCD method (Fuchs *et al.*, 1995) applies the fracture mechanics theory of Bažant (1984) to concrete anchors, by explicitly including a size effect, wherein the failure stress of concrete is assumed to be an inverse function of the specimen/foundation size. While the theory is presented for concrete anchors, no experimental data is available to verify/examine the CCD method in the context of shear keys in base plates.

With respect to (2) and (3) described earlier, the design of shear lugs itself is presented in Fisher (1981), Goldman (1983), Tronzo (1984) and more recently in the AISC *Steel Design Guide 1* (Fisher & Kloiber, 2006). The AISC *Design Guide* recommends the lug be treated as a cantilever beam with a uniform bearing stress on the face of the lug, from which the lug thickness and weld size can be determined. The design guide also mentions that bending in the base plate may be an issue for large shear loads and/or column weak axis loading. However, a literature search did not reveal any experimental investigations addressing this issue.

In summary, studies investigating the response of base plate shear key bearing are extremely limited. Owing to the unavailability of experimental data for shear lugs, the aforementioned research synthesis by Grauvilardell *et al*. (2005) states that research on this topic is priority.

2.4 OBJECTIVES OF CURRENT RESEARCH

As discussed in the preceding sections, several topics regarding shear transfer in base plates are unresolved and may be addressed through further experimentation and analysis, especially in the context of large scale prototypes. Based on consultation with the AISC

oversight committee and consideration of experimental budgets, the main objectives of the current study are to examine three mechanisms (surface friction, anchor rod bearing and shear key bearing) commonly used to resist shear in exposed column base plate connections. While several failure modes are possible for each of these mechanisms, the specific issues addressed by this study are now summarized –

1. For surface friction, the major objective to is characterize the coefficient of friction between steel and grout, and more importantly, between the steel and grout interface when leveling shim stacks are used.

2. For anchor rod bearing, the major objective is to characterize the strength of the anchor rod itself under the combination of axial tension, shear and flexure. Three issues are important in this context. First, the effective bending length and bending shape of the anchor rod must be characterized to determine the flexural stresses in the rod. Second, the effects of interaction/contact between the anchor rods and base plate on the strength of the anchor rods must be examined. Third, geometric second order effects due to large displacement of the rods should be considered. Concrete failure modes are not explicitly investigated.

3. For shear key bearing, the major objective is to investigate the strength capacity associated with the side blowout of a shear key embedded near a free edge in an unreinforced concrete footing. Other failure modes, such as shear key yielding or base plate failure due to the forces imposed by the shear key are not considered.

In addition to providing experimental data and analysis for each of these shear mechanisms, a key objective of the current study is to verify existing design methods and to provide improved design guidelines for shear transfer. Chapter 3 describes the results of the experimental program in detail, including an analysis of the test observations.

Chapter 3

Experimental Program and Test Results

3.1 INTRODUCTION

Observations from seven large scale tests are reported to investigate shear transfer in exposed column base plates. Three mechanisms, commonly used in current structural design practice, are examined: surface friction, anchor rod bearing and shear key bearing. While similar tests have been conducted previously in broader contexts, the tests described in this chapter focus on shear transfer mechanisms from the specific perspective of exposed column base plates. For example, the surface friction tests investigate the effect of shim stacks typically used in base plates for column erection (as opposed to only considering pure steel on grout friction). Similarly, tests involving the anchor rods investigate the effect of anchor rod bending, rather than only considering the interaction of axial and shear stresses. The shear key tests provide entirely new experimental data on concrete blowout behavior in an unreinforced footing.

The large scale experiments, along with the ancillary tests (also described in this chapter) provide data which can be used to evaluate current design guidelines and capacity predictions, such as those outlined in the AISC *Steel Design Guide Series 1* (Fisher & Kloiber, 2006). This chapter describes the experimental program in detail by providing an overview of the large scale test setup, testing procedures and test results. While this chapter presents key data and representative response plots associated with the discussion of experimental observations, detailed data for all experiments is provided in Appendix B. An analysis of observations and a brief assessment of current design guidelines are provided for each shear transfer mechanism investigated. This chapter also presents a summary of the ancillary tests, including anchor rod tension tests, standard concrete cylinder compression tests and grout cylinder compression tests. An inventory of the ancillary tests, along with material descriptions, is given Appendix A.

3.2. ANCILLARY TESTS

Three types of ancillary tests were conducted to characterize the materials used in the base plate tests. These include (1) anchor rod tension tests, (2) standard concrete cylinder compression tests and (3) grout cylinder compression tests. Tables 3.1-3.3 summarize key results obtained from the ancillary tests and Appendix A includes a detailed inventory of the ancillary test data.

3.1.1 Anchor Rod Tension Tests

Tension tests were conducted on samples taken from the same batch of ASTM F1554 Grade 55 anchor rods used for the base plate tests. Four unthreaded rod specimens (two for each rod size used in the large scale tests, 3/4" and 1-1/4" diameter) were tested quasi-statically under monotonic tension to determine anchor rod material properties. Two uniaxial strain gages were attached to the rods to identify initial yielding behavior.

As summarized in Table 3.1, the mean ultimate strength $F_{u,rod}$ is 96.4 ksi for the 3/4" diameter rod and 75.0 ksi for the 1-1/4" diameter rod. These values are approximately within the ASTM specified ultimate strength range of 75-95 ksi (AISC, 2005). The average yield strength $F_{y,rod}$ (as determined by the 0.2% offset method) is 66.8 ksi for the 3/4" diameter rod and 54.4 ksi for the 1-1/4" diameter rod. The yield strength of the smaller 3/4" diameter rod is approximately 21% greater than the minimum specified strength of 55 ksi, whereas the yield strength of the 1-1/4" diameter rod is about equal to the specified strength. Complete results of the rod tension tests are provided in Appendix A.

3.1.2 Standard Concrete Test Cylinders

Four pedestals representing the concrete foundation for the base plate tests (see Figure 3.1), measuring 4 feet by 7 feet in plan area and 32.5 inches in height, were cast using commercial ready-mixed concrete specified with a 4,000 psi twenty-eight day compressive strength and 4.0" slump. The concrete was delivered in two trucks and each batch had a measured slump of 3.5". Prior to testing, all concrete pedestal specimens were air cured well beyond 28 days (i.e. between 3-5 months). At this age, similar

concrete is approximately 13% stronger than the measured twenty-eight day compressive strength (ACI 209, 2006). Note that for the purpose of analysis, the twenty-eight day compressive strength is considered. A total of 12 concrete compression test cylinder specimens (three cylinders sampled from the concrete used for each pedestal) were collected (as per ASTM C31, 2008) and tested after twenty-eight days of curing (as per ASTM C39, 2005). The average ultimate compressive strength f'_c of all test cylinders is 4,760 psi (standard deviation = 260 psi), about 19% greater than specified (4,000 psi). The average ultimate compressive strength of the concrete from each pedestal is shown in Table 3.2, along with other information such as cylinder density. Detailed information regarding the concrete, including the test results of each individual compression test, is archived in Appendix A.

3.1.3 Grout Test Cylinders

General construction, mineral-aggregate non-shrink grout was installed between the steel base plate and concrete pedestal for all large scale tests. Tests were conducted to examine the compressive strength of the grout used for each base plate test. The grout compressive strength is especially important for the large scale tests involving the shear key, where the failure surface encompasses both concrete and grout and grout bearing failure is a possible failure mode. Twenty-eight grout cylinders (four samples from the grout used for each large scale test), measuring 6" tall and 3" in diameter, were tested in compression at a loading rate of approximately 3.5 kips/second. The standard ASTM method for testing grout strength (ASTM C109, 2007) was not used. This method, also known as a "grout cube test", is applicable for masonry grout applications. Except for the smaller cylinder size, the grout was tested and collected using the same methods as for standard concrete cylinders (i.e. ASTM C31 and ASTM C39). For logistical (laboratory schedule) and construction reasons, the grout pad from each large scale test had different cure times and water content. This variation in the cure time and water content was replicated for each grout test cylinders. The average compressive strengths of the grout is presented in Table 3.3, along with other information such as the corresponding large scale test number, curing time, water content, and density. The average compressive strength of the grout ranged between 5,780 and 7,210 psi. Standard practice typically

requires the grout to have a compressive strength at least twice as large as the compressive strength of the supporting concrete (i.e. 8,000 - 10,000 psi grout in the case of the concrete used in the large scale experiments). Due to testing schedule constraints, the grout was not cured to full strength. Detailed information regarding the grout, including the test results of each individual compression test and product data from the manufacturer, is archived in Appendix A.

3.3 LARGE SCALE EXPERIMENTS: TEST SETUP AND PREPARATION

Table 3.4 presents the test matrix for the base plate tests. The table includes key information about each experiment, including information regarding the shear mechanism investigated and the applied loading. One concrete pedestal (which represents the foundation/footing) was used for all the friction tests (Tests #1, #2 and #3), as well as one anchor rod test (Test #4). A new pedestal was used for each of the other three tests (Tests #5, #6 and #7). Figure 3.1 shows a representative photograph of the concrete pedestal.

The three mechanisms investigated for the base plate tests, indicated in Table 3.4, represent popular design alternatives for shear transfer in exposed base plates and are featured in the AISC *Steel Design Guide 1* (Fisher & Kloiber, 2006). Moreover, these mechanisms were enumerated as being important by the AISC (AISC RFP 6807, 2006) in response to which this study was initiated. Referring to Table 3.4, surface friction is examined under cyclic shear and various compressive axial load levels. To reflect common construction procedures, two friction tests (Tests #1 and #2) included steel shim stacks beneath the base plate. For comparison, a third friction test (Test #3) investigated a steel on grout interface without the shim stacks. Two tests (Test #4 and #5) were conducted to investigate the response of anchor rods in a grouted base plate connection under combined shear and tensile loading. Two differently sized anchor rods (3/4" and 1-1/4" diameter), with a welded plate washer detail, were investigated. Two other tests (Tests #6 and #7) focused on a shear key bearing mechanism. Recall that a literature review did not reveal any prior tests which evaluated shear keys loaded toward a free edge, even though this detail is often suggested for exposed base plates with high shear

forces. Two shear key embedment depths, 5.5 inches and 3.0 inches below the concrete surface, were tested under monotonic shear with small axial compression force.

3.3.1 Test Setup

The base plate tests were conducted at the UC Berkeley Network for Earthquake Engineering Simulation (NEES) Structures Laboratory in Richmond, California. Figure 3.2a schematically illustrates the test setup and a photograph is provided in Figure 3.2b. Referring to Figure 3.2a, a large steel beam-column loading frame provided a rigid load path for both compressive and tensile axial loading. The loading frame was braced laterally onto a concrete reaction wall. Horizontal (i.e. lateral) loads were applied via two steel assemblies bolted directly onto the base plate (see Figure 3.3), thus applying direct shear loading with negligible moment at the base connection. Two MTS series 244 150-kip dynamic actuators provided the vertical (axial) loading while two MTS series 244 220-kip dynamic actuators provided the horizontal (shear) loading. The test assembly, including the base plate, was designed to remain undamaged during testing and was reused for all seven tests. However, the base plate was modified for certain tests, including the welding (and removal) of plate washers (for Tests #4 and #5) and the welding (and shortening) of the shear key (for Tests #6 and #7). The total self weight of the set-up, determined by the vertical actuator load cells, was approximately 17.2 kips. This weight was subtracted from the axial loads recorded from the vertical actuators to determine the net axial load in the base plate connection.

3.3.1.1 Test Setup for the Friction Tests: Tests #1, #2 and #3

For Tests #1 and #2, steel shim stacks (see Figure 3.4) were used to support the base plate on the concrete pedestal during column erection. While other erection procedures were considered, the shim stack method is commonly used in current practice (Fisher & Kloiber, 2006). The shims were thermally cut from steel bar stock, each approximately 4 inches by 2 inches in area and 1/2 inch thick. Each shim stack consisted of two shims, resulting in a one inch clear distance between the surface of the concrete and the base plate, thereby providing a one inch grout pad thickness. The shims were heavily oxidized and had a slightly rough surface, especially around the shim edges. Deposits resulting

19

from thermal cutting were chipped away from the surface of the shims but the shims were not de-burred nor treated in any other way. Thus, the shims were fabricated to reflect standard construction practice. As shown in Figure 3.5, different shim stack positioning was used for Test #1 and #2. Test #3, designed to examine friction between steel and grout, did not feature shim stacks and the column was lowered by the vertical actuators to provide a grout pad thickness of one inch.

Anchor rods were absent for all friction tests in order to prevent unwanted strength contribution from rod bearing. Grout was installed by pouring a flowable mix through one anchor rod hole in the base plate until it flowed out through the other three anchor rod holes. A short tube, placed over one anchor rod hole, was used to provide head pressure to distribute the grout. The concrete pedestal surface was moistened to ensure an easy flow of the grout. Post-test visual inspection of the grout pad confirmed that the grout was evenly distributed and contained few air voids (see Figure 3.6). For all friction tests, the grout was contained within an approximate 26" by 26" foam dam, thus providing a 4.70 square foot grout pad area (see Figs. 3.5 and 3.6). Excess grout was removed from the base plate anchor rod holes prior to curing. Compressive loading, equal to the test setup assembly weight (17.2 kips; 25 psi), was maintained in the connection during curing to preserve the steel to grout bond.

Since frictional response is sensitive to surface properties, it is relevant to discuss the surface condition of the base plate. Before the first friction test, the surface condition of the ASTM A529 Grade 50 base plate was typical of freshly fabricated steel. The plate contained some mill scale and did not have any visible signs of oxidation. To reflect field conditions, the surface was not treated (sanded nor polished, etc.) in any way. After the first friction test, the plate sustained buffing damage from the grout and small patches of scouring damage due to the steel shim stacks, but no other damage was visible. Prior to the next two friction tests, residual grout was removed from the plate and the surface was wiped clean with a damp cloth. As shown previously in Fig. 3.5, different shim stack positioning was used for Tests #1 and #2 such that the scoured plate surface from Test #1 did not coincide with the shim stack locations of Test #2.

3.3.1.2 Test Setup for the Anchor Rod Tests: Tests #4 and #5

Figure 3.7 shows a schematic of the rebar details of the concrete pedestals used for the anchor rod tests (Test #4 and #5). As indicated in the figure, the concrete pedestals include specifically designed rebar details to ensure failure of the anchor rod itself, rather than failure within the concrete. Four anchor rods were used and the rod layout was approximately 24" inches square for all tests (see Figure 3.8). The anchor rod holes in the two inch thick base plate were 2-1/16" in diameter, the recommended size for 1-1/4" diameter anchor rods stated in the AISC *Steel Design Guide 1* (Fisher & Kloiber, 2006). Note that since the same base plate was reused for both rod sizes, the rod hole size was larger than the recommended hole diameter of 1-5/16" for the 3/4" diameter anchor rods. As recommended by the AISC *Steel Design Guide 1* (Fisher & Kloiber, 2006), plate washers, provided for the anchor rods, were fillet welded to the base plate to reduce the amount of slip before the shear loading was transferred to all rods. Machined square plate washers, measuring 2.5" x 2.5" x 1/4" with an internal diameter of 0.8 inch (≈ rod diameter + 1/16"), were used for the 3/4" anchor rods of Test #4 and plate washers, measuring 3.5" x 3.5" x 1/2", with holes approximately 1.3 inches in diameter (≈ rod diameter + 1/8"), were fabricated from thermally cut plate stock for the 1-1/4" diameter rods of Test #5. The sizes and hole diameters of these plate washers reflect recommendations from the AISC *Steel Design Guide 1* (Fisher & Kloiber, 2006). Additional washers were placed (un-welded) over the rods on top of the plate washers to prevent dishing of the welded plate washers due to the large tension forces in the rods. A photograph of this detail is shown in Figure 3.9. Nuts were hand tightened snug with an additional 1/8 turn. For both tests, a stiff grout mix was placed on the concrete pedestal and the base plate was lowered on to it. The grout was compacted to an approximate 1-1/4" thickness for Test #4 and an approximate 1" thickness for Test #5. Excess grout was removed from the anchor rod holes prior to curing. The threads of the anchor rods extended approximately 2 inches below the surface of the concrete to ensure failure in the threaded region.

3.3.1.3 Test Setup for the Shear Key Tests: Tests #6 and #7

For Tests #6 and #7, an I-shaped shear key, fabricated from plate stock, was welded (with 1.5" fillet welds) to the center of the base plate (see Figure 3.10 and 3.11). The shear key was designed to remain undamaged during testing. For Test #6, the shear key was 7 inches long. After this test, the shear key was thermally cut to reduce its length to 4.5 inches for Test #7. The bearing width of the shear key for both tests was 6". Referring to Fig. 3.1, grout pockets were provided in the concrete pedestals, measuring 9" x 9" in plan, 7" deep for Test #6 and 4" deep for Test #7. The distance from the shear key bearing surface to the edge of the concrete pedestal was about 20.25 inches. Grout was installed by pouring a highly flowable mix through two grout holes in the base plate. Shims were used for both shear key tests to provide a grout thickness of 1.5", resulting in an approximate shear key embedment depth (below the surface of the concrete) of 5.5" for Test #6 and 3.0" for Test #7. Anchor rods (3/4" in diameter) were cast in the pedestal to mimic the reinforcing aspect of the anchor rods, but the rods were not bolted to the base plate in order to isolate the strength of the shear key. Figure 3.12 shows the reinforcement layout of the pedestals used for the shear key tests. It is important to note that the anticipated blowout area (i.e. failure region) of the concrete pedestal was free of any reinforcement or other obstructions (with the exception of the anchor rods), to ensure that failure was obtained in the concrete only. For Tests #6 and #7, the concrete pedestals were attached to the laboratory strong floor by tension rods that terminated below the anticipated blow out area (refer Fig. 3.12), so as not to interfere with the concrete blowout failure mechanism.

3.3.2 Loading Protocol

Table 3.5 indicates the loadings applied in the base plate tests. Detailed loading plots for each test are presented in Appendix B. As indicated in Table 3.5, the friction tests involved the application of different axial load levels, followed by cyclic lateral displacement based loading as indicated in Fig. 3.13. As shown in the figure, the cyclic loading history consists of sets of increasing reversed lateral slip cycles (three cycles per set), with amplitudes of 0.1", 0.2", 0.4", 0.8" and 1.0". It is relevant to note that while several loading protocols are available for structural component testing, they are typically

expressed in terms of interstory drifts with the intent of testing deformation sensitive components. Similar protocols are not readily available for "stiff" mechanisms such as the shear transfer examined in these tests. Thus, the lateral deformation histories applied in this study are adaptations of other such protocols (i.e. Krawinkler *et al.*, 2000) to reflect deformation demands that may be expected during shear transfer. For Test #1, constant axial loads levels were applied in increasing orders of magnitude such that the steel-grout bond was broken at the lowest axial load level. Three axial loads were applied (43, 112 and 261 kips), and the cyclic lateral loading history (see Fig. 3.13) was applied at each stage. These axial loads correspond to concrete foundation bearing stresses of about 64, 166, and 386 psi, which is approximately two to ten percent of the nominal ultimate compressive strength (4,000 psi) of the concrete. For Test #2 and #3, the axial loads were applied in reverse (i.e. decreasing) order, thereby breaking the grout bond at the highest load level.

Referring to Table 3.5, similar loading was applied for the anchor rod tests (Tests #4 and #5), except that the constant axial load was tensile. Table 3.5 indicates the level of tensile load applied to each of the anchor rod bearing tests. Considering equal load distribution between the rods, the axial load levels were about 31% (Test #4) and 39% (Test #5) of the ultimate tensile capacities of the anchor rods (based on the measured material properties).

For the shear key tests, a relatively small level of axial compressive load (between 0-27 kips for Test #6 and 15 kips for Test #7) was applied to prevent liftoff of the column from the concrete pedestal. For both tests, lateral (shear) deformations were applied monotonically in one direction until failure. Subsequently, the loading was reversed and applied monotonically in the opposite direction until failure was achieved.

3.3.3 Instrumentation

Figure 3.14 illustrates the typical instrumentation layout for the base plate tests. In addition to the loads and displacements monitored by the four actuators themselves, instrumentation was installed on the specimens and loading frame to measure

displacements and strains. These instruments included position transducers attached to the base plate and concrete pedestal to measure base plate and concrete pedestal motion in three dimensions, thus enabling an accurate monitoring of the relative slip between the base plate, concrete pedestal and laboratory strong floor. Similarly, displacement transducers were installed to monitor unwanted out-of-plane motion of the test loading frame. Strain gages were attached to the testing rig to monitor deformations within the test setup. For Tests #4 and #5, two uniaxial strain gages were attached to the anchor rods (at two inches below the upper threads; about five inches below the surface of the concrete) to measure rod axial strain. Strain gages were also attached to the shear key for Test #6 (see Figure 3.11). For Tests #4 and #5, embeddable concrete strain gages were installed to monitor concrete strains near the anchor rods. Embeddable concrete strain gages were also installed, in the vicinity of the concrete failure region, for Test #6 and #7. Prior to and following testing, the geometry of the concrete pedestal for Test #6 was measured by a high definition laser scanner to generate three dimensional plots of the failure surface (see Figure B.14 in Appendix B).

3.4 LARGE SCALE TEST RESULTS

This section presents key observations from the base plate tests. In addition, the test results are analyzed and an evaluation of current design guidelines is given. Detailed experimental data is archived in Appendix B. A summary of results and a discussion of design implications are presented in Chapter 4. The discussion of the test observations is divided into three sections, each focusing on one specific shear transfer mechanism, i.e. surface friction, anchor rod bearing and shear key bearing.

3.4.1 Surface Friction

As discussed in the previous sections, Tests #1-3 involved the application of three compressive axial loads levels (43, 112, and 261 kips; with corresponding bearing stresses of about 64, 166, and 386 psi) between the base plate and grout interface. For each constant compressive load level, a lateral displacement-based load protocol (illustrated in Figure 3.13) was applied. Figure 3.15 shows the representative response of the friction tests (shown here for Test #3). This figure shows a large initial lateral

(frictional) force due to steel-grout bonding followed by a square shaped hysteretic response indicative of Coulomb friction behavior. Similar behavior is observed for all friction tests (refer Appendix B). Note that all slip occurs between the grout and the steel base plate, rather than the grout and the concrete pedestal.

Figure 3.16 shows the condition of the grout, base plate and shim stacks after Test #1. In addition to mild abrasion marks observed over the entire base plate, moderate scouring damage to the base plate was localized at the locations of the shim stacks. For Test #1, only two shim stacks exhibited significant scuffing damage, indicating that not all shims came into complete contact with the base plate during column erection. On the other hand, Test #2 showed approximately equal scuffing damage to all shims, suggesting that all were in complete contact with the base plate. Aside from mild spalling of the extreme perimeter of the grout pad, no damage to the grout (other than abrasion by the steel base plate) was observed for all surface friction tests. Moreover, for all friction tests, no damage to the concrete was observed, and the grout retained its bond to the concrete.

Figure 3.17 plots the frictional force versus cumulative slip of the base plate for Test #2 (similar graphs for the other friction tests are presented in Appendix B). The quantities are plotted over the entire duration of Test #2, illustrating the large jumps in frictional force when the normal (axial) load is changed. Figure 3.18 plots the corresponding frictional force normalized by the normal (axial) load (thus providing an effective coefficient of friction) for each friction test. As observed from Figure 3.18, the lateral resistance (i.e. the effective coefficient of friction), varies significantly during the duration of each normal load level. In addition, for each experiment (refer Appendix B and Figure 3.18), the initial force required to overcome the steel-grout bond resistance is significantly higher (approximately twice) than the frictional force remaining after the bond is broken. Thus, characterization of the coefficient of friction is somewhat subjective. Four key observations are made to develop a strategy to characterize the coefficient of friction in a consistent and conservative manner –

1. For all friction tests (Tests #1, #2 and #3), the initial resistance corresponding to steel-grout bond breakage is significantly higher than the frictional force following bond breakage. This bond resistance arises from chemical bonding (i.e. constitutive behavior) that is distinct from sliding friction resistance. Moreover, this bond resistance may not be available in field conditions where the bond could be broken during construction or over the life of the building due to overloads. Thus, shear resistance corresponding to the bond force is not considered in the characterization of the coefficient of friction because it may provide an unconservative and unrealistic estimate.

2. For both the experiments with shim stacks, i.e. Tests #1 and #2, the effective coefficient of friction follows a consistent pattern of evolution. After the initial bond breakage, the shear resistance remains relatively constant during the initial displacement cycles. Subsequently, the shear resistance increases, which may be attributed to the shim stacks gouging into the underside of the base plate (see Figure 3.16). As this mechanism occurs only after significant cumulative lateral slip, this increase in the friction coefficient may not be suitable for design. Accordingly, coefficient values corresponding to shim stack gouging are not considered in the analysis.

3. The minimum coefficient of friction values extracted from Tests #1 and #2 are shown in Figure 3.18a and Figure 3.18b, respectively. Following the observations discussed above, these values, which are considered in the determination of the friction coefficient (1) are the lowest frictional forces observed for each axial load level and (2) do not include the increased frictional resistance due to shim stack gouging nor steel-grout adhesion. For Test #2, an increase in resistance from steel shim gouging is evident during the first level (261 kips) of axial compressive loading. Thus, only one friction coefficient value is extracted from Test #2 (see Fig. 3.18b). For Test #1, two values can be extracted since the increase in frictional resistance is delayed until the second level (112 kips) of axial loading. This delay suggests that steel shim gouging

occurs at lower levels of cumulative slip for higher levels of compressive axial loading.

4. Figure 3.18c shows the values extracted from Test #3 for the determination of the friction coefficient. These values do not consider the initial larger force corresponding to bond breakage and include the lowest frictional force points observed for each of the three different gravity load levels. Since Test #3 does not feature shim stacks, a significant increase in frictional resistance due to steel shim gouging is not observed . Slight dips in the effective coefficient of friction observed subsequent each change in axial load level (as seen in Figure 3.18a-3.18c) occur during cyclic displacement amplitudes of 0.1" (recall Figure 3.13) under which the slip velocity is slower (4.2 x 10^{-3} inches/sec) than the rest of the loading (1.4 x 10^{-2} inches/sec). Thus, there is a possibility that frictional resistance is sensitive to slip velocity. Prior friction tests of non-metallic materials on steel (Fenz, 2002) show that frictional resistance decreases as the slip velocity tends to zero.

Figure 3.19 plots the frictional force values (extracted as described in the preceding discussion) versus the normal (axial) load values collected from the friction tests. These values are also listed in Table 3.6. Figure 3.19 also shows a linear regression line (with the intercept set to zero) for the data set from Test #1 and #2, from which the coefficient of friction is determined as 0.46 (for a base plate on a grout pad with shim stacks). A similar regression line for Test #3 results in a coefficient of 0.45 (for base plate on a pure grout pad). Both these regression lines have a high R^2 value (greater than 0.98) indicating a good fit and confirming the expected linear frictional response. Appendix B presents comprehensive data regarding the surface friction tests (i.e. Tests #1, #2 and #3). A review of this data indicates that the values presented in Figure 3.19 and Table 3.6 for the determination of the friction coefficient are the most conservative, whereas including additional data (i.e. considering shim stack gouging and steel-grout bond adhesion) shows significant deviation from the expected linear relationship for friction.

The AISC *Steel Design Guide 1* (Fisher & Kloiber, 2006) lists the coefficient of friction as 0.55 for steel on grout. This is adapted from ACI 349-85 which states, "*μ = 0.55 for grouted conditions with the contact plane between grout and as-rolled steel exterior to the concrete surface*". This value is based on a reported value of 0.53 from Cannon *et al.* (1975). Recent tests by Nagae *et al.* (2006), report a coefficient of friction value between steel and mortar as 0.52. The value determined by the current study (0.45) is lower than these previously reported values. A study investigating the coefficient of friction between a steel base plate and *concrete* (Cook & Klingner, 1991) reports an average coefficient of 0.43. It is important to note that the friction coefficient may be highly sensitive to the condition of the steel surface, as well as grout properties and construction procedures. For example, under the current study, the grout was allowed to cure for only about one week due to laboratory scheduling requirements. Moreover, the coefficient friction may be highly sensitive to the presence of mill scale on the steel base plate. A series of friction tests between steel and concrete by Baltay and Gjelsvik (1990) indicates that the coefficient of friction for a mill scale steel surface is less than that for a machined (i.e. polished) surface for bearing stress levels below 10,000 psi. The report describes that the mill scale is harder than the steel and is therefore not penetrated by the concrete/grout particles at lower bearing stress levels, resulting in a lower coefficient of friction. The conservative value $μ = 0.45$ for the coefficient of friction between a steel base plate with mill scale and grout pad (with or without steel shim stacks) is recommended based on experimental data from the current study.

3.4.2 Anchor Rod Bearing

Tests #4 and #5 investigate base plate shear resistance via four anchor rods under a combination of imposed axial tensile loads and shear/flexural loading. As described previously, the connection includes welded plate washers and grout between the base plate and concrete pedestal. The main difference between Tests #4 and #5 is the nominal anchor rod size; Test #4 features 3/4" diameter anchor rods while Test #5 features 1-1/4" diameter rods. All rods were ASTM F1554 Grade 55 ksi steel and were installed such that the rod threads ran below the surface of the concrete pedestal; i.e. the threads were included in the shear plane. Due to the threads, the minimum root diameter for the 3/4"

bolts was 0.64" and 1.10" for the 1-1/4" bolts. Table 3.5 indicates the tensile axial load applied to each anchor rod test. Compared to the measured strengths presented previously in Table 3.1, the applied axial tension load was approximately 31% of the ultimate load (of all four rods) for Test #4 and 39% for Test #5. The axial load was held constant and was followed by the application of cyclic lateral displacements (as described previously and illustrated in Figure 3.13).

Qualitatively, both anchor rod experiments (Tests #4 and #5) followed a similar progression of events. Visual inspection indicated that the application of tensile axial loading instantly broke the bond between the steel base plate and the grout pad. Figure 3.20 plots the vertical displacement (averaged from four locations on the base plate) versus the initial axial load for both tests. Under initial tensile axial loading, the base plate displaced vertically upward 0.035" for Test #4 and 0.07" for Test #5. As observed through anchor rod strain data, the axial load distribution during initial vertical loading was not uniform for all rods, especially for Test #4 (see Figure 3.21). However, no rods yielded during the initial base plate uplift. Subsequent to this, the axial loading produced no discernible indications of damage, except that the gap between the base plate and the grout pad increased as continuing lateral deformations were applied. Figure 3.22 plots the base plate vertical displacement (averaged from four locations on the base plate) during the course of the cyclic lateral loading (expressed as cumulative lateral displacement). Prior to failure, the base plate displaced vertically approximately 0.35" for Test #4 and 0.50" for Test #5, illustrating axial elongation of the anchor rods caused by the cyclic lateral displacement of the base plate under constant axial tension.

Figures 3.23 and 3.24 plot lateral load versus lateral base plate displacement for Tests #4 and #5, respectively. An analysis of these plots is provided in a later section. Both tests were concluded when one rod fractured during a cyclic displacement excursion (see Figure 3.25). For Test #4 (3/4" diameter rod), rod fracture occurred during the 4th amplitude of the 0.8" cycle and for Test #5 (1-1/4" diameter rod) during the 1st excursion of the 1.0" cycle. Table 3.7 summarizes the experimental results for both anchor rod tests, including the peak lateral load observed for each slip direction. In addition, Table 3.7 lists

29

predicted anchor rod strengths (to be discussed later). The fracture points are indicated on the load deformation curves in Figs. 3.23 and 3.24. Fig. 3.26 overlays a photograph of the fractured anchor rod from both tests with the locations of the base plate, plate washers, grout and concrete.

Inspections made after Test #4 (3/4" rods) reveals damage occurred to the grout pad in the form of localized spalling around the anchor rods. Furthermore, at two anchor rods locations, the grout cracked and completely separated from the concrete pedestal (see Figure 3.27a). However, no damage to the concrete pedestal was observed for Test #4. An anchor rod from Test #4 fractured at about 1/4" from the top of the concrete surface (i.e. within the grout pad − refer overlay schematic in Fig. 3.26a). Test #5 showed evidence of slight concrete damage (local spalling cones around the perimeter of each rod, generally 2" to 4" in diameter and 1" to 1.25" deep − see Fig. 3.27b) and extensive grout damage (see Fig. 3.27c). For Test #5, the anchor rod fractured within the concrete pedestal, about one inch below the surface of the undamaged concrete (refer overlay schematic in Fig. 3.26b). After the completion of Test #5, two of the anchor rods were excavated from the concrete and exhibited significant residual deformations up to about one inch below the surface of the damaged concrete (i.e. where the rod threads terminated). For both tests, damage to the grout was so extensive that pieces of the grout pad completely separated from the concrete pedestal. Cracking of the grout pad was observed during the 0.2" amplitude displacement cycle for both anchor rod tests. Note that the grout was installed up to the edge of the steel base plate such that the edge distance between the rods and grout pad was approximately five inches.

Referring to the load-deformation Figures 3.23 and 3.24, a complex hysteretic response, controlled by several phenomena, is observed. The following explanation of the response presented in this section is based on visual observations during testing, post-test inspection of the deformed anchor rods and damaged grout, as well as theoretical analyses of the anchor rods. Appendices C and D summarize the theoretical analyses of the anchor rod tests; Appendix C provides an examination of current design methods while Appendix D provides a detailed analysis incorporating geometric and material

nonlinearities. Several observations may be made from Figures 3.23 and 3.24, the observed response of the specimens and the associated analyses (Appendix D). These are now summarized –

1. The large initial lateral force observed in Test #4 (see Figure 3.23) is attributed to stubs of grout (approximately 0.75" tall) which were not completely removed from the four base plate anchor rod holes. The highly confined grout stubs constrained the movement of the anchor rods or the base plate, thus requiring a relatively high load to break. This highly brittle mode of failure (and its corresponding peak load) is neglected in the analysis since it corresponds to a certain construction procedure which can not be relied on in practice.

2. For the anchor rod tests, it is challenging to characterize a peak load since the rod response is controlled by several phenomena, including the yielding of the anchor rods in bending followed by an increase in strength due to second order geometric effects as the bolted end of the yielded rods displaces laterally, thereby resulting in a post-yield increase in lateral load. Figure 3.28 illustrates this effect, in which the axial force in the rods increase as they deform, resulting in increased lateral resistance of the base plate. In fact, the peak loads observed in the load-deformation plots (Figures 3.23 and 3.24) are an artifact of the loading history since they coincide with displacements of load reversal. Thus, it is not appropriate to consider only the observed peak load from the experiments in the development of predictive models and design approaches. However, the experiments provide important information regarding overall response of the anchor rod mechanism, which may be used to inform design considerations. Accordingly, Table 3.7 lists the peak lateral load observed for each slip direction.

3. For both anchor rod tests, the initial yielding and the post-yield hardening (due to geometric nonlinear behavior of the rods) are followed by strength as well as stiffness degradation at repeated cyclic displacement excursions (see Figures 3.23 and 3.24). This degradation may be attributed to damage of the grout in the

vicinity the rod under cyclic lateral loading (see Fig. 3.28 for a schematic). The damage to the grout progressively increases the effective bending length of the rod, resulting in lower strength and stiffness. In fact, the analysis presented in Appendix D indicates that this degradation in strength and stiffness can be simulated with a reasonable degree of accuracy through an assessment of an appropriate effective bending length.

4. At relatively large lateral base plate displacements, two phenomena occur. First, increased axial forces are developed in the anchor rods due to large lateral displacements of the bolted end of the rod. Figure 3.29 illustrates this effect by plotting the average axial rod strains versus slip for the first 0.8" amplitude displacement excursion. Second, the inside edge of the base plate hole impinges on some or all anchor rods (see Fig. 3.28 for a schematic), thereby resulting in a sudden decrease in the effective bending length of the anchor rod. This produces the stiffening observed in the specimen response (see Figs. 3.23 and 3.24). Although the observed stiffening behavior is consistent with tension stiffening (as would be observed from rod deformation due to large lateral base plate displacements), the analysis presented in Appendix D indicates that a similar sudden increase in tension stiffening would become dominant at deformations well in excess of those observed in the experiments. In addition, the unsymmetrical nature of the observed response (especially in Test #5; see Figure 3.24), as well as observations from fractured rods (see Figure 3.26) confirms that the observed stiffening behavior is attributed to the anchor rod bearing within the base plate hole, rather than within the plate washer (Figure 3.28 illustrates this effect).

5. Referring back to the load-deformation plots (i.e. Figures 3.23 and 3.24), reversal of loading produces a pinched hysteretic response as the effective lateral stiffness of the rods decreases as they approach their original (vertical) position and increases as they are deformed in the reverse direction. In addition, as discussed previously, the hysteretic behavior is marked by some strength degradation at

repeated lateral displacement amplitudes, likely attributed to damage of the grout surrounding the rods and/or accumulating plastic strain in the rods themselves.

6. Referring to the load-deformation plots (i.e. Figures 3.23 and 3.24), unsymmetrical response was observed for both tests. Asymmetry was especially evident in Test #5 (1-1/4" anchor rod), where the maximum base plate shear load in one direction was significantly higher (by 79%), as compared to the maximum shear load in the reverse direction. This unsymmetrical response may be attributed to the irregular placement of anchor rods within the holes Figures 3.31 and 3.32 illustrate the as-built anchor rod placement for Tests #4 and #5; note the extremely tight placement of two of the rods for Test #5. When the plate was pushed in the direction of minimum clearance between the rod and the edge of the anchor rod hole in the base plate, it made contact with the rod at low lateral plate displacements. As discussed previously, this caused a reduction in the bending length of the rod, resulting in stiffening behavior. Figure 3.30 illustrates this effect schematically. In the reverse direction, the larger clearance between the rod and edge of the hole delayed this response. In fact, a similar stiffening response is observed for Test #4 as well – however, due to the placement of the rods (and the extremely oversized holes), it is more symmetric as compared to the response observed in Test #5. Recall that the holes in the base plate were sized for the 1-1/4" diameter anchor rods; the smaller 3/4" rod had a greater hole clearance than typically prescribed. The effect of the base plate bearing on the anchor rod is demonstrated by a large kink in the rod at the location of the bottom of the base plate for Test #5 (see Figure 3.26b). A visual examination of the anchor rods after testing confirms that the bottom edge of the base plate made contact with at least two of the small rods (for Test #4) and all four of the large rods (for Test #5).

Appendix C provides the current method for characterizing the anchor rod mechanism capacity. A more exhaustive analysis of anchor rod response, including an explicit consideration of second order geometric effects, is provided in Appendix D.

Figures 3.33 and 3.34 re-introduce the load-deformation curves for Tests #4 and #5 introduced earlier, with a focus on examining the efficacy of various strength prediction approaches. As discussed earlier, it is inappropriate (as well as impractical) to accurately characterize the measured peak loads from the tests. Thus, instead of characterizing the strength prediction approaches in terms of conventional test-to-predicted strength ratios, the predicted strengths determined as per various approaches are overlaid on Figs. 3.33 and 3.34 (as well as listed in Table 3.7) for a qualitative assessment. Three methods are considered to estimate the predicted strengths; two methods consider the interaction of axial force, bending moment and shear in the anchor rods, whereas the third method considers the interaction only of axial force and shear. The three strength prediction methods are now briefly summarized –

1. *Method One – strength prediction considering axial force, shear and bending over a length equal to the thickness of base plate plus half the thickness of the welded plate washer:* This strength estimate $R^{PVM}_{measured,eliptical}$ [1] (See Figs. 3.33 and 3.34) reflects the interaction of axial, shear and flexure stresses in which the anchor rod is assumed to deform in double (reverse) curvature over a length corresponding to the distance between the top of the grout pad and the center of the welded plate washer (see schematic in Figure 3.28). A similar procedure is suggested by the AISC *Design Guide 1* (Fisher & Kloiber, 2006) using the shear/tension interaction equation (Eq. C-J3-5a) provided in the AISC Steel Construction Manual (AISC, 2005). A sample calculation using this approach is provided in Appendix C. In the current analysis, measured (rather than nominal) parameters are used for $R^{PVM}_{measured,eliptical}$. In addition, an elliptical stress interaction equation is used. For Test #4, $R^{PVM}_{measured,eliptical}$ is calculated as 10.8 kips, whereas it is calculated as 35.5 kips for Test #5. From Figures 3.33 and 3.34 these estimates of strength are lower than the observed strengths. However, two points are

---

[1] The subscript "elliptical" refers to the nature of the material interaction relationship used in the calculation. The subscript "measured" refers to a consideration of a tabulated rod net tensile area. Later discussion, including Appendix C, outlines an alternate trilinear material interaction relationship as well as a consideration of a nominal unthreaded rod area measurement.

relevant in this regard. First, as described previously, the high initial strength observed for Test #4 may be attributed to the presence of grout in the plate holes. Once this grout is damaged, $R^{PVM}_{measured,eliptical}$ provides a reasonably conservative estimate of the strength of the rods. For Test #5, it is especially informative to consider the negative quadrant of data, which is not affected by the base plate bearing on the anchor rod. Even in this case, $R^{PVM}_{measured,eliptical}$ provides a reasonable and conservative approximation of the strength, not considering the stiffening due to geometric nonlinearities discussed earlier.

2. *Method Two – strength prediction considering axial force, shear and bending over a length equal to the thickness of grout and base plate plus half the thickness of the welded plate washer:* The second approach is similar to the first one, except that the assumed effective bending length equals the sum of the thickness of the base plate, half the thickness of the plate washer, as well as the thickness of the grout pad. The strength calculated as per this approach (overlaid on Figures 3.33 and 3.34) is denoted as $R^{PVM*}_{measured,eliptical}$ (calculated as 6.84 kips for Test #4 and 25.0 kips for Test #5 – see Appendix C for a detailed calculation). As expected, with the increased bending length, the strength estimates are lower (33% on average) than those predicted by Method One. Consequently, this estimate of strength is highly conservative with respect to the experimental data and reflects the observed response only at high levels of base plate slip (approximately greater than 0.2") after substantial strength degradation has occurred. This is not entirely unexpected, given that the strength degradation is associated with grout damage, and the progressive increase of anchor rod bending length.

3. *Method Three – strength prediction considering only axial force and shear:* This estimate of strength $R^{PV}_{measued,eliptical}$ (which equals 71.1 kips for Test #4 and 158 kips for Test #5) disregards anchor rod bending, but instead considers only the interaction between axial force and shear (see Appendix C for a detailed calculation). In addition to these estimated strengths, it is evident from Figures

3.33 and 3.34 that Method Three results in the highest estimates of strength. In fact, $R^{PV}_{measued,eliptical}$ predicts the peak strength in both anchor rod tests with a higher degree of accuracy, as compared to Methods One and Two. However, a closer inspection reveals that $R^{PV}_{measued,eliptical}$ may provide unreliable (and unconservative) estimates of shear strength in the base plate connection, since the observed increase in strength due second order geometric effects requires an assumed displacement, which may be difficult to quantify for design. Moreover, if designed for this strength, the anchor rods may undergo large cyclic inelastic deformation, possibly resulting in fatigue failure.

Based on the above observations, it is evident that bending of the anchor rods should be considered in the strength determination for shear transfer in a grouted base plate with a welded plate washer and oversized anchor rod hole detail. A post-test visual inspection of the anchor rods confirms reversed curvature bending behavior (see Fig. 3.25). Three other factors may increase the strength of the anchor rod connection, including (1) large displacements causing the base plate (rather than the welded plate washers) to come into contact with the anchor rods, resulting in a reduction of the bending length, (2) irregular placement of the anchor rods, resulting in constrained bending and (3) geometric nonlinear effects which develops increased tension forces in the deformed anchor rod. Fortunately, these three effects result in strength capacities which are higher than capacities based on current design guidelines that consider rod bending. However, the increased strength associated with these alternate mechanisms depends on factors that may not be possible to prescribe during design and construction. Thus, based on the experiments conducted in this study, it is recommended that flexure, as well as axial and shear stresses, be considered when characterizing the strength of the anchor rods in bearing. However, incorporating flexural response requires the consideration of an appropriate bending length. The current approach prescribed in the AISC design guide (i.e. assuming the bending length equal to the thickness of the base plate plus half the thickness of the welded washer) provides the most reasonable strength estimate for design. Although some inelastic deformations are associated with this force level, they are relatively small.

The other alternative bending length considered, (i.e. assuming the bending length equal to the base plate and grout thickness, plus half the thickness of the plate washer), provides a somewhat conservative strength prediction. While the strength determined based on this increased length reflects response at larger displacements (subsequent to strength degradation), it does not reflect initial response. Thus, this alternative bending length may be more appropriate under situations of base plate cyclic deformations.

As outlined in Appendix C, all the strength estimates discussed above are based on the interaction equation presented below between shear and tensile stress –

$$\left(\frac{f_t}{F_{nt}}\right)^2 + \left(\frac{f_v}{F_{nv}}\right)^2 = 1 \tag{3.1}$$

Where: F_{nt} = ultimate tensile capacity of rod

f_t = tensile stress in rod (from flexure and tensile loads)

F_{nv} = ultimate shear capacity of rod

f_v = shear stress in rod

It is relevant to note, in addition to the interaction equation presented above, the AISC Steel Construction Manual presents a trilinear interaction equation (Equation [C-J3-6a] in the Commentary) as an alternative to Equation [3.1]. This trilinear approach is presented in Appendix C. In addition, the AISC *Steel Design Guide 1* assumes the anchor tensile stress area to be of 75% the nominal (unthreaded) rod area. However, the net tensile area of the rod may be more accurately characterized by the number of threads per inch and the measured unthreaded diameter (e.g. see Table 7-18 in the 2005 AISC Manual). The results presented in Figures 3.33 and 3.34 (and Table 3.7) are based on this more accurate (i.e. measured) net tensile area of the anchor rod. The use of the alternate (trilinear) interaction equation and the nominal dimensions will, in general, produce slight deviations from the predictions presented in this study. While these deviations depend on

specific rod size and configuration, for the tests presented in this study, these alternate capacity predictions produced strength estimates that were similar (within approximately 10%) as compared to the predictions presented in this chapter (i.e. using a measured diameter and an elliptical stress interaction equation; see Appendix C for details).

The proposed strength prediction method detailed above is significantly conservative as compared to test observations. The analysis presented in Appendix D indicates that if geometric nonlinearities are included, strength estimates more consistent with observed response may be obtained. However, since the force obtained from this analysis is a function of displacement (being a direct consequence of geometric nonlinearities), it is difficult to consider it for design, especially for stiff mechanisms, where the deformation demands cannot be appropriately characterized.

It is relevant to note that, under certain situations, the base plate connection will develop additional resistance from friction that would develop from clamping action which arises when the base plate displaces laterally leading to increased tension forces in the rods. Recall that for the current study, the base plate completely uplifted from the grout pad for the entire lateral loading protocol. Thus, clamping action of the base plate is beyond the scope of this report. The reader is referred to Gresnigt *et al.* (2008) for an analysis that also includes clamping action of the base plate.

3.4.3 Shear Key Bearing

Referring to the test matrix presented in Table 3.4, Tests #6 and #7 feature a concrete block with a pocket (see Fig. 3.1), into which a shear key (a built-up I-beam stub; see Fig. 3.10) was inserted. These tests investigate the failure modes and capacities associated with the shear key bearing mechanism. As outlined in the Chapter 2 and in the AISC *Steel Design Guide 1* (Fisher & Kloiber, 2006), shear key failure may be associated with several failure modes, including concrete/grout bearing failure, shear blowout edge failure of the concrete foundation or failure of the shear key itself, either through yielding or through fracture of the welds which connect the shear key to the base plate. Additionally, the shear key may induce flexural yielding failure in the base plate. In the

present study, the main focus is on the shear blowout edge failure of the concrete foundation. As explained earlier, the predicted failure region of the concrete pedestal used to represent the foundation did not contain rebar nor any other obstructions (with the exception of the anchor rods) to enable characterization of the strength capacity associated with concrete alone (i.e. not including the effect of steel reinforcement). For both tests, the shear key was installed in the center of the concrete block such that an edge distance of 20.25" was provided between the shear key bearing surface and the pedestal perimeter (see Fig. 3.35). Two shear key embedment lengths (measured from below the surface of the concrete) were tested: 5.5" for Test #6 and 3.0" for Test #7. The shear key was 6" wide for both tests, thus providing a 33 square inch bearing surface for Test #6 and 18 square inches for Test #7. A small amount of axial tension force was applied to the column during both tests to reduce the self weight of the test setup. However, since the axial loading was applied in load control, some compressive axial load was maintained during each of the tests (up to 27 kips for all tests; see Table 3.5 and Appendix B for details). This relatively small compressive load in the column ensured that the base plate did not completely lift off the concrete pedestal during testing. As a result, a small amount of resistive frictional force was present, and a corresponding correction is applied before analysis of the measured shear key strengths.

Under a relatively small axial compressive load, both shear key experiments (Tests #6 and #7) involved the application of lateral (i.e. shear) monotonic loading to failure. Representative load-deformation plots are shown in Figure 3.36 and key results, such as observed peak load values, are listed in Table 3.8. Referring to Figure 3.36, load-deformation plots are shown for the positive and negative loading directions. Data collected for the reversed loading direction is assumed to reflect undamaged initial conditions since the concrete behind the shear key's initial loading direction remained virtually undamaged. Thus, while the second (i.e. "negative") load-deformation plot corresponds to a damaged concrete pedestal, the peak load values (as well as the load-deformation plot itself) are not substantially different as compared to the load-deformation plot for the "undamaged" condition of the concrete pedestal (average peak load difference = 5%).

Figure 3.37 shows photographs and schematics illustrating the typical evolution of damage as lateral loading progressed for both Test #6 and #7. Two distinct load drops are observed. The first load drop (about 20-40% of the peak load) corresponds to the formation of a long vertical crack running down the center of the concrete pedestal (see Figure 3.37a). At this point, cracks were also observed on the grout pad underneath the base plate. This center crack on side of the concrete pedestal increased in width and length as the lateral resistance continued to increase (see Figure 3.37b). This failure mode is similar to flexural response in concrete beams (MacGregor & Wight, 2004), where flexure cracks perpendicular to the beam axis form before inclined shear cracking leads to ultimate failure. The absence of steel reinforcement in the failure region precludes analysis by the strut-and-tie method.

After the initial load drop, the load steadily continued to increase until a second (and final) peak in load was observed, accompanied by diagonal cracks on both sides of the pedestal about 30 degrees perpendicular to the loading direction (see Figure 3.37c). This type of cracking is consistent with shear blowout failure reported in the literature on concrete design (e.g. MacGregor & Wight, 2004). The post-test condition of the pedestal of Test #6 is shown in Figure 3.38. Figure 3.39 shows the failure surface of the concrete pedestal from Test #6 and Test #7 (which was extracted manually after testing). Appendix B includes a contour plot (generated by three dimensional laser scanning) and pictures of the concrete failure surfaces for all shear key tests. The steel shear key itself did not show any signs of damage. In fact, strain data recorded by strain gages on the shear key (see Fig. 3.11) did not indicate any yielding. The anchor rods, which were embedded within the failure region, showed permanent deformation in the direction of loading indicating that they might have contributed to the strength of the failure mechanism. No concrete or grout bearing damage was observed in the region directly in front of the shear key's load path. Note that the final peak load values occur at relatively small lateral displacements (approximately less than 0.2" for all shear key tests), indicating the high stiffness of the failure mode associated with this type of detail.

Table 3.8 summarizes key experimental results from the shear key tests including the two peak lateral loads corresponding to the first ($V_{peak}^{initial}$) and the second ($V_{peak}^{ultimate}$) force drops in each test. These peak load values are illustrated in the load-deformation plots of Figure 3.36. Referring to Table 3.8, $V_{peak}^{effective}$ represents the peak load observed during the second (i.e. ultimate) failure mode minus the friction force. This friction force is determined from the axial load at the time of the second failure mode (see Table 3.8) using a coefficient of friction determined in Section 3.4.1 for a steel-grout interface ($\mu = 0.45$). In addition to the observed peak load values, Table 3.8 also includes predicted strengths for the shear key bearing tests. Two methods are considered to estimate the strength corresponding to the observed blowout failure mode of the concrete. One of these methods, commonly referred to as the 45 degree cone method, is prescribed by ACI-349 (2006) for the concrete shear capacity of embedded shear lugs and is featured in the AISC *Design Guide 1* (Fisher & Kloiber 2006). As per an adaptation of this method, the strength capacity corresponding to shear blowout is determined as follows –

$$V_n^{45} = \left(4\sqrt{f_c'}\right) A_{45}, \quad lb \qquad [3.2]$$

Where: f_c' = concrete compressive strength, psi

A_{45} = effective stress area based on a 45 degree projected plane, inches^2 (see

Figure 3.40a)

The 45 degree cone method assumes a uniform tensile stress of $4\sqrt{f_c'}$ acting on an effective stress area defined by projecting a 45 degree plane (note - not a cone surface) from the bearing edges of the shear lug to the concrete free surface. The bearing area of the shear lug is excluded from this projected area. Figure 3.40a illustrates the projected area used for this method, while Appendix E provides detailed calculations determining this area.

The second estimate of strength V_n^{CCD} is based on the concrete capacity design (CCD) method which has been adapted by ACI-349 (2006) for anchorages in concrete under tension or shear loading. As per this method, the strength is calculated as –

$$V_n^{CCD} = \frac{1}{\sqrt{c}}\left(\frac{40}{9}\sqrt{f_c'}\right)A_{35}, \quad lb \qquad [3.3]$$

Where: c = free edge distance from the shear key, inches

f_c' = concrete compressive strength, psi

A_{35} = effective area based on a 35 degree projected plane, inches^2 (see Figure 3.40b)

The CCD method assumes an effective area defined by projecting a 35 degree plane from the bearing edges of the shear lug to the free surface, excluding the bearing area of the shear lug. A detailed derivation of Equation [3.3], indicating its adaptation from the CCD method proposed originally by Fuchs *et al.* (1995), is presented in Appendix E. Referring to Equations [3.2] and [3.3] above, the main difference between the two strength equations is associated with the size-effect in concrete derived from fracture mechanics theory (Bažant, 1984). Equation [3.2] predicts that the strength associated with concrete blowout is directly proportional to the projected effective stress area. While this is often true for smaller specimens, where the specimen dimension is approximately 10-20 times the aggregate size (Bažant, 1984), failure in larger specimens is typically governed by fracture mechanics, since the initiation of cracking in the concrete, rather than the development of a uniform stress over a failure surface, controls the strength associated with blowout. Similar analogies may be found in other structural components, for example in steel, wherein some situations and details with a sharp crack do not achieve their full strength as would be predicted through an ultimate strength approach that considers only yielding. Research by Bažant (1984) and others (Fuchs *et al.*, 1995) has shown that this size effect may be successfully incorporated by expressing the "nominal" failure stress as a function of the specimen size (conveniently characterized by the

embedment free edge distance c), i.e. $\sigma_{failure} = f(1/\sqrt{c}, \sqrt{f'_c})$. Thus, for larger specimens, the failure stress is smaller as compared to that for relatively smaller specimens. As per the CCD method, the projected area for determination of the nominal stress is based on a 35 degree projection as illustrated in Figure 3.40b. The reader is referred to Fuchs *et al.* (1995) for more details regarding the CCD method.

Along with the experimental data outlined earlier, Table 3.8 includes predicted strength capacities and test-to-predicted load ratios based on the two estimates described above. In the context of the above discussion, a review of Table 3.8 and Figs. 3.36-3.39 reveals several points that are relevant to the strength characterization due to shear key bearing and concrete blowout failure –

1. Referring to the representative shear load versus base plate slip response (Figure 3.36) and the failure progression photographs (Figure 3.37), the two load peaks are associated with distinct failure modes; (1) flexural splitting of the free edge followed by (2) side blowout. For the positive loading direction (i.e. loading on the undamaged pedestal), the second failure mode corresponds to the largest capacity for both tests. Although the initial flexural splitting failure mode corresponds to a drop in load, ultimate failure corresponds to concrete blowout in a shear mode. Thus, the loads corresponding to this event, corrected for friction (i.e. $V_{peak}^{effective}$), are included in the analysis of the results and in further discussion.

2. An inspection of the test-to-predicted ratios $V_{peak}^{effective} / V_n^{45}$ (mean = 0.51; COV = 0.14) indicates that the 45 degree cone method (currently proposed by the AISC *Design Guide 1*) may be unconservative for large edge distances (i.e. large concrete foundations) due to the size effect discussed in the preceding discussion.

3. The test-to-predicted ratios determined with respect to the CCD method indicate the inclusion of the concrete size effect in the analysis provides more accurate estimates of strength (mean $V_{peak}^{effective} / V_n^{CCD} = 1.07$; COV = 0.19).

4. A slight bias is observed such that both the 45 degree cone method as well as the CCD method gives higher strength predictions for the deeper 5.5" shear key (mean $V_{peak}^{effective} / V_n^{CCD} = 1.22$; mean $V_{peak}^{effective} / V_n^{45} = 0.55$) as compared to the 3.0" deep shear key (mean $V_{peak}^{effective} / V_n^{CCD} = 0.92$; mean $V_{peak}^{effective} / V_n^{45} = 0.46$). Due to the geometry of the concrete pedestal, the effective stress area A_{35} is nearly identical for the two shear key lengths (less than 1% difference), while the area A_{45} differs by about 10% for the two shear key embedment lengths. This suggests that the longer shear key is stronger on a unit basis, as compared to the shorter one. This may be attributed to the larger local bearing stresses associated with the smaller shear key embedment length. As evidenced in numerical studies (e.g. Ožbolt *et al.*, 2007), this higher bearing stress increases the likelihood of early crack initiation and failure.

5. For both tests, the angle of the failure surface in plan view (i.e. the top of the pedestal) is approximately 30 degrees perpendicular to the load (e.g. see Figs. 3.37 and 3.38). In elevation view (i.e. the side of the pedestal), the angle of the failure surface is between 40-60 degrees to the load (e.g. see Figure 3.39). Thus, the overall failure surface area is within the range predicted by the 45 degree cone method and the CCD method.

Based on the above observations, the CCD method provides a relatively accurate estimate of strength for embedments with large free edge clear distances (i.e. large concrete foundations), where the strength is controlled by fracture initiation. Although not tested as part of this study, it is anticipated that for small edge distances, where the strength is governed by development of the concrete tensile strength over the failure area, the CCD method might provide unconservative results. Thus, it is recommended that the reliable strength of concrete blowout due to shear key bearing be calculated as the minimum of the two estimates, such that for smaller edge distances, the 45 degree cone method will govern, while for larger edge distances, the CCD method will govern –

$$\phi V_n = \min\left\{ \phi_{CCD} \frac{1}{\sqrt{c}} \left(\frac{40}{9} \sqrt{f_c'} \right) A_{35}, \phi_{45} \left(4\sqrt{f_c'} \right) A_{45} \right\}$$

[3.4]

Where: ϕ_{CCD} = strength reduction factor of the CCD method = 0.75 (ACI 349, 2006)

ϕ_{45} = strength reduction factor of the 45 degree cone method = 0.85 (ACI 349, 2006)

The two functions in Equation [3.4], along with the observed effective peak loads, are plotted in Figure 3.41 for clarity. Referring to this equation, two important observations are presented. First, the effective stress areas calculated as per the two methods are based on different geometries, i.e. one is based on a 45 degree angle, whereas the other (i.e. the CCD method) is based on a 35 degree angle (see Figure 3.40). The area calculated for the 45 degree cone method is based on physical interpretation, since this method assumes that the concrete tensile strength is activated over this area. On the other hand, the expression for the CCD method is based on fracture mechanics, i.e. all of the projected area is not simultaneously engaged. In fact, in situations where the CCD method governs, failure occurs due to the initiation of cracking over a small region in the vicinity of the shear key. Once crack initiation occurs, the load drops steadily as the shear cracks grow and the failure region expands. Thus, the area A_{35} in Equation [3.3] above does not bear any physical significance in the context of the final failure surface, but rather may be interpreted as a basis for the characterization of the nominal stress required to produce fracture. As for the second observation, assuming that the projected areas can be calculated based only on the edge distance c (i.e. the dimension of the shear key is small as compared to the concrete foundation and the foundation is large enough to capture the entire projected area), Equation [3.4] above indicates that the CCD method will govern for edge distances greater than approximately 6 inches (i.e. 5-10 times the aggregate size, which is in approximate agreement with the fracture mechanics theory proposed by Bažant [1984]).

The size effect in concrete is diminished in the presence of steel reinforcement which increases the ductility of the concrete pedestal, thereby providing the opportunity for the

redistribution of stresses over a larger volume of material. However, the beneficial effect of reinforcement is difficult to quantify in the absence of additional testing.

In some cases, the shear key may be positioned close to a corner, or the foundation may not be deep enough to develop the full projected effective area (i.e. A_{45} or A_{35}). Appendix E outlines methods and provides schematics for calculating these areas in the presence of these boundary effects.

Table 3.1 – Summary of anchor rod tension tests

Nominal unthreaded diameter (inches)	$F_{y,rod}$[1] (ksi)	$F_{u,rod}$[2] (ksi)	E[3] (ksi)
3/4	66.8	96.4	32,000
1-1/4	54.4	75.0	31,100

[1]Measured yield stress, based on 0.2% offset method
[2]Measured ultimate strength
[3]Measured Young's modulus

Table 3.2 – Summary of concrete compression tests

Concrete pedestal specimen[1]	Corresponding base plate test number	Delivery truck	Concrete density (lbs/ft^3)	Average 28-day compressive strength (psi)	Standard deviation of compressive strength (psi)
A	1,2,3,4	A	146	4,570	290
B	5	A	146	4,760	60
C	6	A	145	4,650	320
D	7	B	145	5,030	90

[1] Three 6"-by-12" test cylinders were collected for each concrete pedestal specimens

Table 3.3 – Summary of grout compression tests

Corresponding base plate test number[1]	Water content (gallons per 50 pounds of grout)	Curing time (days)	Grout density (lbs/ft^3)	Average compressive strength (psi)	Standard deviation of compressive strength (psi)
1	1	9	128	5,780	1,050
2	1	13	127	7,070	760
3	1	7	128	6,230	390
4	7/8	4.5	130	6,130	1,100
5	7/8	7	131	7,210	970
6	1-1/8	9	126	6,030	850
7	1-1/8	7	127	5,800	1,050

[1] Four 3"-by-6" test cylinders were collected from the grout for each base plate test

Table 3.4 – Base plate test matrix

Test #	Mechanism investigated	Test detail	Loading description
1	Surface friction	Shim stacks plus grout	Cyclic shear with various levels of constant axial compression
2			
3		Grout only	
4	Anchor rod bearing	3/4" diameter anchor rods with welded plate washers	Cyclic shear with constant axial tension
5		1-1/4" diameter anchor rods with welded plate washers	
6	Shear key bearing	6" bearing width with 5.5" embedment depth	Monotonic shear with small compressive axial load
7		6" bearing width with 3.0" embedment depth	

Table 3.5 – Base plate test loading details

Test #	Loading iteration	Axial load (kips)	Axial loading type	Lateral (shear) loading
1	1	43	Constant compression	Cyclic displacement (see Figure 3.13)
1	2	112		
1	3	261		
2	1	261		
2	2	112		
2	3	43		
3	1	261		
3	2	112		
3	3	43		
4	1	40	Constant tension	Cyclic displacement to failure (see Figure 3.13)
5	1	108		
6	1	0 to 10	Small compression	Monotonic push to failure
6	2	17 to 27		Monotonic push in opposite direction to failure
7	1	15		Monotonic push to failure
7	2	15		Monotonic push in opposite direction to failure

Table 3.6 – Base plate surface friction test results

Grout detail	Corresponding test number	Axial compression (kips)	Shear force (kips)	Coefficient of friction
With shim stacks	1	43.0	17.51	0.41
With shim stacks	2	112	44.51	0.40
With shim stacks	2	261	125	0.48
No shim stacks	3	43.0	16.5	0.38
No shim stacks	3	112	50.0	0.45
No shim stacks	3	261	119	0.46

Table 3.7 – Anchor rod bearing test results

Test Number	4	5
Nominal unthreaded rod diameter (inches)	0.75	1.25
Measured threaded rod diameter (inches)	0.64	1.10
Measured rod ultimate strength (ksi)	96.4	75.0
Plate washer thickness (inches)	0.25	0.50
Base plate thickness (inches)	2.00	2.00
Average grout height (inches)	1.25	1.00
Imposed tensile axial load (kips)	39.6	108
R_{peak} (kips)[1]	30.2	126
$R_{peak}^{reverse}$ (kips)[2]	28.2	70.4
$R_{measured,eliptical}^{PVM}$ (kips)[3]	10.8	35.5
$R_{measured,eliptical}^{PVM*}$ (kips)[4]	6.84	25.0
$R_{measued,eliptical}^{PV}$ (kips)[5]	71.1	158

[1]Observed peak load

[2]Observed peak load in opposite slip direction

[3]Predicted capacity assuming rod tension, shear and flexure and a bending length equal to the base plate thickness plus half the plate washer thickness

[4]Predicted capacity assuming rod tension, shear and flexure and a bending length equal to the base plate thickness, grout thickness plus half the plate washer thickness

[5]Predicted capacity assuming rod tension and shear

Table 3.8 – Shear key bearing test results

Test Number	6		7	
[1]Shear key embedment length (inches)	5.5		3.0	
Loading direction	positive	negative	positive	negative
[2]Axial load (kips)	2.0	28.5	15.4	15.4
Frictional resistance (kips)	0.9	12.8	6.9	6.9
[3]$V_{peak}^{initial}$ (kips)	186	185	141	135
[4]$V_{peak}^{ultimate}$ (kips)	194	172	149	143
[5]$V_{peak}^{effective}$ (kips)	193	159	142	136
[6]V_{n}^{45} (kips)	318	318	302	302
$V_{peak}^{effective} \big/ V_{n}^{45}$	0.61	0.50	0.47	0.45
[7]V_{n}^{CCD} (kips)	144	144	151	151
$V_{peak}^{effective} \big/ V_{n}^{CCD}$	1.34	1.10	0.94	0.90

[1]Shear key width = 6"; edge distance = 20.25"
[2]Axial load at final (ultimate) peak lateral load
[3]Observed initial peak load
[4]Observed second (ultimate) peak load
[5]Observed ultimate peak load adjusted for frictional resistance
[6]Predicted capacity using 45 degree cone method
[7]Predicted capacity CCD method
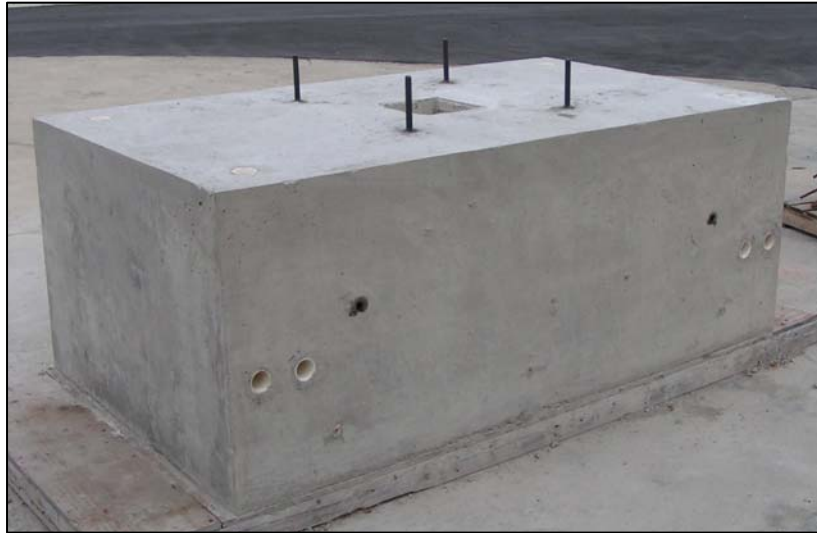
Figure 3.1 – Concrete pedestal with anchor rods and shear key pocket
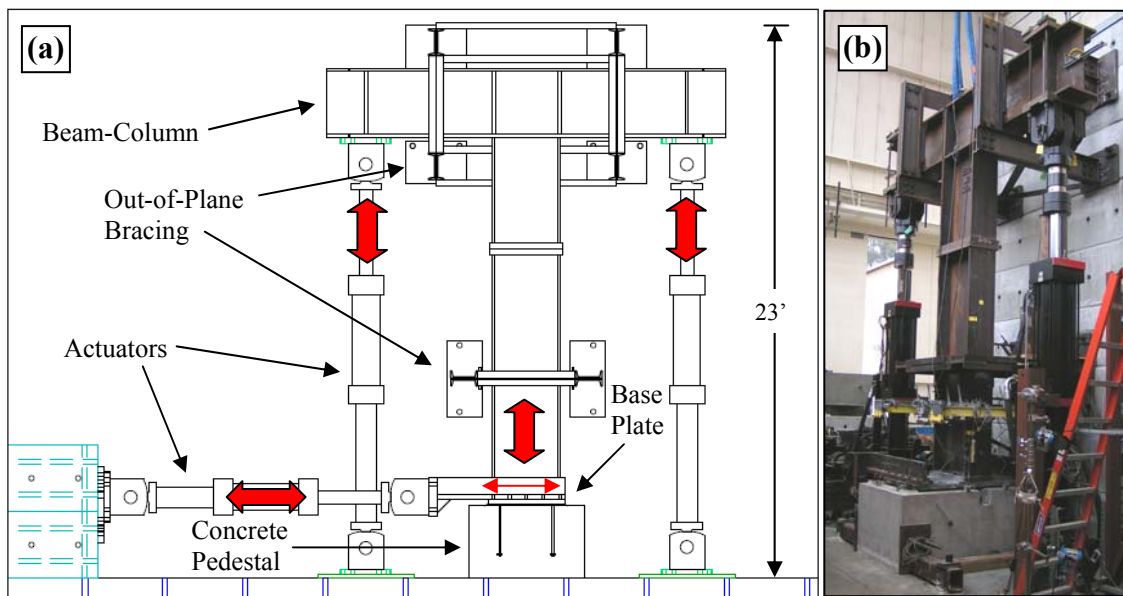
Figure 3.2 – Base plate shear test setup (a) schematic (to scale; rear reaction wall omitted for clarity) and (b) photograph
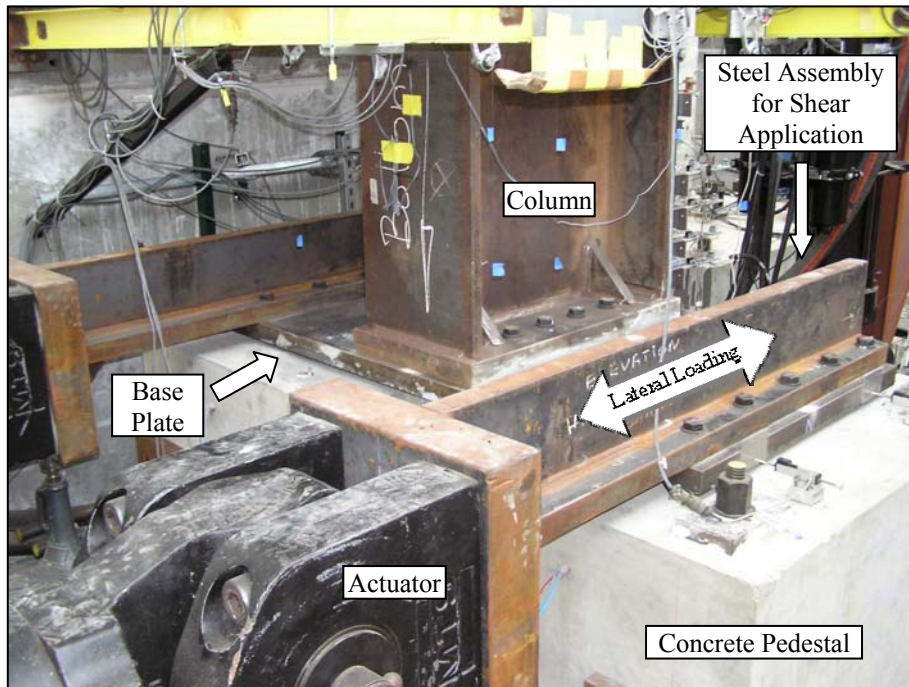
Figure 3.3 – Steel shear loading assembly for base plate tests

Figure 3.4 – Steel shim stacks used for friction Tests #1 and #2
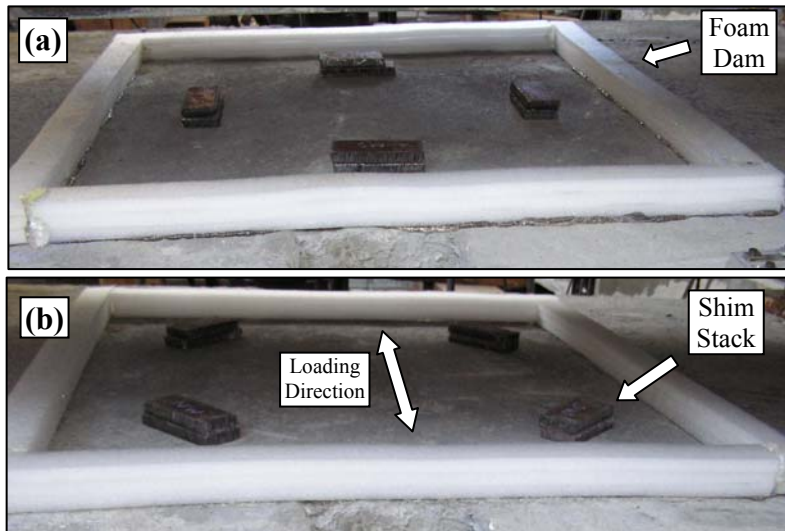
Figure 3.5 – Shim stack positioning for (a) Test #1 and (b) Test #2
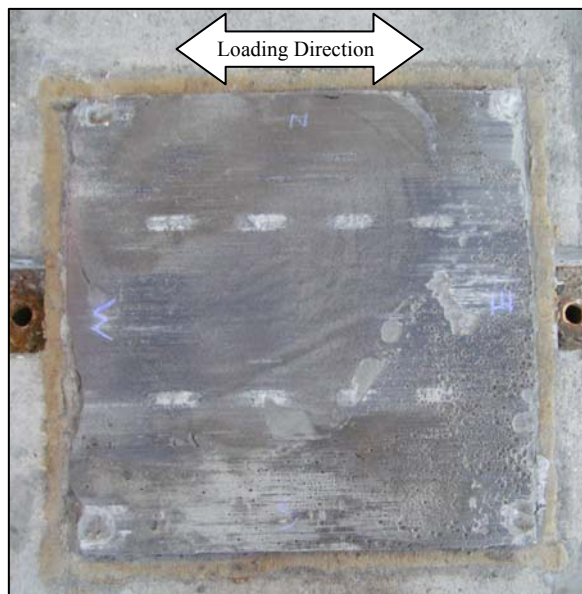
Figure 3.6 – Post-test photograph of grout pad for Test #3
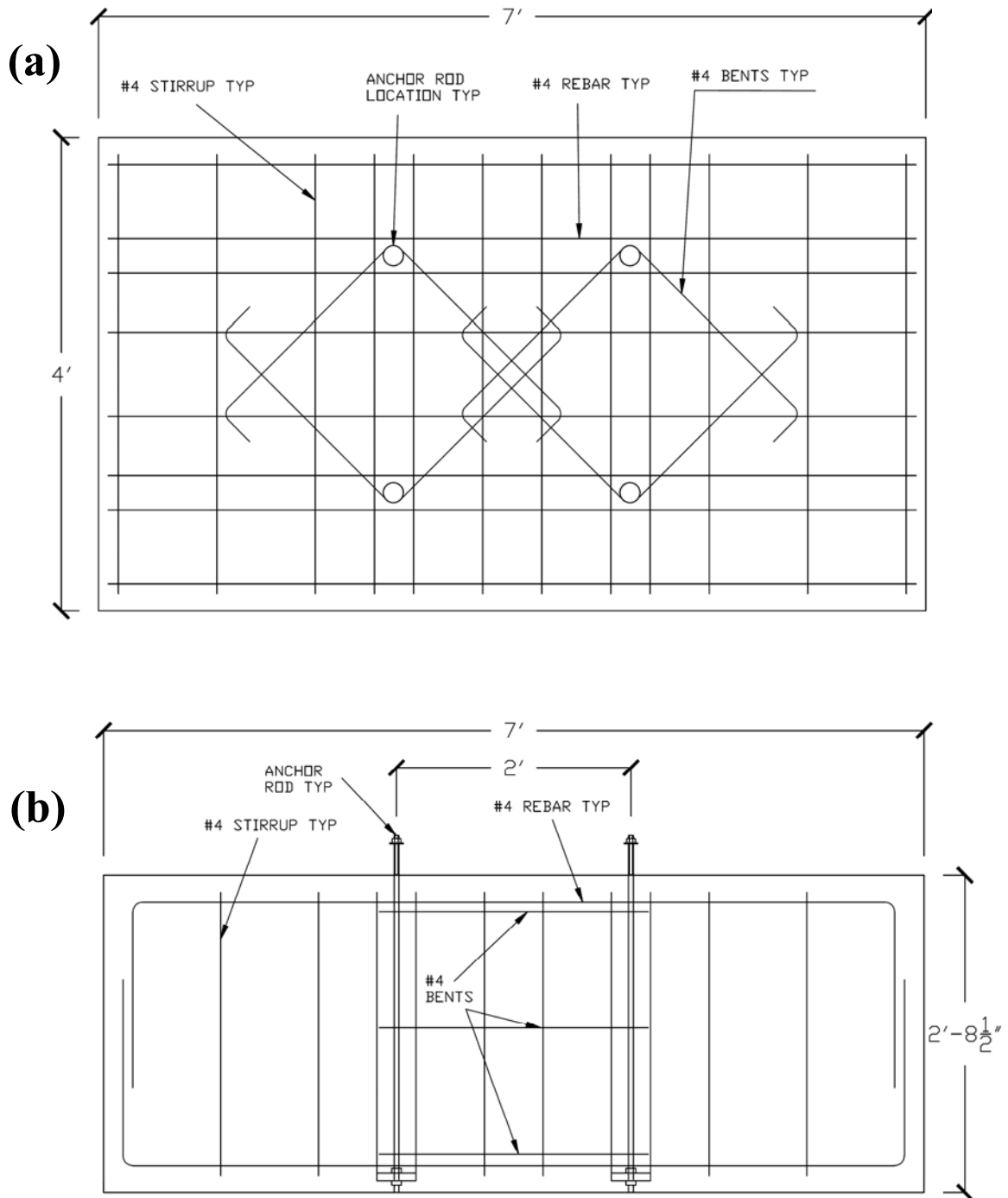
Figure 3.7 – Schematic (a) plan view and (b) elevation view of reinforcing bar details used in the concrete pedestals for the anchor rod tests #4 and #5
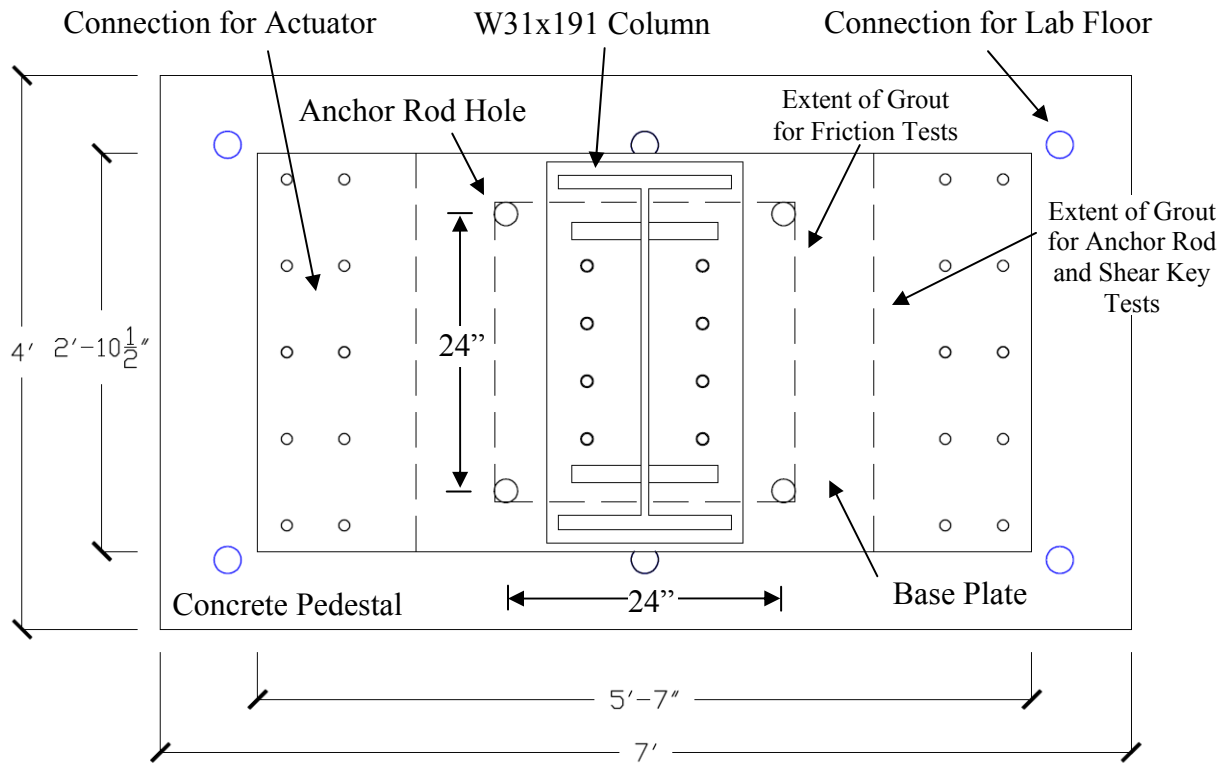
Figure 3.8 – Schematic plan view of base plate specimen (to scale)

Figure 3.9 – Welded plate washer detail (shown here for Test #5)
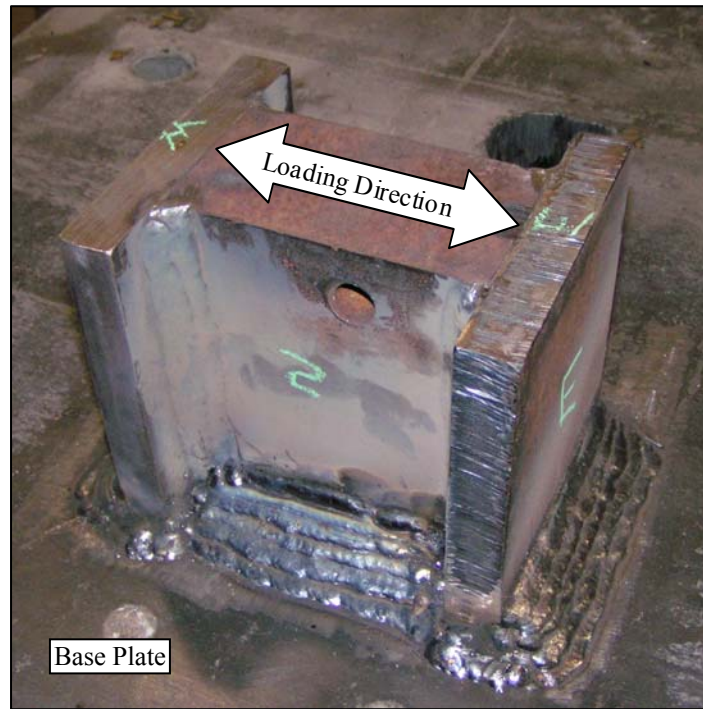
Figure 3.10 – Welded shear key (shown here for Test #6)
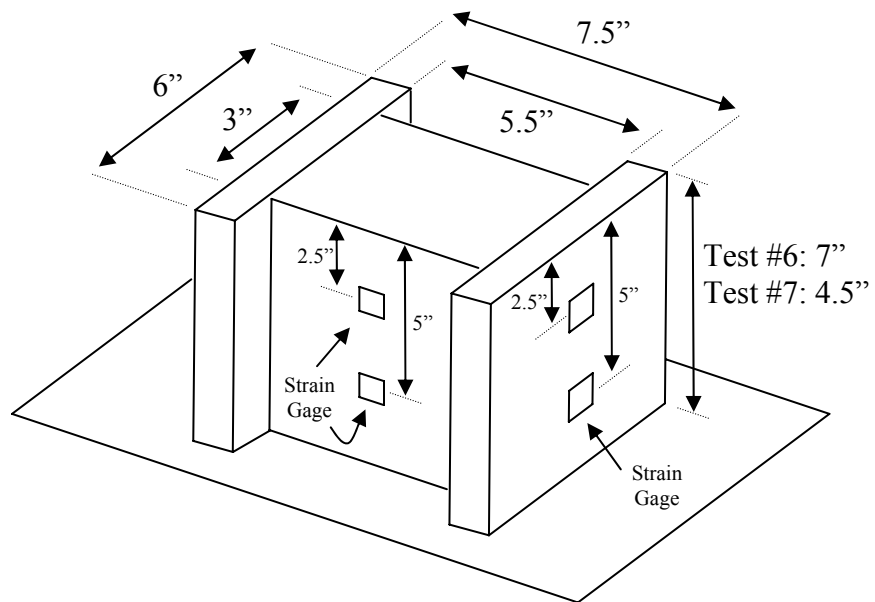
Figure 3.11 – Schematic detail of shear key geometry

(a)

(b)
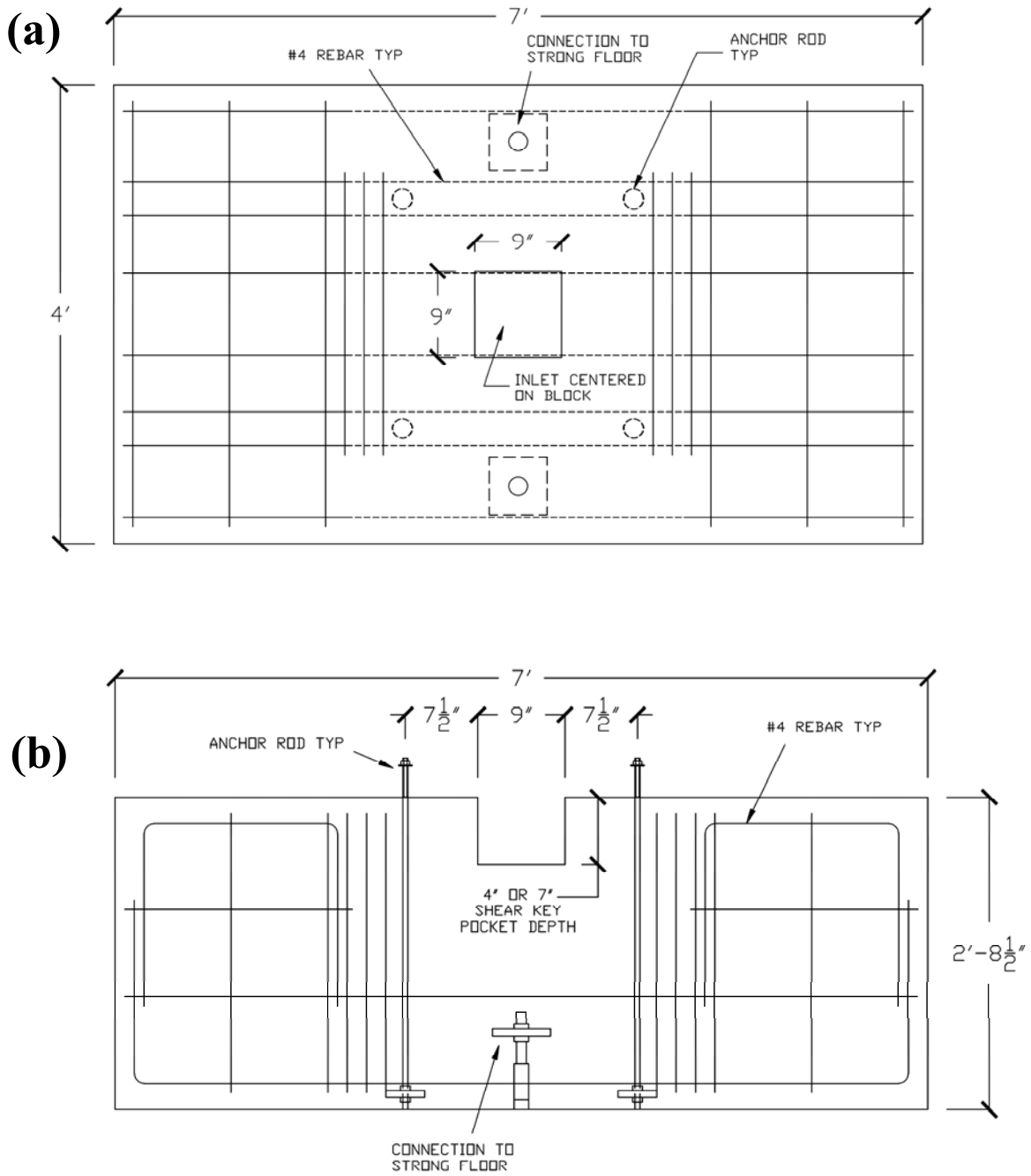
Figure 3.12 – Schematic (a) plan view and (b) elevation view illustrating rebar details in the concrete pedestals for the shear key tests (Test #6 and #7)
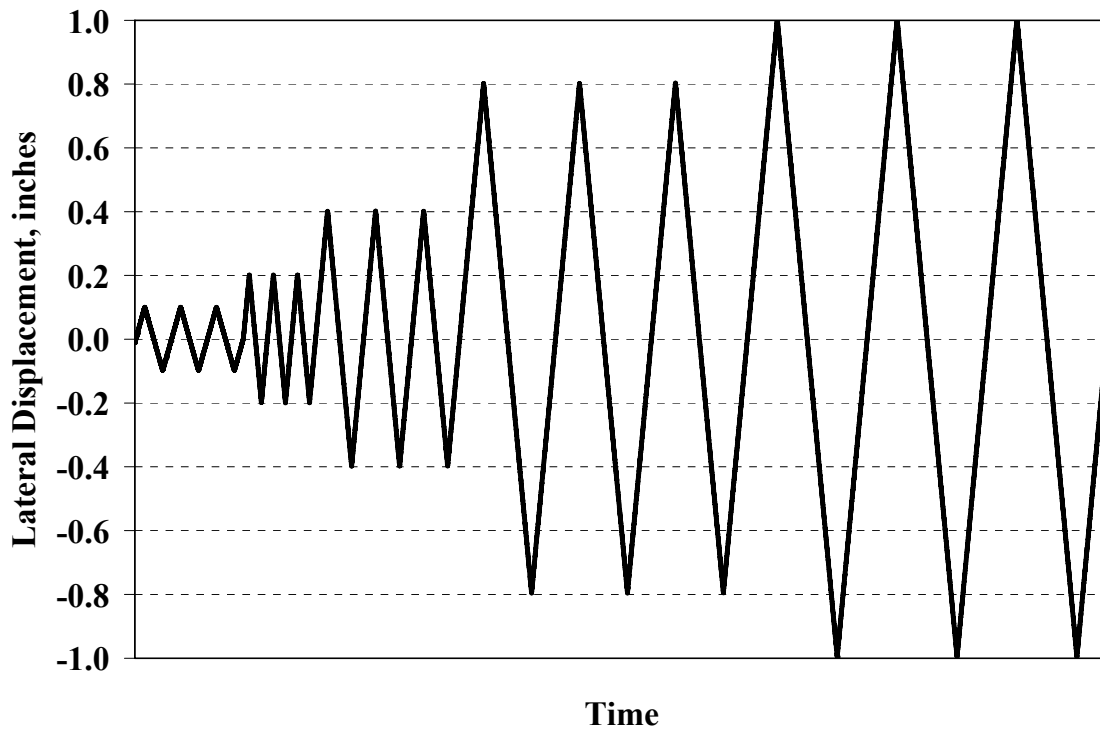
Figure 3.13 – Typical lateral loading protocol for large scale surface friction and anchor rod bearing tests (Tests #1 - #5)
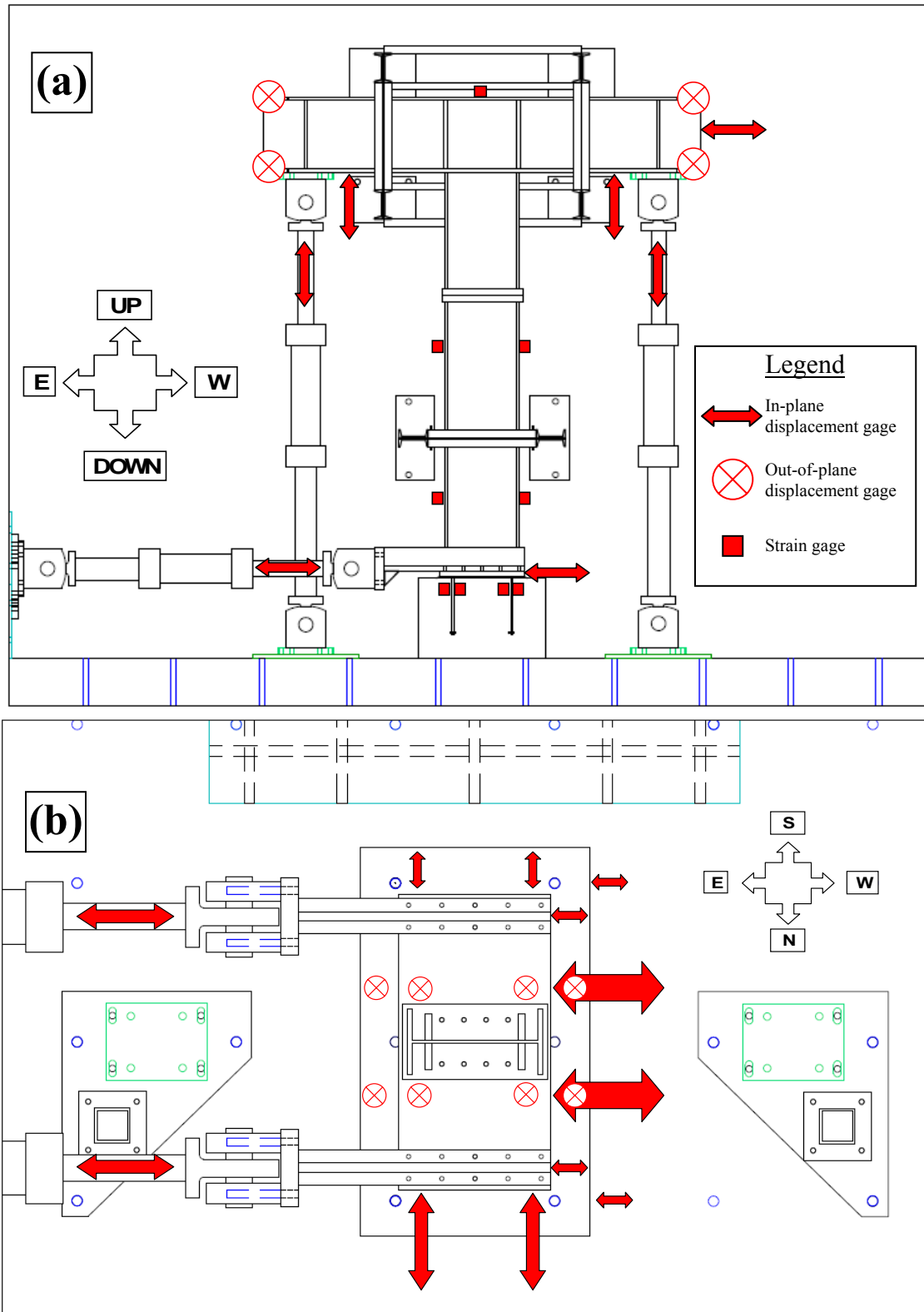
Figure 3.14 – Schematic illustrating instrument locations (to-scale)
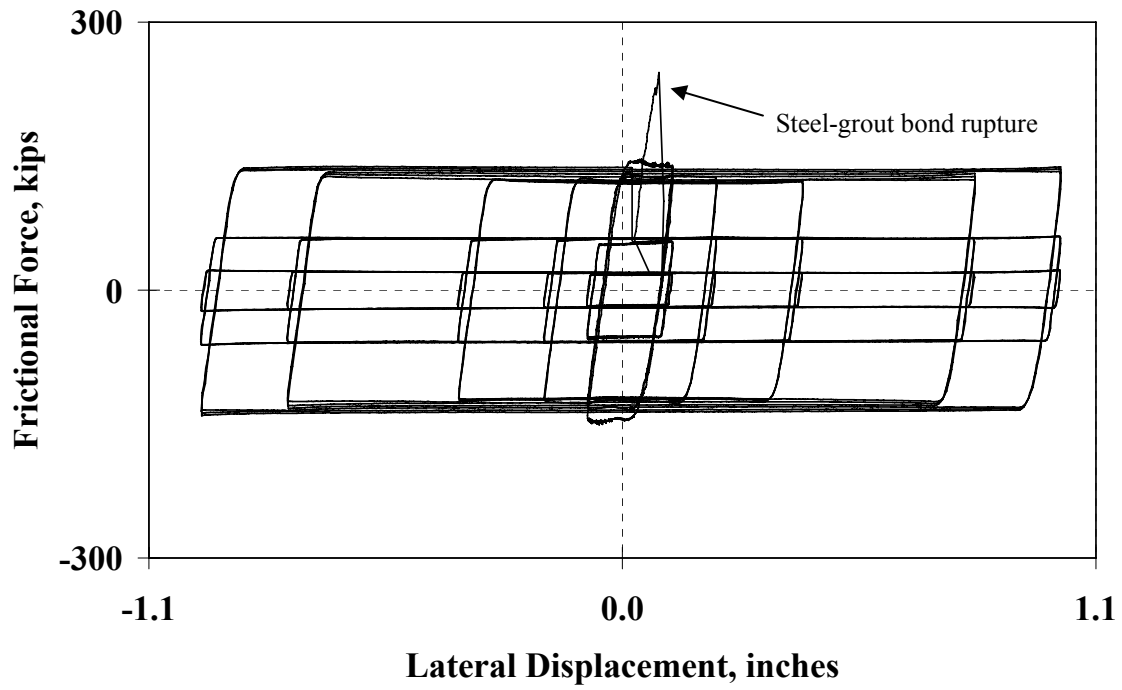
Figure 3.15 – Representative response plot of the surface friction tests (shown here for Test #3)
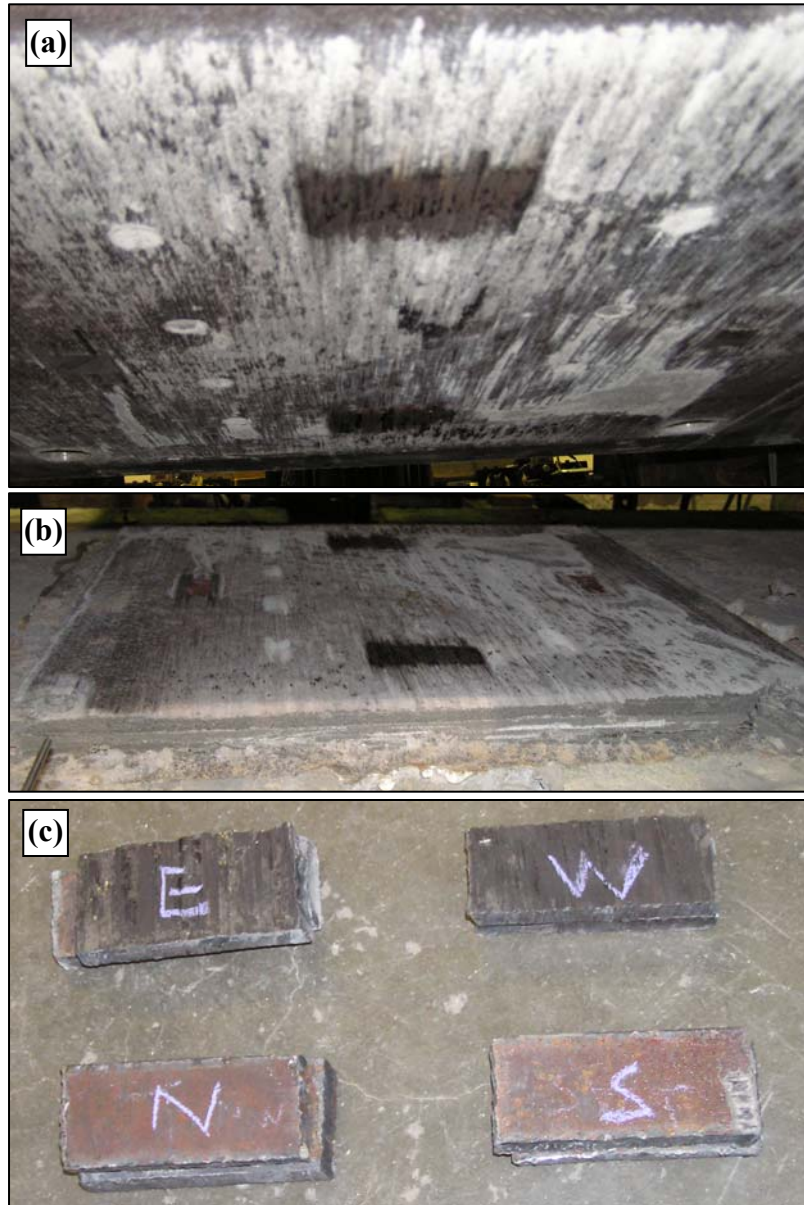
Figure 3.16 – Condition of (a) the underside of the base plate, (b) the grout pad and (c) shim stacks after Test #1
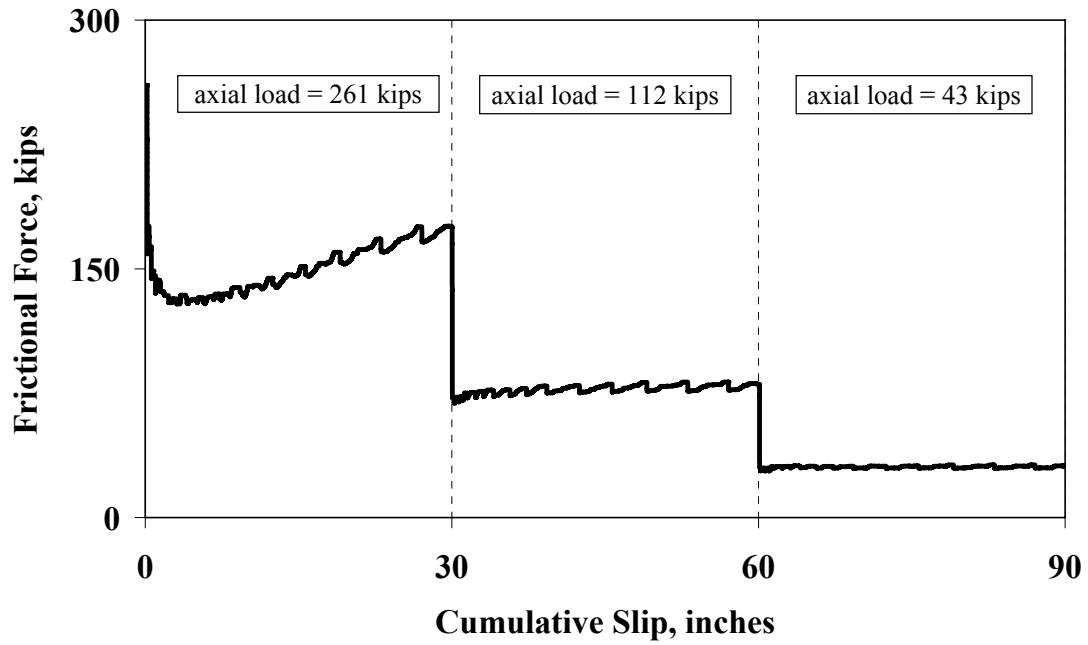
Figure 3.17 – Frictional force versus cumulative slip for Test #2
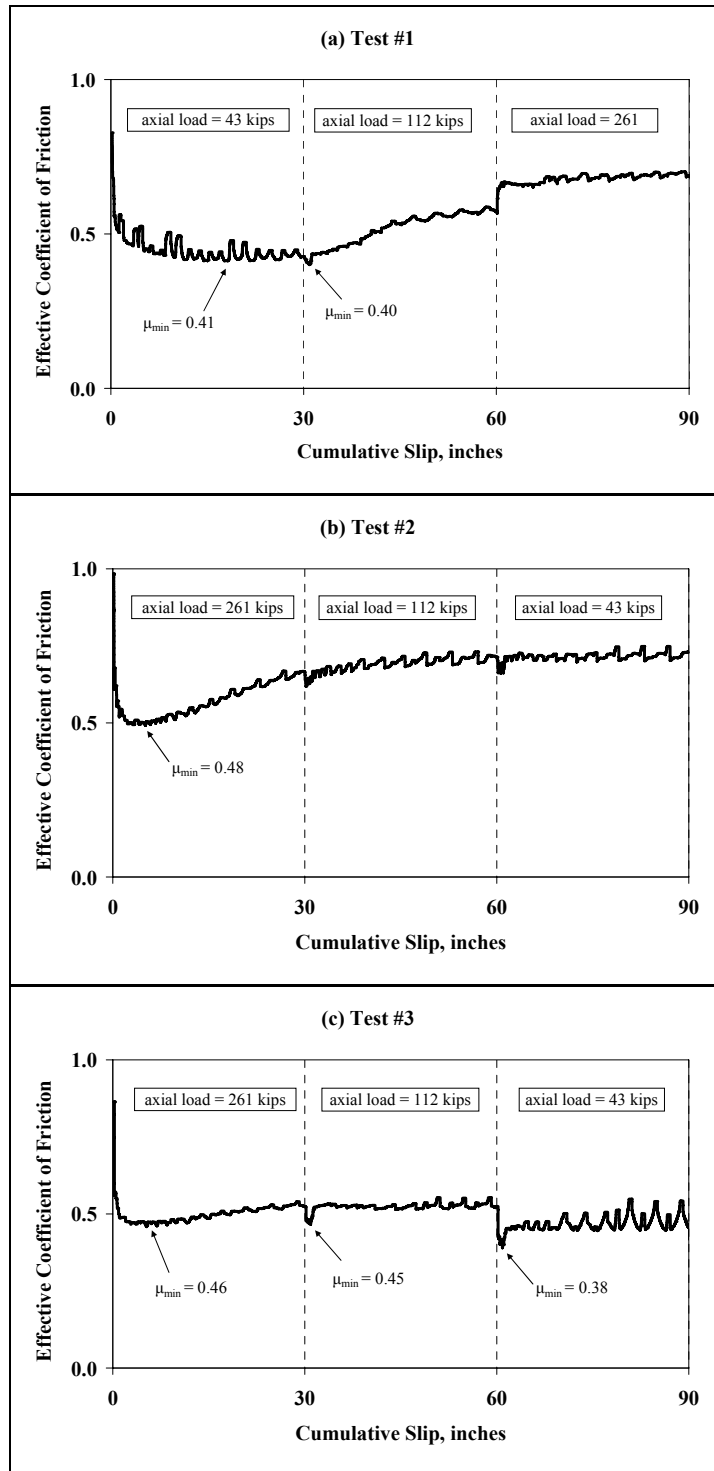
Figure 3.18 – Response progression of each friction test illustrating the extracted coefficient of friction values used for analysis
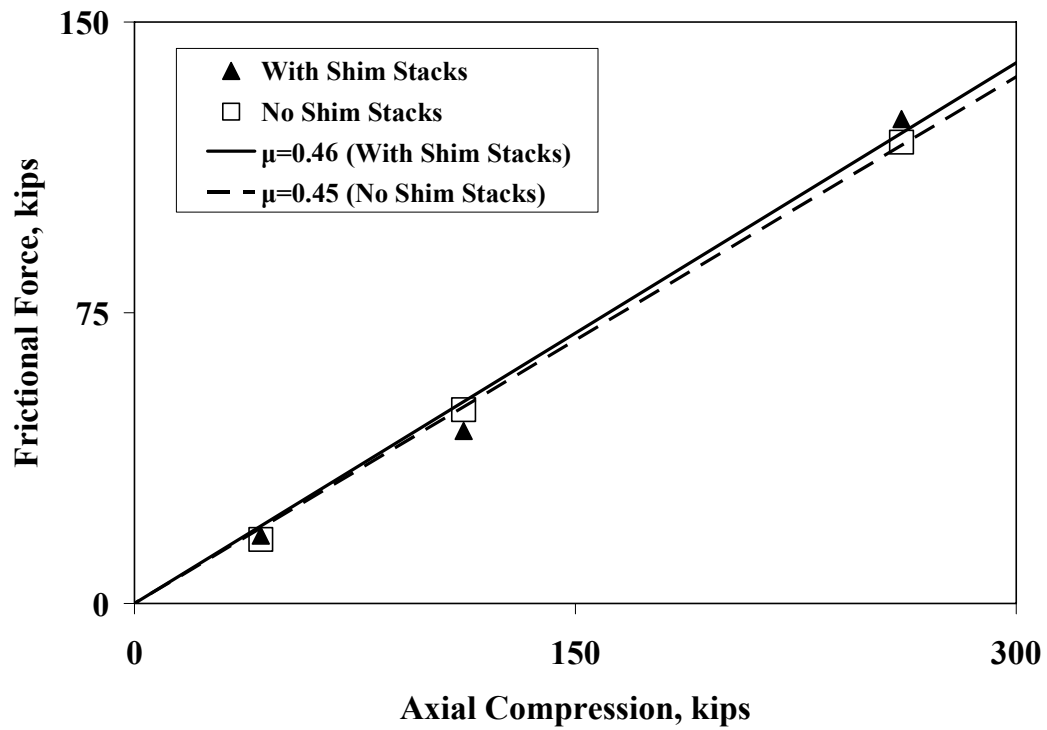
Figure 3.19 – Summary of friction tests illustrating the extracted data points used to determine the coefficient of friction
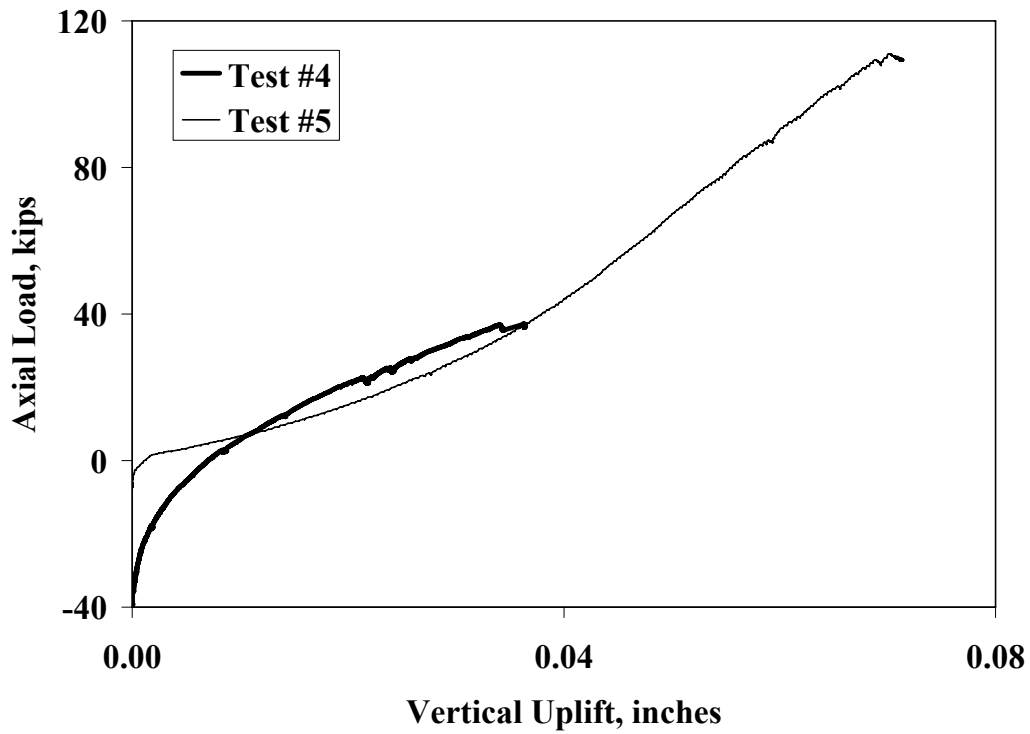
Figure 3.20 – Vertical uplift versus axial load during the initial axial tension loading of the anchor rod bearing Tests #4 and #5
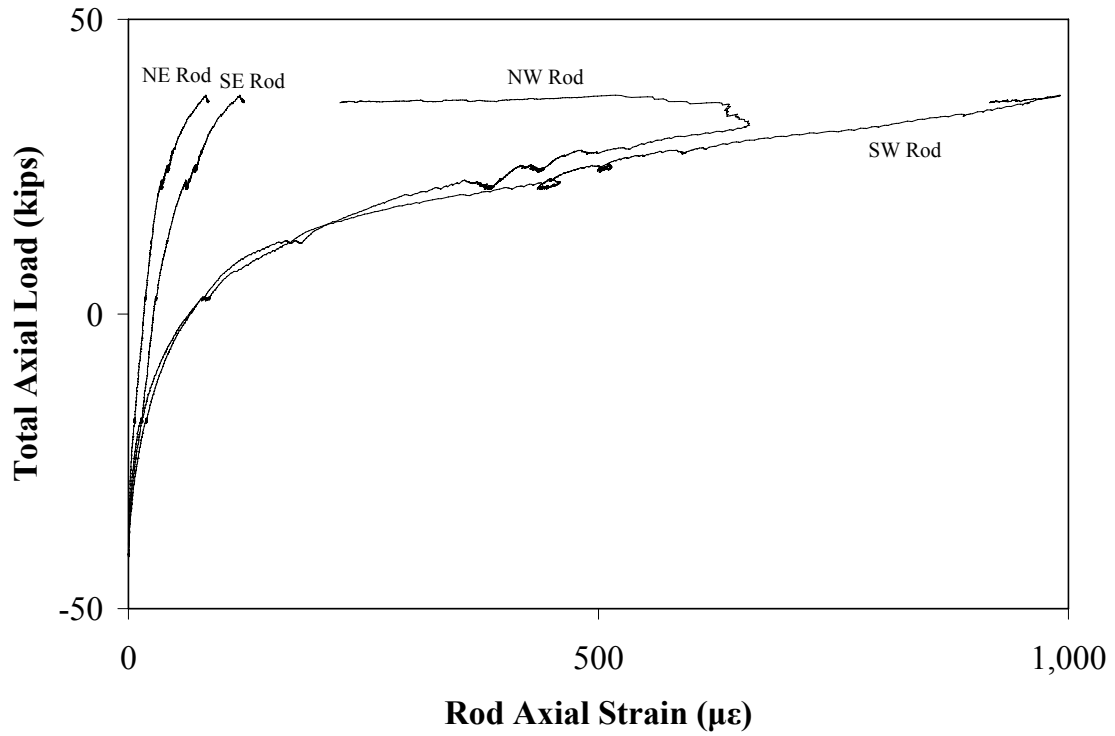
Figure 3.21 – Anchor rod axial strains during initial axial uplift of base plate Test #4 (3/4" diameter rods)
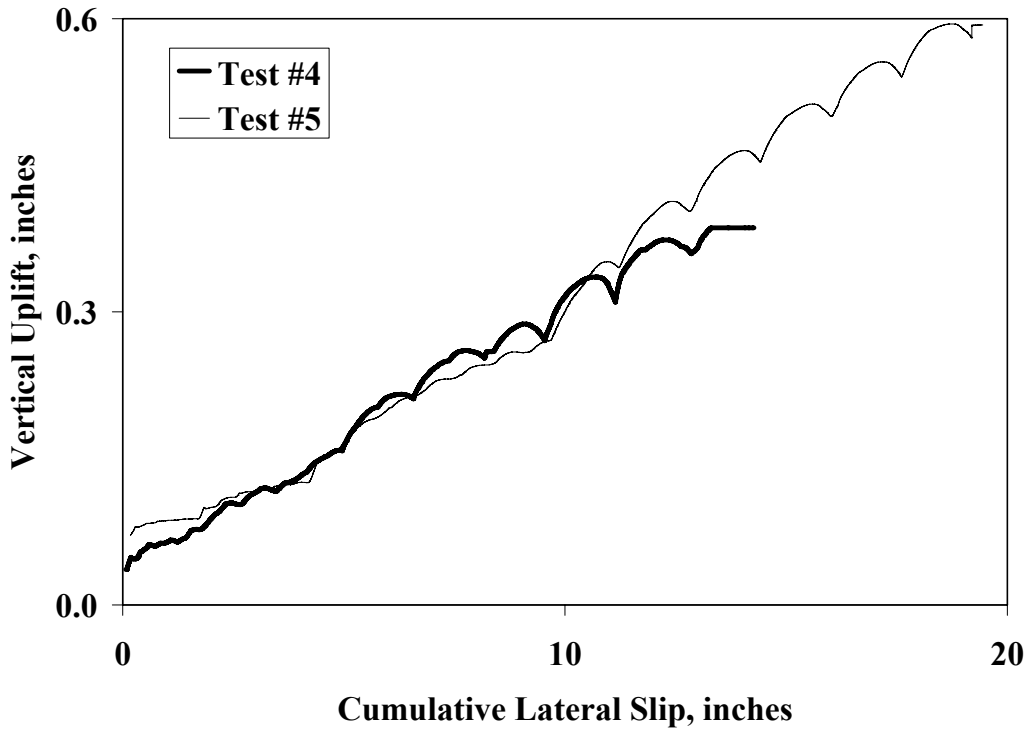
Figure 3.22 – Vertical displacement of base plate versus cumulative lateral slip during lateral loading of both anchor rod bearing Tests #4 and #5
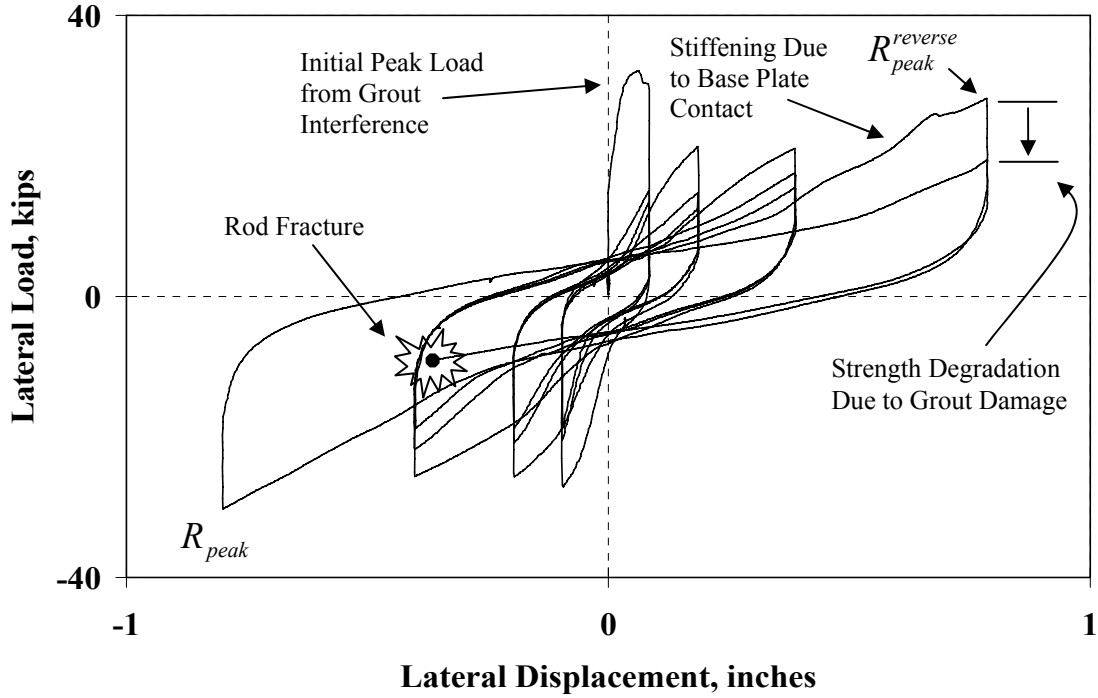
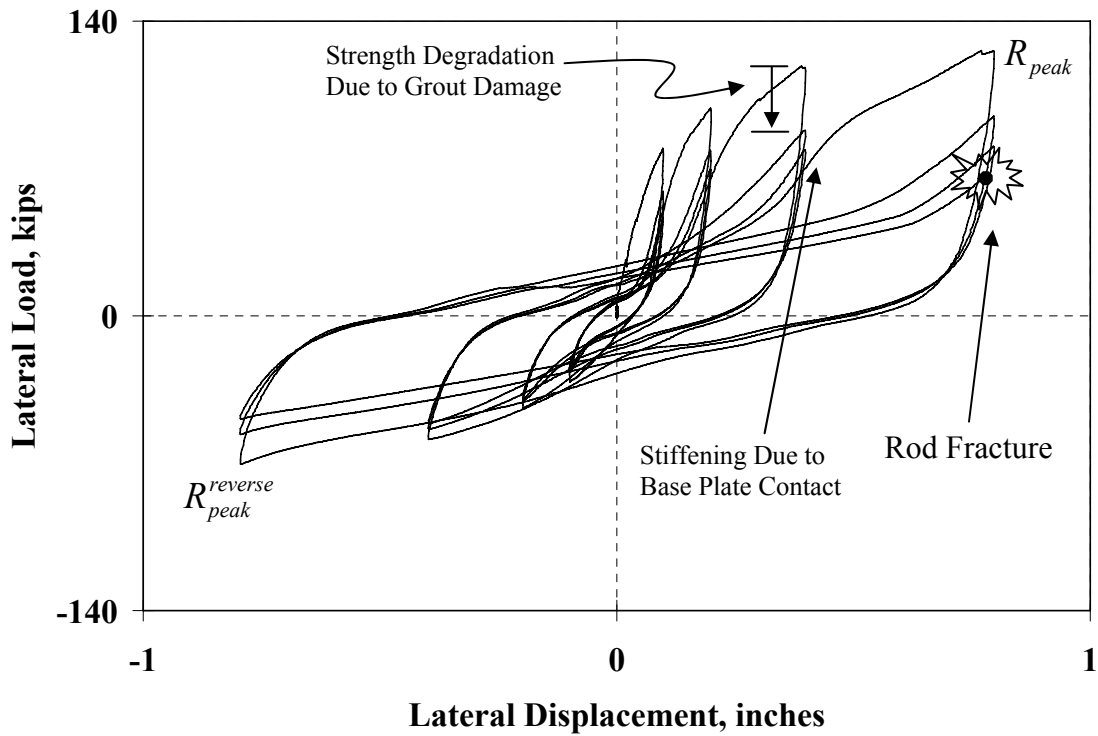**Figure 3.23** – Load versus displacement response of Test #4 – 3/4" diameter anchor rod

Figure 3.24 – Load versus displacement response of Test #5 – 1-1/4" diameter anchor rod
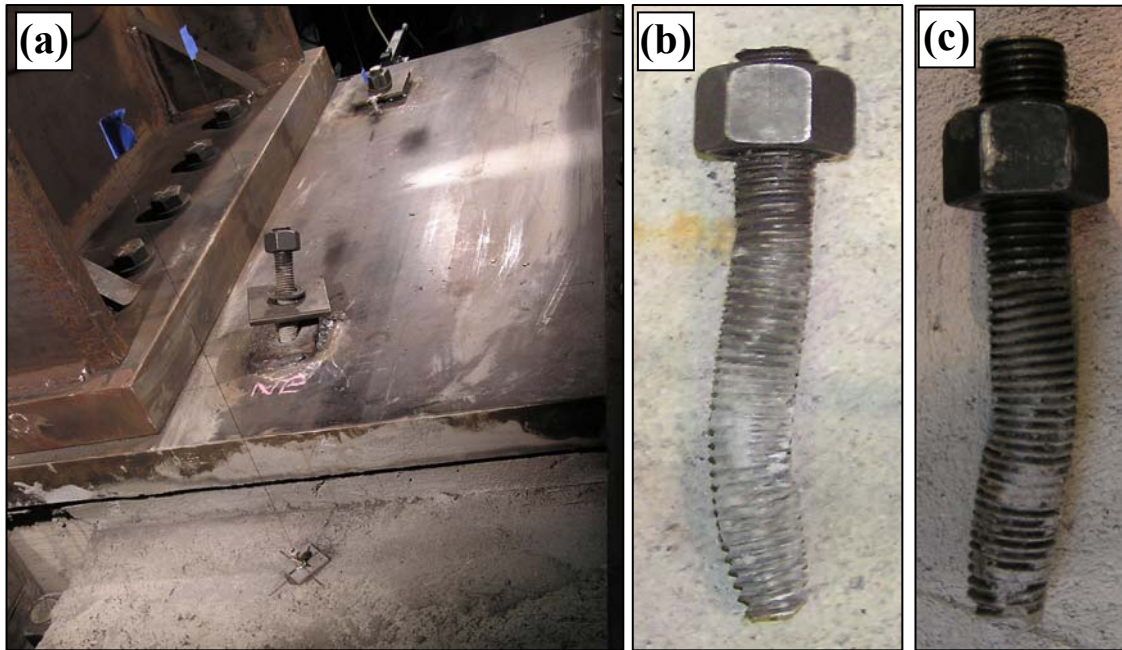
Figure 3.25 – Post-test photographs showing (a) rod fracture of Test #4, (b) fractured 3/4" diameter rod from Test #4 and (c) fractured 1-1/4" diameter rod from Test #5
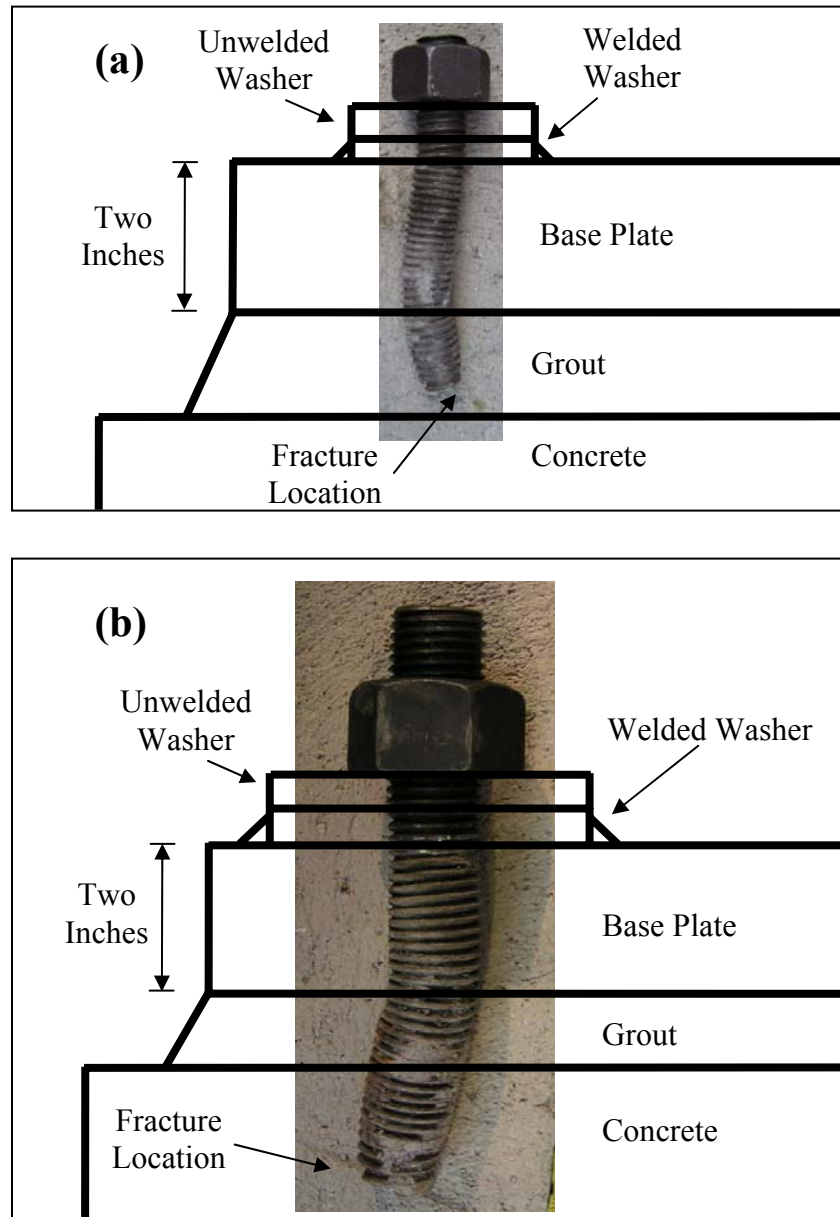
Figure 3.26 – To-scale illustration of fractured (a) 3/4" diameter anchor rod and (b) 1-1/4" rod relative to base plate, grout and concrete
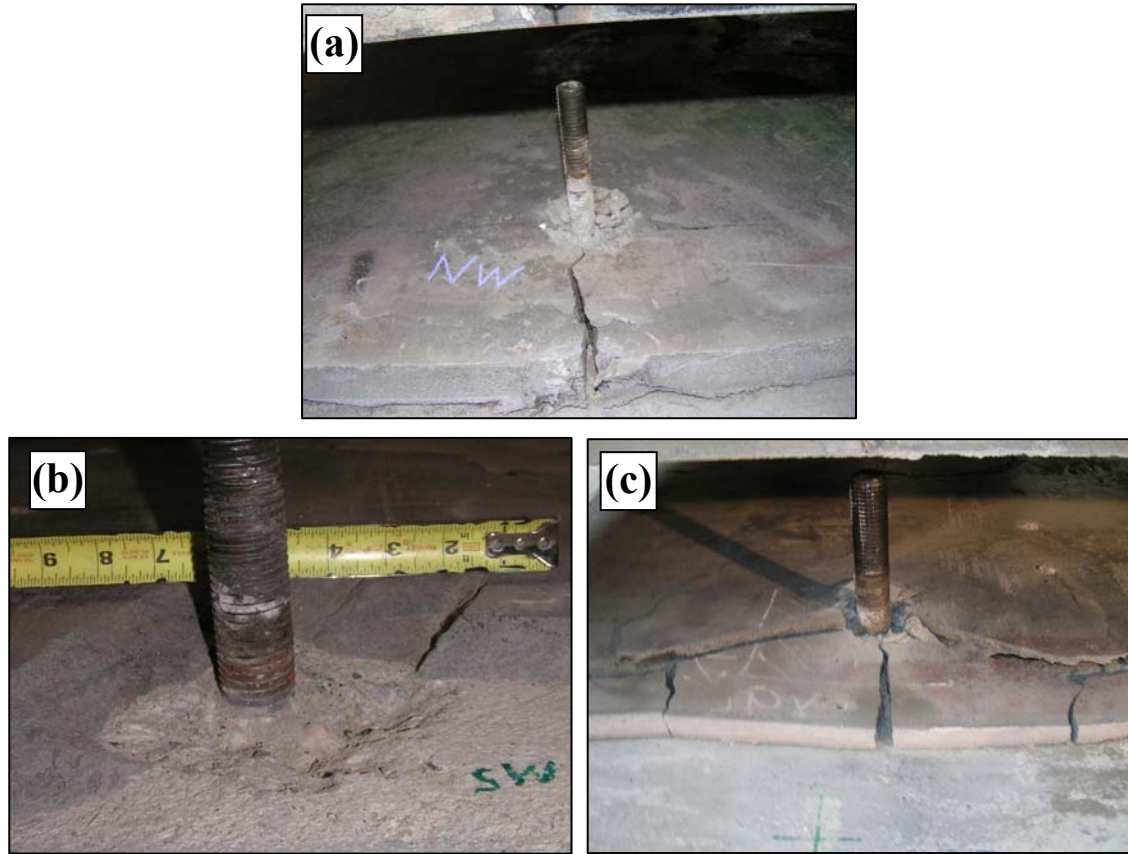
Figure 3.27 – Post-test photographs showing (a) grout damage of Test #4; (b) concrete damage of Test #5 and (c) grout damage of Test #5
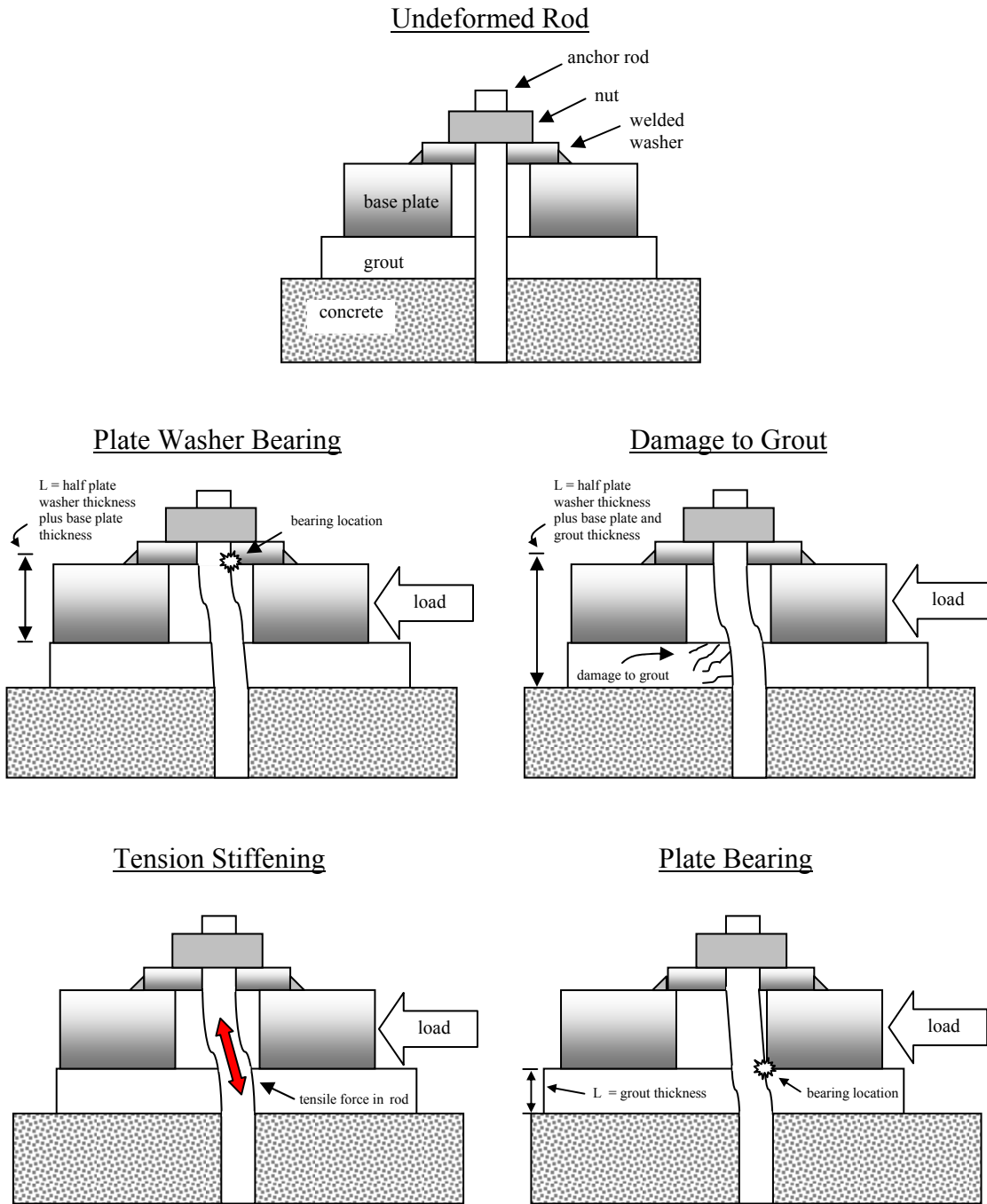
Undeformed Rod

anchor rod

nut

welded washer

base plate

grout

concrete

Plate Washer Bearing

L = half plate washer thickness plus base plate thickness

bearing location

load

Damage to Grout

L = half plate washer thickness plus base plate and grout thickness

load

damage to grout

Tension Stiffening

load

tensile force in rod

Plate Bearing

load

L = grout thickness

bearing location

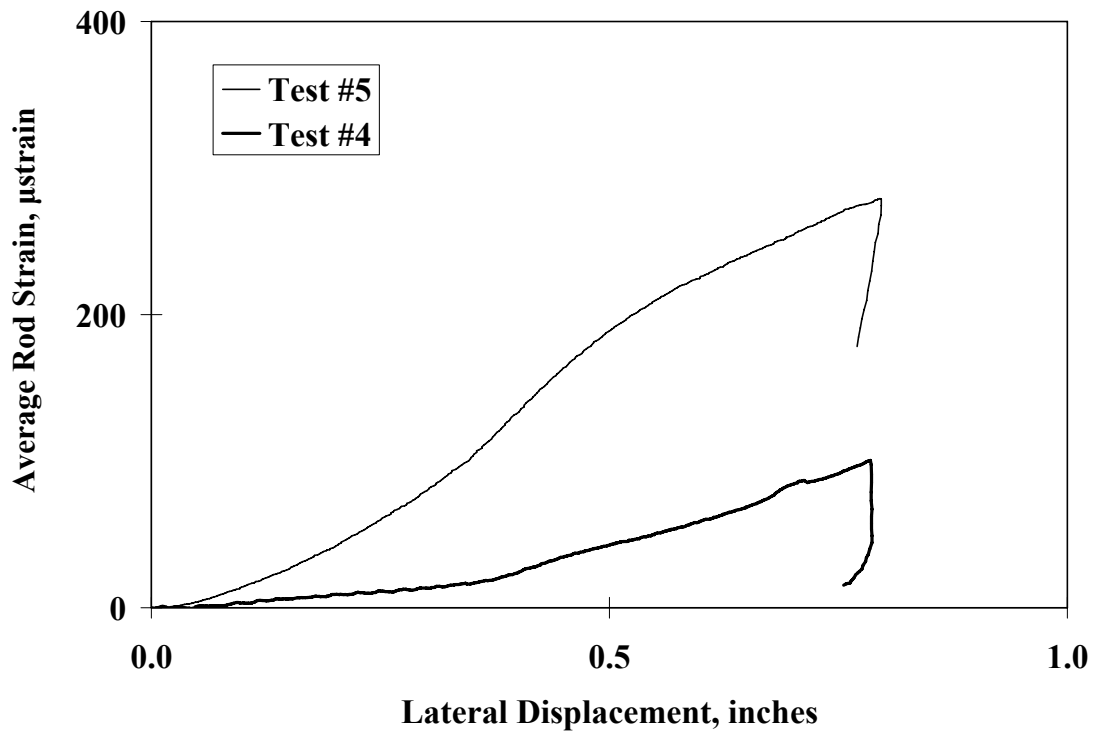**Figure 3.28** – Schematic illustrating various phenomenon in the anchor rod bearing mechanism

Figure 3.29 – Average (relative) axial strain measured from all anchor rods during the first lateral displacement excursion to 0.8"
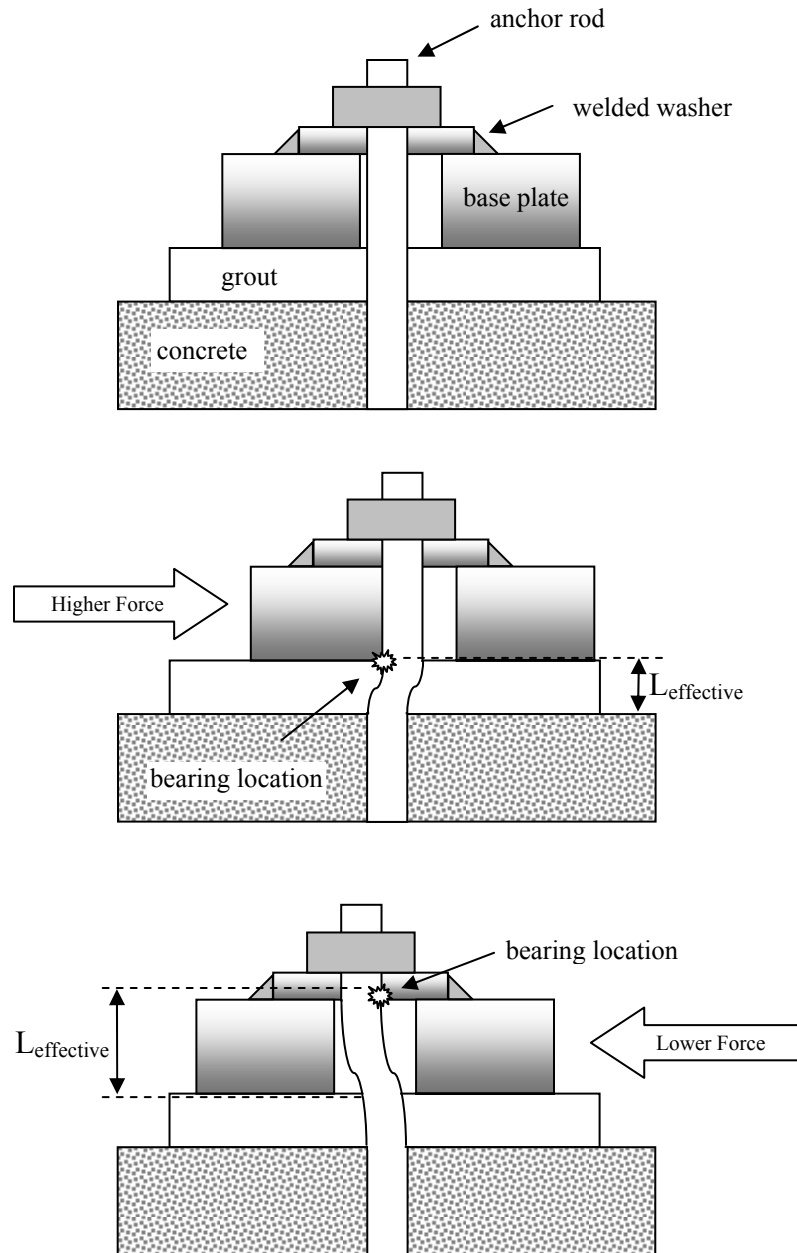
Figure 3.30 – Schematic illustrating the mechanism causing the asymmetry in anchor rod bearing load-deformation response
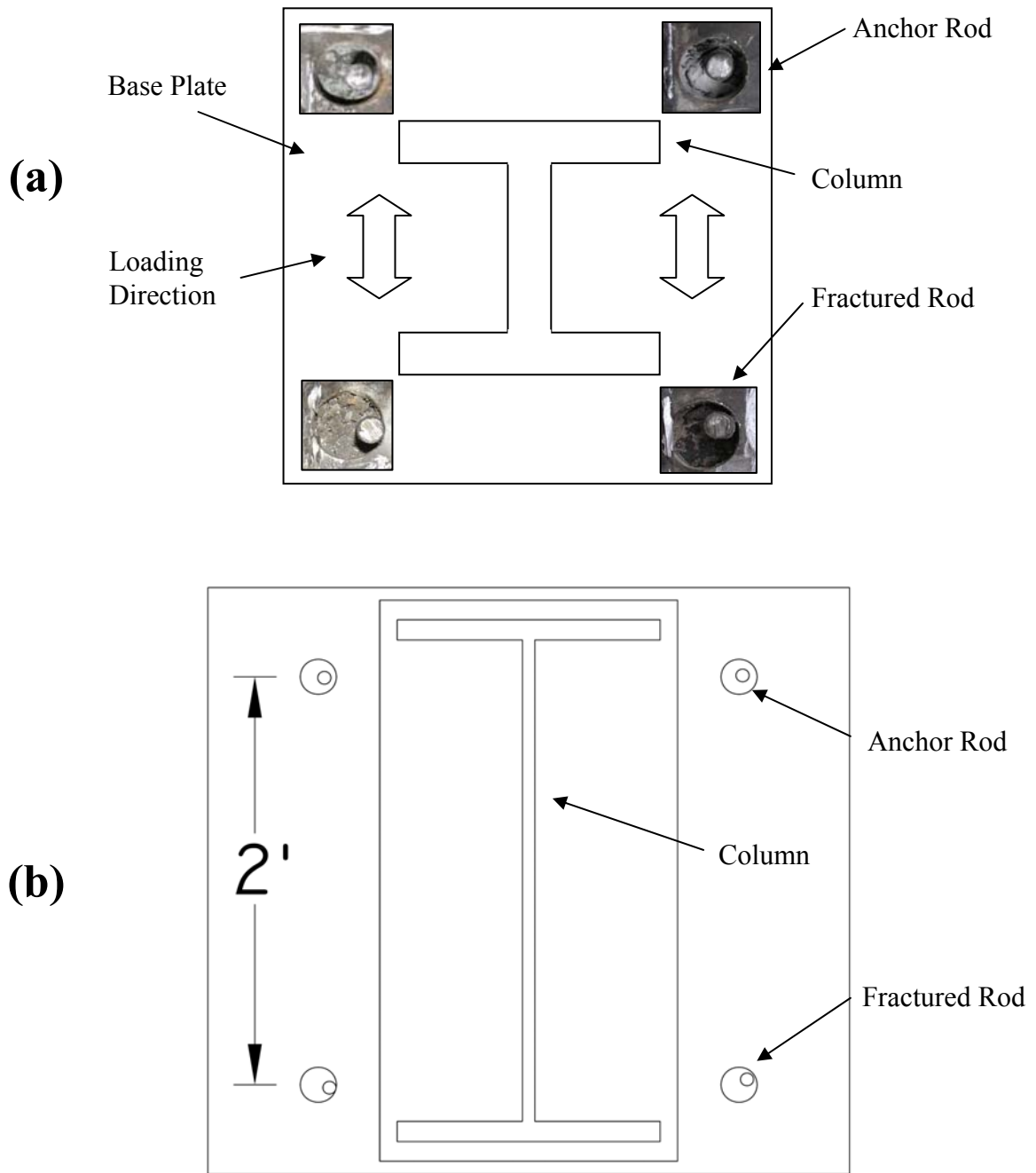
Figure 3.31 – (a) Superimposed photographs and (b) to-scale schematic indicating as-built anchor rod positioning for Test #4 (3/4" diameter rods)

(a)

Base Plate

Anchor Rod

Column

Loading
Direction

Fractured Rod

(b)
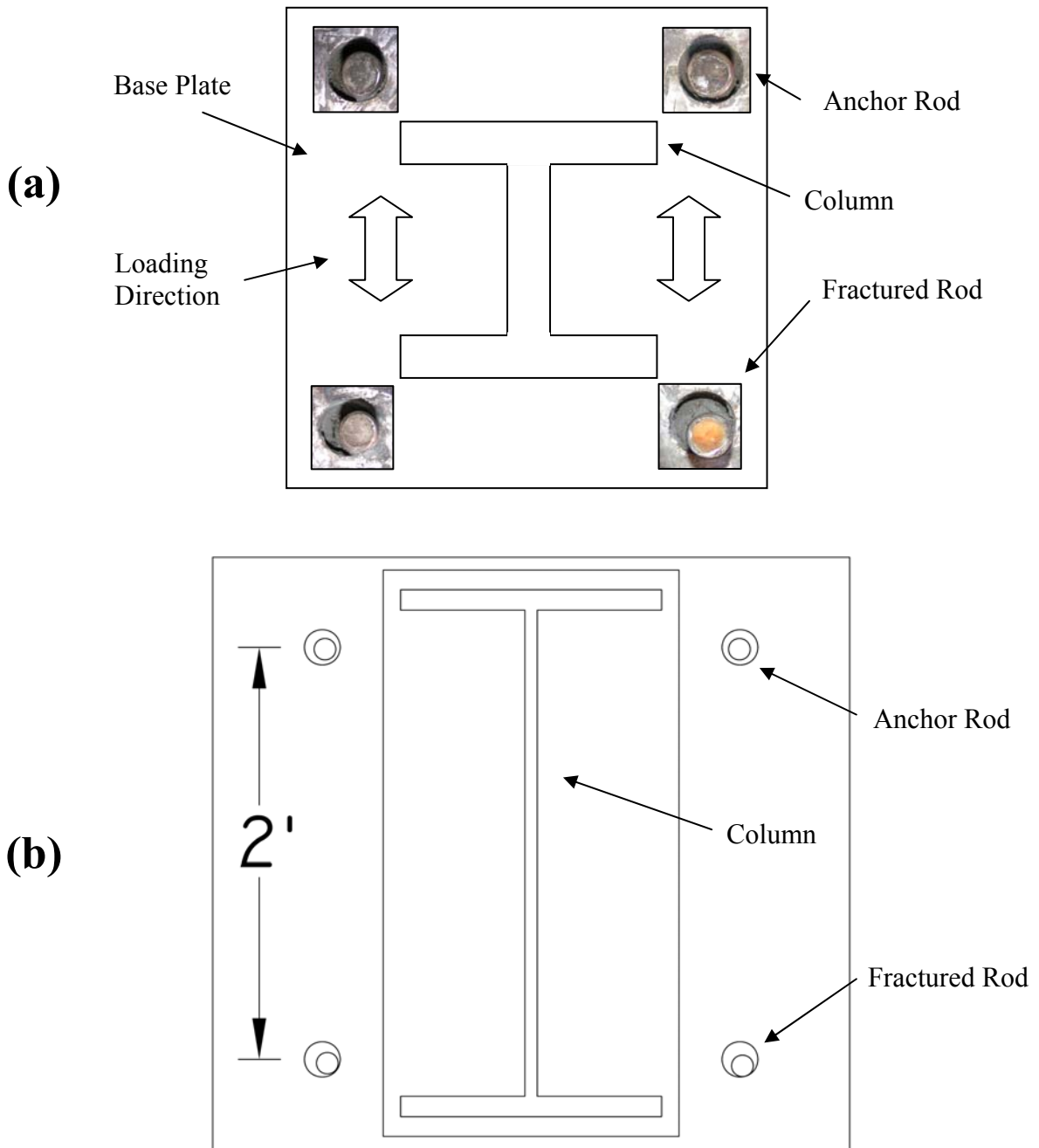
2'

Anchor Rod

Column

Fractured Rod

Figure 3.32 – (a) Superimposed photographs and (b) to-scale schematic indicating as-built anchor rod positioning for Test #5 (1-1/4" diameter rods)
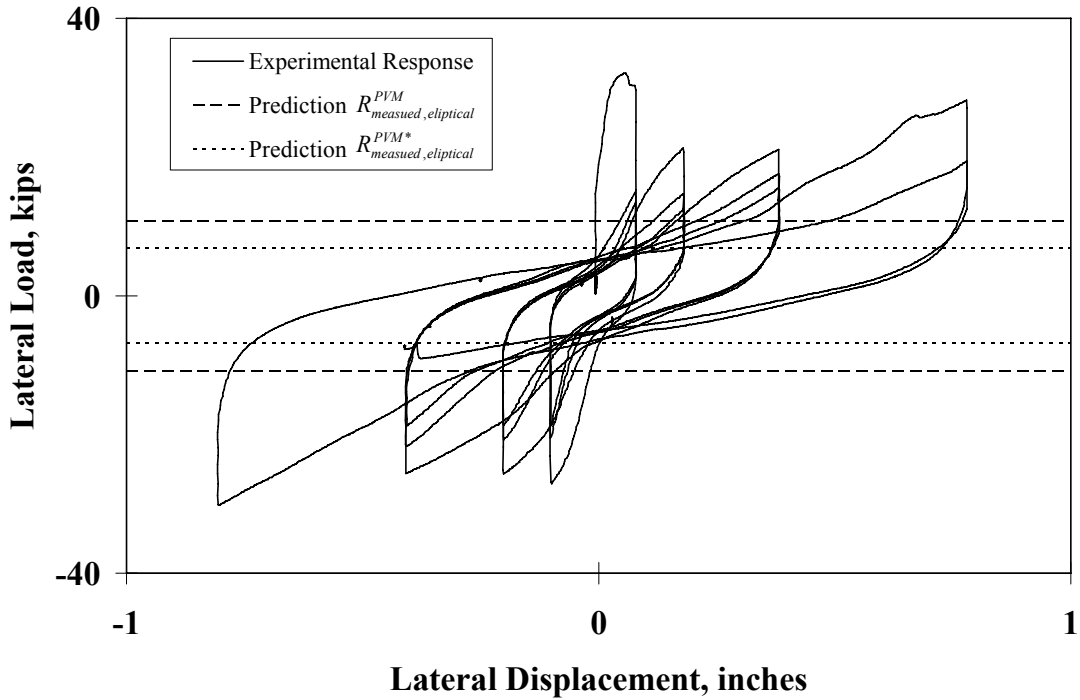
Figure 3.33 – Anchor rod strength estimates and observed response for Test #4 (3/4" diameter anchor rod); PV estimate out of range
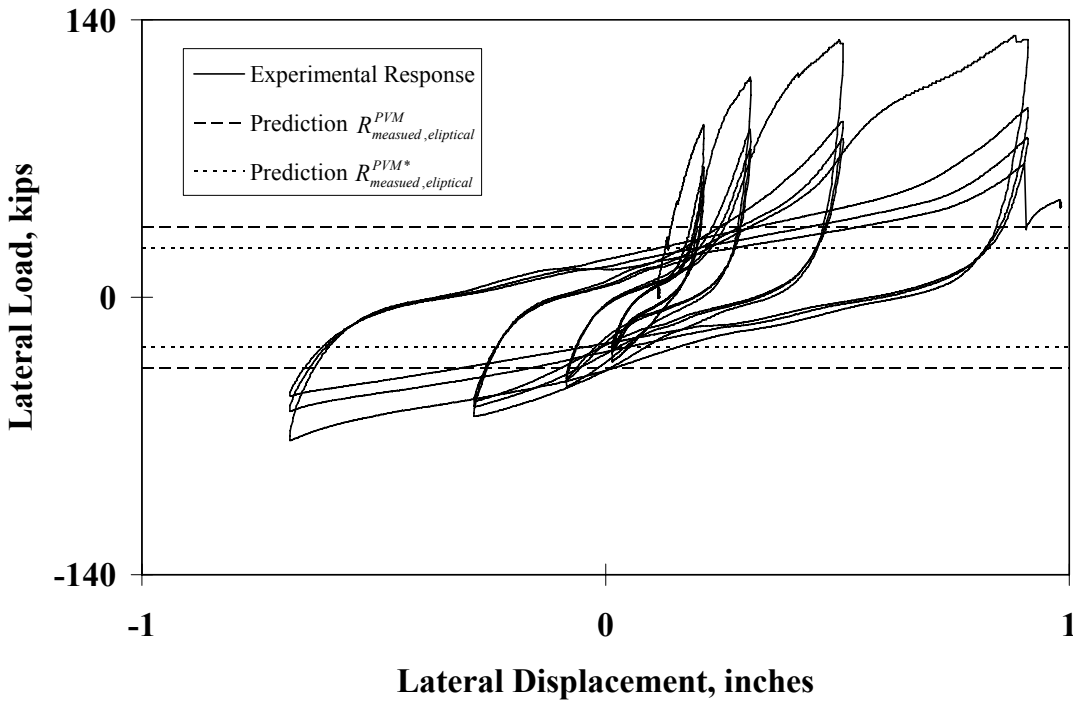

Figure 3.34 – Anchor rod strength estimates and observed response for Test #5 (1-1/4" diameter anchor rod); PV estimate out of range
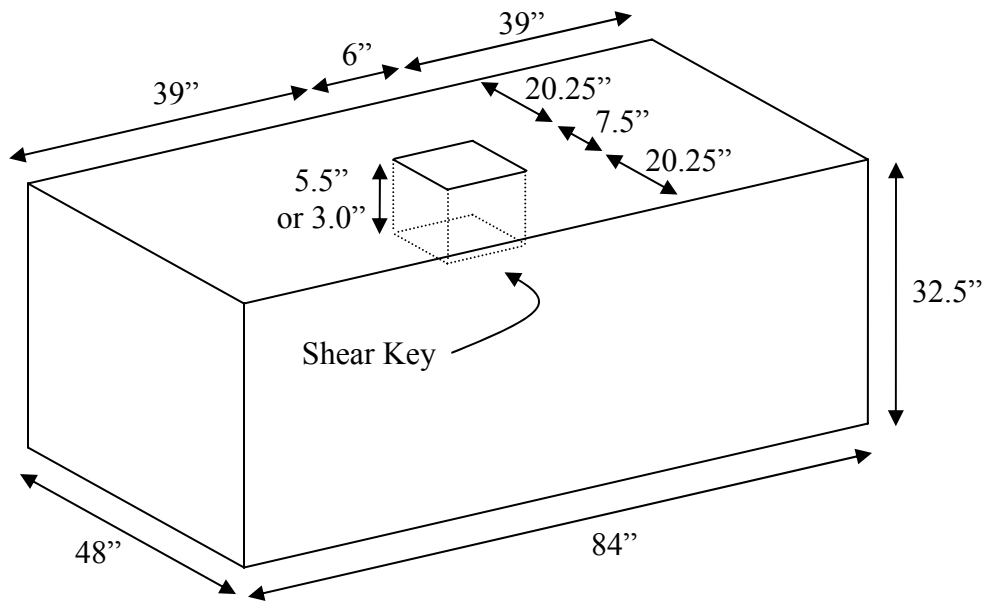
Figure 3.35 – Dimensions of concrete pedestal with shear key pocket
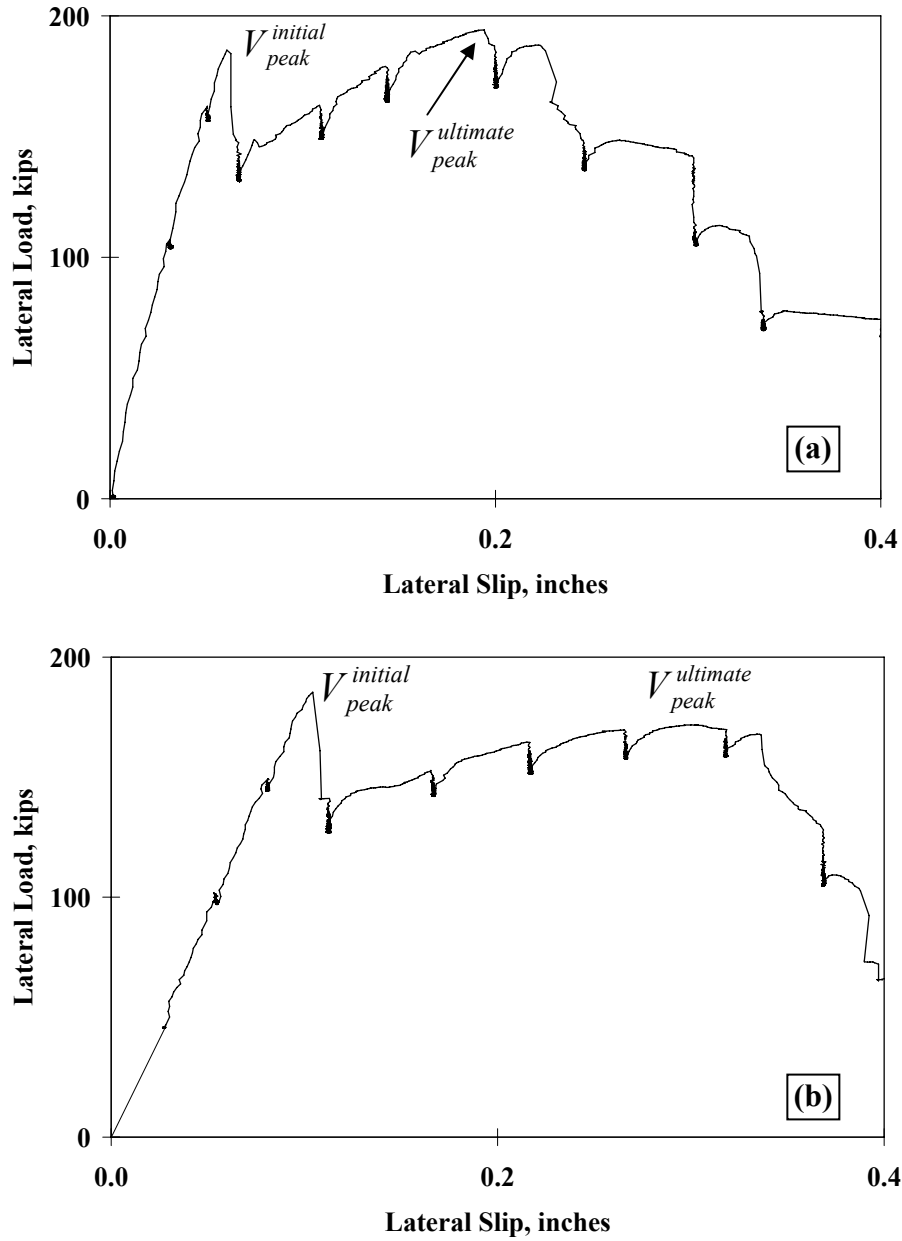
Figure 3.36 – Representative load-displacement response for the shear key tests; shown here for Test #6 – 5.5" shear key depth (a) the positive loading direction and (b) the negative loading direction
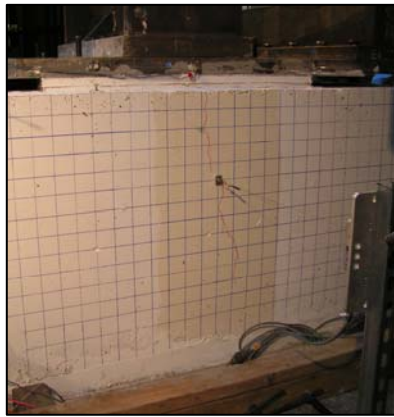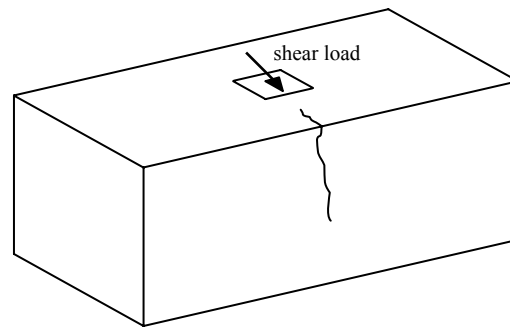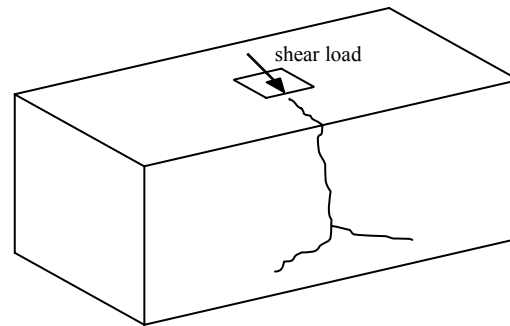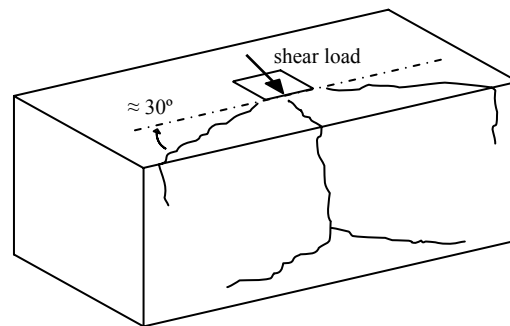
Figure 3.37 – Damage progression of initial loading of Test #6 at (a) 0.066" slip (b) 0.144" slip and (c) 0.246" slip (refer Figure 3.36a)
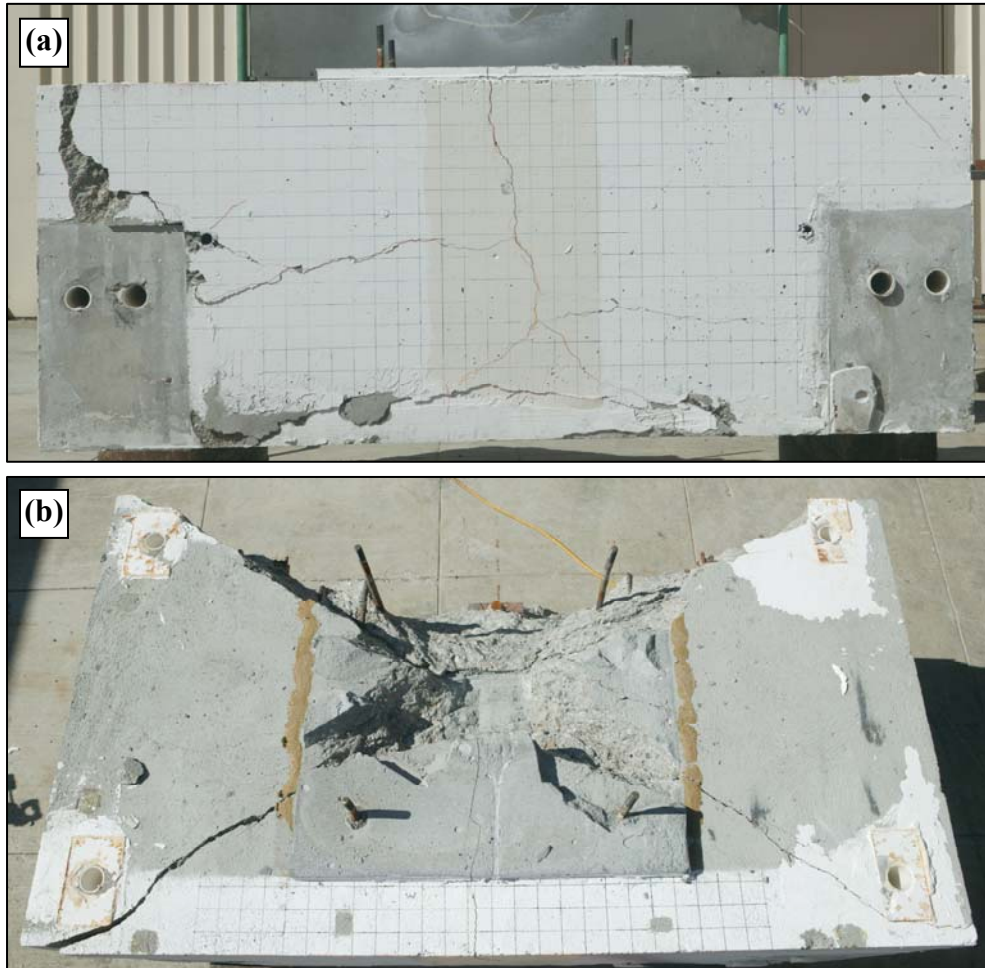
Figure 3.38 – Post test photographs of Test #6 (a) elevation view (b) plan view
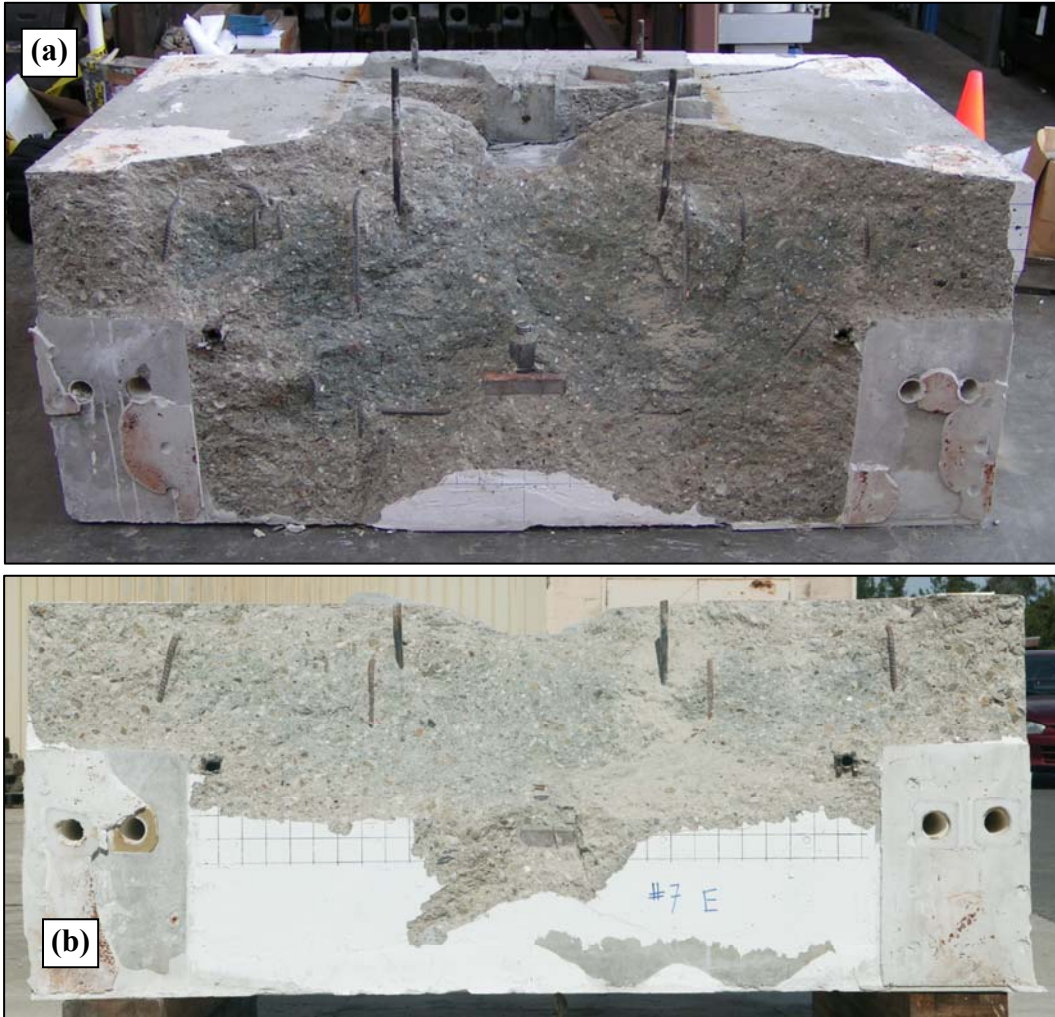
Figure 3.39 – Failure surface of (a) Test #6 and (b) Test #7
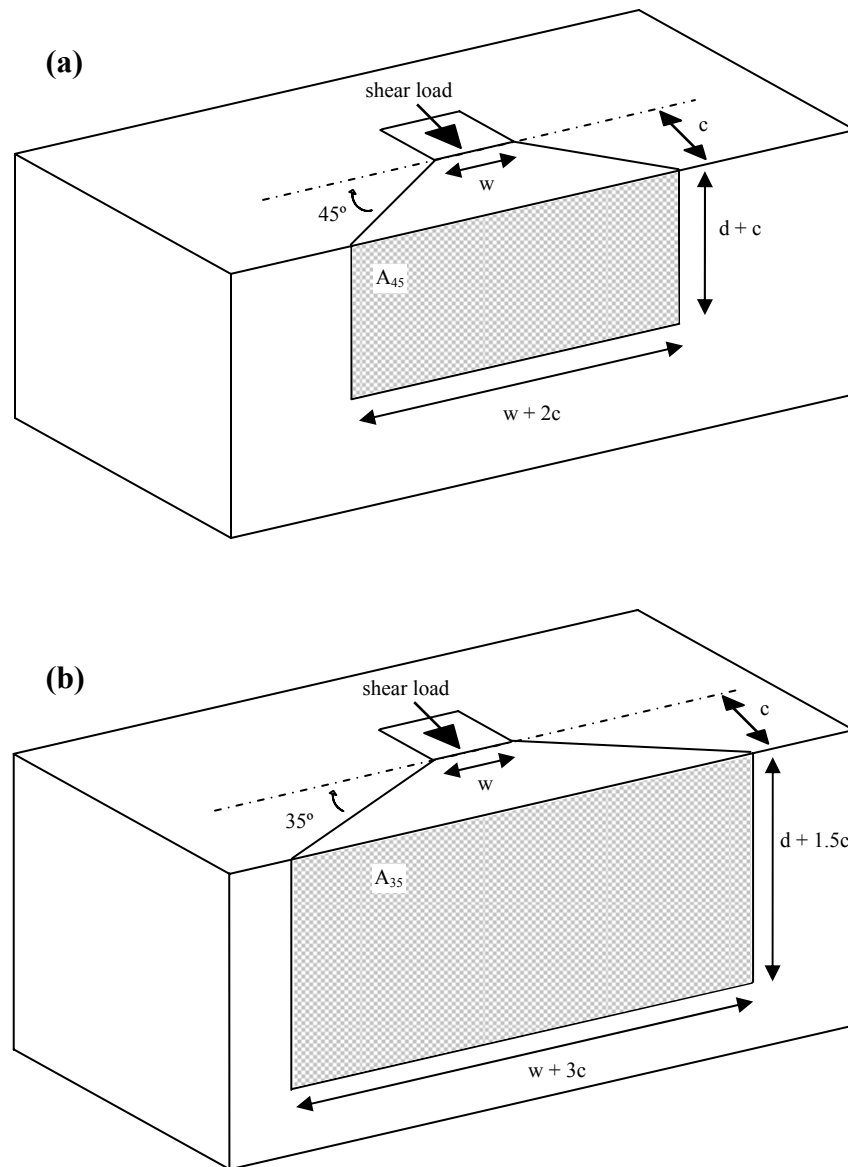
Figure 3.40 – Schematic illustrating the effective stress area assumed by (a) the 45 degree cone method and (b) the CCD method (c = edge distance; w = shear key width; d = shear key embedment depth)
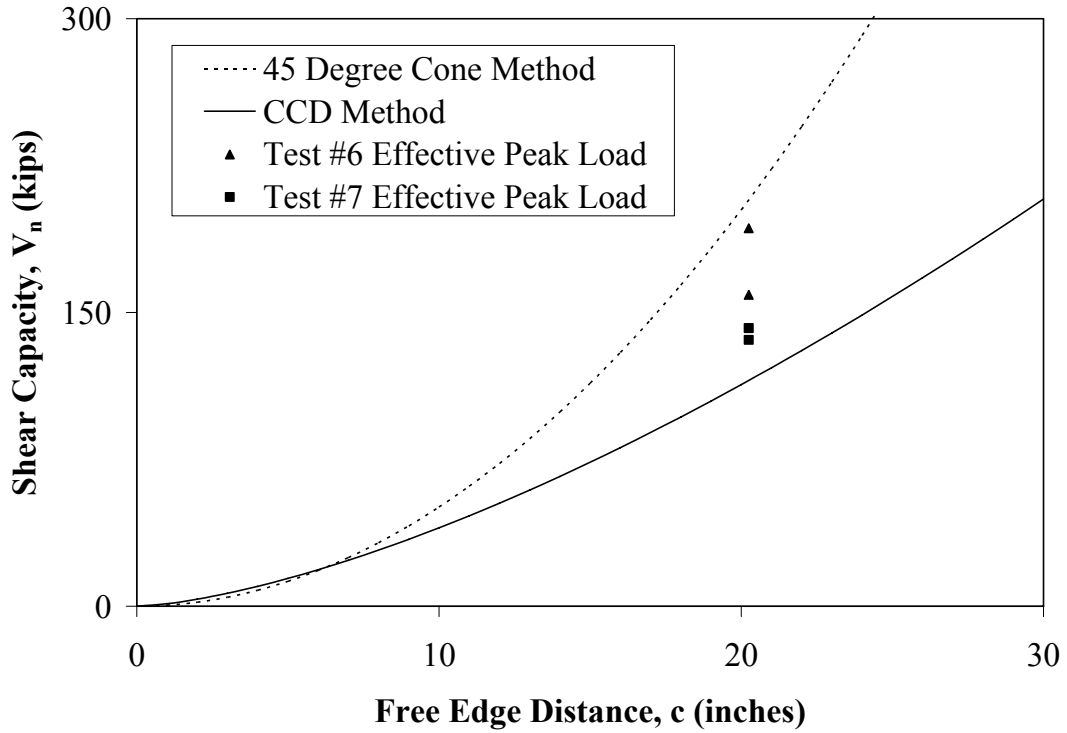
Figure 3.41 − Plot relating the shear capacity of a shear key embedded in concrete ($f_c' = 4000$ psi) a distance "c" to a free edge using the 45 degree cone method and the CCD method; experimental observations included

Chapter 4

Summary and Conclusions

4.1 SUMMARY

Current methods and equations for the design of shear transfer in steel column bases, such as those presented in the AISC *Steel Design Guide 1* (Fisher & Kloiber, 2006), have not been fully validated by experimental testing. An independent review of literature, including review of a recently published AISC sponsored synthesis of research on column base connections (Grauvilardell *et al.*, 2005), reveals that large scale experimental tests of shear transfer in exposed column base plates has not been explicitly addressed, although associated mechanisms have been researched in independent contexts. Thus, current design provisions for base plates typically adapt and combine findings from several independent studies, which are, in general, based on small-scale component tests or specific failure mechanisms. Therefore, only limited data is available involving large scale base plate components, where various mechanisms may interact with each other or may be influenced by the construction procedure or geometry of the base connection itself.

To address these issues, an experimental study was conducted to investigate three common shear transfer mechanisms of exposed column base plates which are featured in the AISC *Steel Design Guide 1* including (1) surface friction (2) anchor rod bearing and (3) shear key bearing. Seven large scale base plate tests were carried out; three tests investigated surface friction between the base plate and grout interface (two tests integrated steel shim stacks while one test examined steel on grout), two tests investigated anchor rod bearing (3/4" and 1-1/4" diameter rods) and two tests investigated shear key bearing (5.5" and 3.0" shear key embedment depth below the surface of the concrete). Loading conditions included axial compression, axial tension and monotonic/cyclic shear. The base plate tests were supplemented by ancillary tests to measure anchor rod, concrete and grout properties.

85

4.1.1 Surface Friction

The three base plate tests investigating surface friction involved the application of three different compressive axial loads levels (43, 112, and 261 kips; with corresponding bearing stresses of about 64, 166, and 386 psi) between the base plate and grout interface. Two tests included shim stacks installed in the grout pad while a third test did not contain shims. For each constant compressive axial load level, a lateral displacement-based load protocol was applied. The general behavior for all tests included a significantly large initial lateral resistance due to the steel-grout bond (from chemical adhesion) followed by a square shaped hysteresis plot indicative of Coulomb friction behavior. For the tests featuring the steel shim stacks, frictional resistance ultimately increased as lateral loading cycles continued, most likely attributed to the shims gouging into the base plate. The shear force corresponding to initial bond breakage and shim gouging are ignored for evaluation of the friction coefficient since these mechanisms may not be present in actual base plate conditions and may provide unconservative strength estimates.

Based on the experimental data, a coefficient of friction value of 0.45 is recommended for use in design. This value is lower than previously reported values and 20% lower than the design value featured in the AISC *Design Guide One* (0.55). Friction, a complex phenomenon in general, is sensitive to several factors, such as the properties of the grout and the surface condition of the steel base plate. The presence of mill scale, such as included in this current study, may result in lower coefficient of friction values compared to a machined steel surface.

4.1.2 Anchor Rod Bearing

Two base plate tests investigated the shear resistance of four anchor rods under a combination of imposed axial tensile loads and shear/flexural loading. The connection included welded plate washers and grout between the base plate and concrete pedestal. Each test examined a different nominal anchor rod diameter size; i.e. 3/4" and 1-1/4".

The lateral load versus lateral plate displacement response is similar for both tests. The cyclic loading resulted in immediate nonlinear response of the connection including

stiffening in the rods resulting from geometric nonlinearities introduced due to large lateral displacements of the bolted end of the anchor rod. A pinched hysteretic behavior is observed as well as some strength degradation at repeated lateral displacement amplitudes. Significant grout damage, in the form of cracking and spalling around the anchor rods was observed for both tests. Both tests were concluded when one rod fractured during a cyclic displacement excursion. Asymmetrical response was observed for both tests, attributed to the irregular placement of anchor rods in the holes during construction which induced constrained rod bending in one loading direction.

Three methods were evaluated to calculate the anchor rod bearing strength. Two of these methods incorporate the interaction of axial, shear and flexure stresses while another method considers only the interaction between axial stress and shear. Based on experimental observations, the method that neglects the effect of flexure is determined to be significantly unconservative. Thus, it is recommended that flexure be considered in the design of anchor rods to resist shear.

The main difference between the two strength prediction methods that consider flexure is the effective bending length, over which the anchor rods are assumed to bend in reverse curvature (based on visual inspection of the fractured rods). One of these methods (based on the current approach prescribed in the AISC *Steel Design Guide 1*) assumes that the bending length equals the thickness of the base plate plus half the thickness of the welded plate washer. Analysis of experimental evidence indicates that this assumption is consistent with observed response at small base plate slip levels. However, as base plate slip increases, damage to the grout surrounding the anchor rod results in an increase in bending length, leading to strength degradation during subsequent cyclic loading. A third strength prediction method (which also considers flexure) assumes that the rods bend over a larger length: the thickness of the base plate *and* the grout height plus half the thickness of the welded plate washer. This assumption provides a somewhat conservative strength prediction. While the strength determined based on this longer length reflects response at larger lateral base plate displacements (subsequent to strength degradation), it does not reflect initial response of the connection.

At larger displacements, tension stiffening due to deflection of the bolted end of the anchor rods (as well as rod contact within the base plate holes) result in a significant increase in strength. Considering these effects, the current approach prescribed in the AISC *Design Guide* (i.e. assuming the bending length equal to the thickness of the base plate plus half the thickness of the welded washer) is determined to provide a reasonably conservative strength estimate for design.

4.1.3 Shear Key Bearing

Two base plate tests featured a pocket within a concrete pedestal, into which a shear key was inserted, to investigate the failure modes and capacities associated with a shear key bearing mechanism. Two shear key embedment lengths were investigated (5.5" and 3.0" below the surface of the concrete). The present study focused on the shear blowout edge failure mechanism of the concrete foundation. The predicted failure region of the concrete pedestal used to represent the foundation did not contain rebar nor any other obstructions (with the exception of the anchor rods) to enable characterization of the strength capacity associated with concrete alone (i.e. not including the effect of steel reinforcement). Under small axial compressive loads, both shear key experiments involved the application of lateral (i.e. shear) monotonic loading to failure. Two distinct force peaks are observed. The first force peak, accompanied by a sudden drop in load (between 20-40% of the peak load), corresponds to flexural splitting of the concrete pedestal. After the initial drop in load, the load steadily increased until a second (and final) peak in load was observed. This ultimate peak in load was accompanied by diagonal cracks on both sides of the pedestal, about 30 degrees perpendicular to the loading direction.

Two methods are considered to estimate the strength corresponding to the observed blowout failure mode of the concrete. One of these methods, commonly referred to as the 45 degree cone method, is prescribed by ACI-349 (2006) for the concrete shear capacity of embedded shear lugs and is featured in the AISC *Design Guide 1* (Fisher & Kloiber, 2006). A second estimate of strength is based on the concrete capacity design (CCD)

method, which has been adapted by ACI-349 (2006) for anchorages in concrete under tension or shear loading. The main difference between the two strength prediction methods is associated with the size-effect in concrete derived from fracture mechanics theory (Bažant, 1984). An inspection of the test-to-predicted ratios indicates that the 45 degree cone method (currently proposed by the AISC *Design Guide 1*) may be unconservative for large concrete edge distances (i.e. large concrete foundations) due to this size effect. The 45 degree cone method has a mean test-to-predicted strength ratio of 0.51 (COV = 0.14). The test-to-predicted ratio determined with respect to the CCD method indicates the inclusion of the size effect in the analysis provides a more accurate estimate of strength. In this case, the mean test-to-predicted ratio is equal to 1.07 with a COV equal to 0.19. The longer shear key is observed to be stronger on a unit basis, as compared to the shorter shear key. The larger local bearing stresses of a shorter lug may increase the likelihood of early crack initiation.

Based on experimental observations, the CCD method provides a relatively accurate estimate of strength for embedments with large free edge clear distances (i.e. large concrete foundations), where the strength is controlled by fracture initiation. Although not tested as part of this study, it is anticipated that for small edge distances, where the strength is governed by development of the concrete tensile strength over the failure area, the CCD method might provide unconservative results. Thus, it is recommended that the reliable strength of concrete blowout due to shear key bearing be calculated as the minimum of the two previously described estimates.

4.2 CONCLUSIONS AND DESIGN IMPLICATIONS

Based on the reported test data and consideration of previously published literature, this study has resulted in improved (and more reliable) guidelines and equations to characterize the strength capacity for various failure modes associated with shear transfer mechanisms in exposed column base plates. Examples illustrating the use of these improved methods are included in Appendices C and E.

While these findings may be suitably incorporated into improved design guidelines for shear transfer, it is outside the scope of this preliminary report, whose main objective is

to present the experimental data and associated analyses. Future efforts, including collaboration with the AISC oversight committee, could result in specific design guidelines (in the form of reports or papers) or modifications to the AISC *Steel Design Guide 1*.

The incorporation of these findings into design guidelines may involve a consideration of several issues, some of which are outlined below –

1. It is important to note that owing to the expense associated with large-scale testing, the current data set does not include replicate data sets for statistical analysis. Thus, to apply this data in a design context, appropriate resistance factors (ϕ) should be developed through examination of previous standards, specifications and similar test data.

2. Some of the tests and analyses conducted in this study did not lead to definitive methods to characterize the strength capacity. For example, from the anchor rod tests, the geometric nonlinear effects associated with large displacements, combined with the variation in bearing conditions (including those affected by construction tolerances), resulted in significantly higher strength capacities than predicted by a consideration of axial, bending and shear stresses in the rods. However, it is challenging to characterize this strength since it depends on the deformation capacity of the anchor rods, which may be difficult to characterize accurately. It may be desirable to utilize this overstrength for design, if suitable assumptions can be made regarding the deformation capacity of the anchor rods.

3. In field details, one or more of the mechanisms discussed in the study could be active. Initially, the force will be resisted by the "stiff" mechanisms of friction (if compressive load is present) and shear key bearing (if a shear lug is provided). Once these are overcome, the lateral load may be resisted by other more "flexible" mechanisms, such as anchor rod bearing. Based on the findings of this and other

studies, design provisions may address the combination of various shear transfer mechanisms to resist the applied loads.

In addition to the three mechanisms outlined in this study, several other details are currently used in design practice to resist large shear forces in base plates, such as commonly encountered in high-seismic regions. These alternative details may include embedding the base plate in concrete or attaching the base plate to a grade beam. Design guidelines may include a consideration of these details and appropriate methods to use them in combination with the mechanisms investigated in this study.

Finally, as discussed in the introduction, the experimental results presented in this report are one part of a comprehensive study on column base plates. While this phase of testing focused on shear dominated response, in general, behavior will involve both flexure and shear. Ongoing work focuses on flexural response of base plates, through a series of seven large scale experiments and complementary simulations. Various parameters investigated in the ongoing study include base plate thickness, anchor rod layout and gravity load effects. Although these experiments focus on flexure-dominated response, in the context of this report, they may provide additional information regarding the interactive effects of flexural and shear response.

References

ACI Committee 209. (2006), "Prediction of Creep, Shrinkage and Temperature Effects in Concrete Structures," Farmington Hills, MI.

ACI Committee 318. (2002), "Building Code Requirements for Structural Concrete (ACI 318-02) and Commentary (ACI 318R-02)," Farmington Hills, MI.

ACI Committee 349. (1985), "Code Requirements for Nuclear Safety Related Concrete Structures and Commentary (ACI 349-85/349R-85)," Farmington Hills, MI.

ACI Committee 349. (2001), "Code Requirements for Nuclear Safety Related Concrete Structures and Commentary (ACI 349-01/349R-01)," Farmington Hills, MI.

ACI Committee 349. (2006), "Code Requirements for Nuclear Safety Related Concrete Structures and Commentary (ACI 349-06/349R-06)," Farmington Hills, MI.

Adihardjo, R., and Soltis, L. (1979), "Combined Shear and Tension on Grouted Base Details," Engineering Journal, AISC, Vol. 16, No. 1 (First Quarter), 1979, pp. 23-26.

American Institute of Steel Construction (AISC). (2006), "Fundamentals of Column Bases and Exposed Seismic Base Design," Request for Proposal (RFP) 6807, August 11, 2006.

American Institute of Steel Construction (AISC). (2005), "Seismic Design Manual," American Institute of Steel Construction, Chicago, IL.

American Institute of Steel Construction (AISC). (2005), "Steel Construction Manual," 13th Edition, American Institute of Steel Construction, Chicago, IL.

Astaneh-Asl, A. (2008), "Seismic Behavior and Design of Base Plates in Braced Frames," SteelTIPS, Technical Information and Product Service, Structural Steel Educational Council.

Astaneh-Asl, A., Bergsma, G. (1993), "Cyclic Behavior and Seismic Design of Steel Base Plates," Proceedings, Structures Congress, ASCE 1993; 409–14.

ASTM Standard C 31. (2008), "Standard Practice for Making and Curing Concrete Test Specimens in the Field," ASTM International, West Conshohocken, PA.

ASTM Standard C 39. (2005), "Standard Test Method for Compressive Strength of Cylindrical Concrete Specimens," ASTM International, West Conshohocken, PA.

ASTM Standard C 109. (2007), "Standard Test Method for Compressive Strength of Hydraulic Cement Mortars (Using 2-in. or [50-mm] Cube Specimens)," ASTM International, West Conshohocken, PA.

Bailey, J.W., and Burdette, E.G. (1977), "Edge Effects on Anchorage to Concrete," Research Series No. 31, Aug. 1977, Department of Civil Engineering, University of Tennessee, Knoxville.

Ballio, G., and Mazzolani, F.M. (1983), "Theory and Design of Steel Structures," Chapman and Hall, London and New York, pp. 257-264.

Baltay, P., and Gjelsvik, A. (1990), "Coefficient of Friction for Steel on Concrete at High Normal Stress," Journal of Materials in Civil Engineering, Vol. 2, No. 1, February, pp. 46-49.

Bažant, Z.P. (1984), "Size Effect in Blunt Fracture: Concrete, Rock, Metal," Journal of Engineering Mechanics, ASCE, 110(4), 518–535.

Burda, J.J., and Itani, A.M. (1999), "Studies of Seismic Behavior of Steel Base Plates," Report No. CCEER 99-7, Reno (NV): Center of Civil Engineering Earthquake Research, Department of Civil and Environmental Engineering, University of Nevada, NV.

Burdette, E.G., Perry T.C., and Funk, R.R. (1987) "Tests of Undercut Anchors," published in ACI Special Publication SP-103.

Cannon, R.W., Burdette, E.G., and Funk R.R. (1975), "Anchorage to Concrete," Report No. CEB 75-32, Tennessee Valley Authority, December 1975.

Cannon, R.W., Godfrey, D.A., and Moreadith, F.L. (1981), "Guide to the Design of Anchor Bolts and Other Steel Embedments," Concrete International, Vol. 3, No. 7 (July 1981), pp. 28-41.

Conrad, R.F., (1969), "Tests of Grouted Anchor Bolts in Tension and Shear," Journal of American Concrete Institute, Vol. 66, No. 9 (September 1969), pp. 725-728.

Cook, R.A., and Klingner, R.E. (1991), "Behavior of Multiple-Anchor Steel-to-Concrete Connections with Surface Mounted Baseplates," Anchors in Concrete - Design and Behavior SP 130, George A. Senkiw and Harry B. Lancelot III, eds., ACI, pp. 61-122.

DeWolf, J.T., and Ricker, D. (1990), "Design of Column Base Plates," American Institute of Steel Construction (AISC), Steel Design Guide Series 1, Chicago, IL.

DeWolf J.T., and Sarisley, E.F. (1980), "Column Base Plates with Axial Loads and Moments," Journal of the Structural Division, ASCE 1980; 106(11):2167–84.

Fahmy, M., Stojadinovic, B., Goel, S.C. (1999), "Analytical and Experimental Studies on the Seismic Response of Steel Column Bases," Proceedings of the 8th Canadian conference on earthquake engineering.

Fenz, D. (2002), "Frictional Properties of Non-Metallic Materials for Use in Sliding Bearings: An Experimental Study," Student Research Accomplishments 2001-2002, pp. 113-118, Department of Civil, Structural & Environmental Engineering, University at Buffalo, NY.

Fisher, J.M. (1981), "Structural Details in Industrial Buildings," Engineering Journal, AISC, Vol. 18, No. 3, Third Quarter, 1981, pp. 83-89.

Fisher, J.M., and Kloiber, L.A. (2006), "Steel Design Guide 1 - Base Plate and Anchor Rod Design," 2nd Ed., AISC 801-06, American Institute of Steel Construction, Inc., Chicago, IL.

Fuchs, W., Eligehausen, R., and Breen, J.E. (1995), "Concrete Capacity Design (CCD) Approach for Fastening to Concrete," ACI Structural Journal 92 (1995) (1), pp. 73–94.

Goldman, C. (1983), "Design of Column Base Plates and Anchor Bolts for Uplift and Shear," Structural Engineering Practice, Vol. 2, No. 2, pp. 103-115.

Grauvilardell, J.E., Lee, D., Ajar, J.F., and Dexter R.J. (2005), "Synthesis of Design, Testing and Analysis Research on Steel Column Base Plate Connections in High Seismic Zones," Structural engineering report no. ST-04-02. Minneapolis (MN): Department of Civil Engineering, University of Minnesota.

Gresnigt, A.M., Romeijn, A., Wald, F., and Steenhuis, C.M. (2008), "Column Bases in Shear and Normal Force," HERON, Volume 53 (2008), Issue 1/2, Special issue: Steel Column Bases.

Kawano, H., Kutani, K., and Masuda, K. (2003), "Experimental Studies on the Shear Resistance of Anchor Bolts in Exposed Type of Steel Column Bases," Journal of Structural and Construction Engineering, Transactions of AIJ, No. 567, May, 2003, pp. 141-148. (In Japanese).

Krawinkler, H., Gupta, A., Medina, R., and Luco, N. (2000), "Loading Histories for Seismic Performance Testing of SMRF Components and Assemblies," SAC Joint Venture, Report no. SAC/BD-00/10. Richmond, CA.

Klingner, R.E., Mendonca, J.A., and Malik, J.B. (1982), "Effect of Reinforcing Details on the Shear Resistance of Anchor Bolts Under Reversed Cyclic Loading," Journal of American Concrete Institute, Vol. 79, No. 1 (January-February 1982), pp. 3-12.

Kulak, G.L., Fisher, J.W., and Struik, J.H.A. (1987), "Guide to Design Criteria for Bolted and Riveted Joints," 2nd edition, John Wiley and Sons, New York, NY.

MacGregor, J., and Wight, J.K. (2004), "Reinforced Concrete: Mechanics and Design," 4th Edition, Prentice-Hall, Upper Saddle River, NJ.

Nagae, T., Ikenaga, M., Nakashima, M., and Suita, K. (2006), "Shear Friction between Base Plate and Base Mortar in Exposed Steel Column Base," Journal of Structural and Construction Engineering, Architectural Institute of Japan, No. 606, August 2006, pp. 217-223. (In Japanese).

Nakashima, S. (1998), "Mechanical Characteristics of Exposed Portions of Anchor Bolts in Steel Column Bases under Combined Tension and Shear," Journal of Constructional Steel Research, 1998, Vol. 46, No.1-3, Paper No.277. (In Japanese).

Occupational Safety and Health Administration (OSHA). (2001), "Safety Standards for Steel Erection," (Subpart R of 29 CFR Part 1926), Washington, D.C.

Ožbolt, J., Eligehausen, R., Periškić, G., and Mayer, U. (2007), "3D FE Analysis of Anchor Bolts with Large Embedment Depths," Engineering Fracture Mechanics, 74, 168-178.

PCI Design Handbook, First Edition, (1971), "Connections," Prestressed Concrete Institute, pp. 6-19, Chicago, IL.

Rabbat, B.G., and Russell, H.G. (1985), "Friction Coefficient of Steel on Concrete or Grout," Journal of Structural Engineering Volume 111, No. 3, March 1985, pp. 505–515.

Rotz, J.V., and Reifschneider, M. (1989), "Combined Axial and Shear Load Capacity of Embedments in Concrete," 10th International Conference, Structural Mechanics in Reactor Technology, Aug. 1989, Anaheim, CA.

Scacco, M.N. (1992), "Design Aid-Anchor Bolt Interaction of Shear and Tension Loads," Engineering Journal, AISC, Fourth Quarter, 1992/Volume 29, No. 4 pp. 137-140.

Shipp, J.G., and Haninger, E.R. (1983), "Design of Headed Anchor Bolts," Engineering Journal, AISC, Vol. 20, No. 2, Second Quarter, 1983, pp. 58-69.

Tronzo, T. M. (1984), "Design of Heavy Steel Column Bases: Handling Forces - Some Practical Procedures," Structural Engineering Practice, Vol. 2, No. 4, pp. 279-300.

Appendix A

Ancillary Test Data

Table A.1 - Anchor rod tension test results

Specimen	Nominal diameter (inches)	Measured original diameter (inches)	Measured necked diameter (inches)	Young's modulus (ksi)	Yield strength[1] (ksi)	Ultimate strength (ksi)
1a	3/4	0.7483	0.501	32,270	66.81	96.54
1b		0.7478	0.500	31,700	66.74	96.32
2a	1-1/4	1.2500	0.773	31,220	54.74	74.93
2b		1.2458	0.765	31,050	54.10	74.99

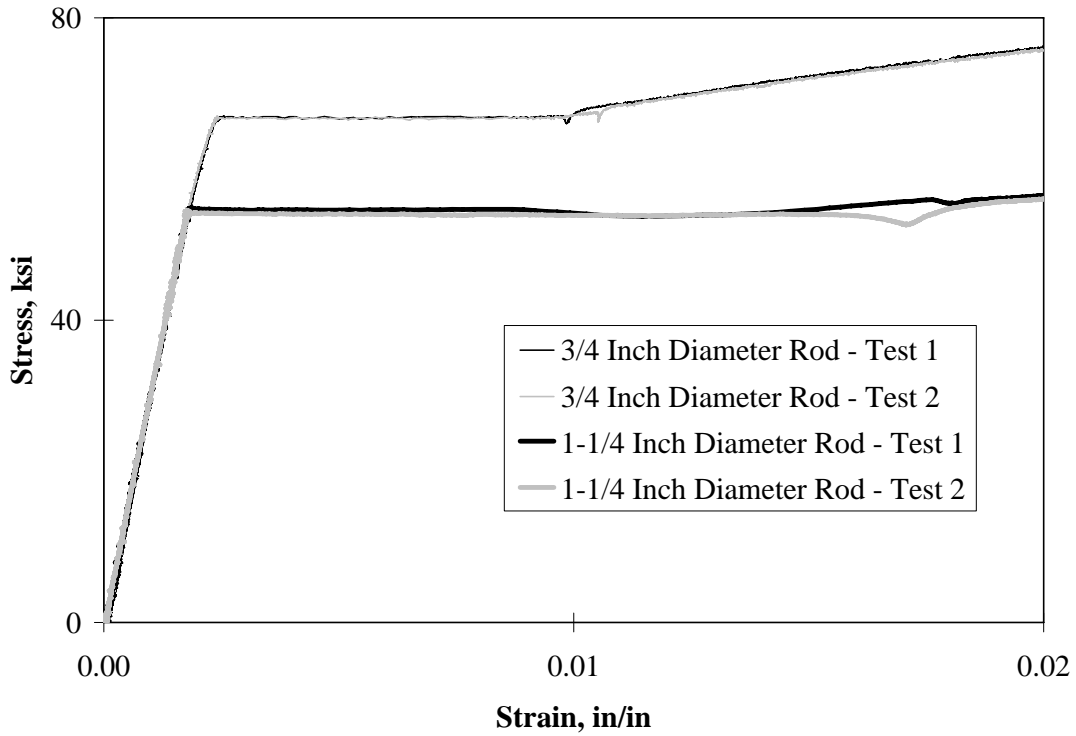[1]Measured yield stress, based on 0.2% offset method

Figure A.1 – Stress-strain response of all anchor rod tension tests

Table A.2 – Concrete cylinder compressive strength test results

Specimen	Truck number	Corresponding large scale test number	Weight (lbs)	Cylinder area[1] (in[2])	Maximum compressive load (kips)	Twenty-eight day compressive strength (psi)
1a			28.50	28.274	136.75	4,837
1b		1, 2, 3 & 4	28.75	28.175	120.00	4,259
1c			28.50	28.128	130.00	4,622
2a			28.75	28.161	135.75	4,820
2b	1	5	28.70	28.185	134.25	4,763
2c			28.50	28.119	132.25	4,703
3a			28.50	28.086	138.00	4,913
3b		6	28.50	28.208	134.00	4,750
3c			28.25	28.138	121.00	4,300
4a			28.50	28.152	139.00	4,937
4b	2	7	28.50	28.166	142.00	5,042
4c			28.25	28.138	144.00	5,118

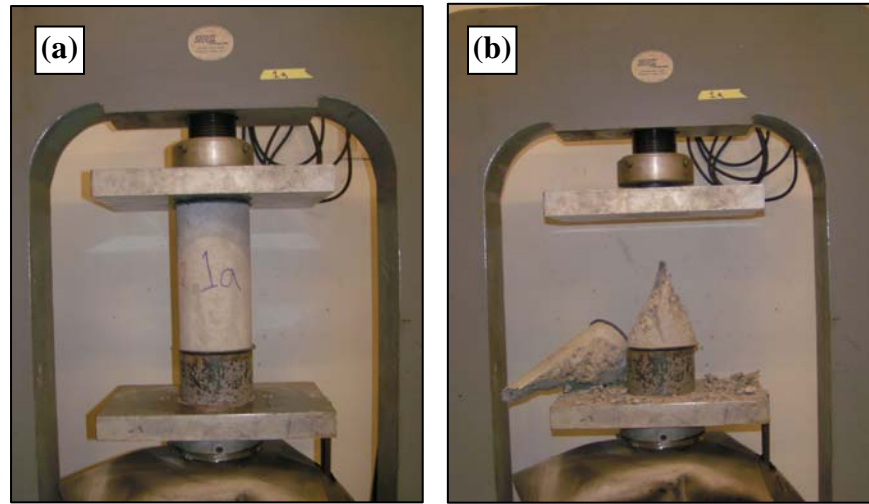[1]Nominal cylinder size = 6" diameter, 12" height

Figure A.2 – Photographs showing representative concrete cylinder test (a) before and (b) after failure

Table A.3 – Grout cylinder compressive strength test results

Specimen	Approx. cure time (days)	Water content (gallons per 50 lbs grout)	Corresponding large scale test number	Weight (pounds)	Cylinder area[1] (in²)	Maximum compressive load (kips)	Compressive strength (psi)
A1	4.5	0.875		3.16	7.13	33.25	4,662
A2	4.5	0.875	4	3.21	7.11	42.00	5,906
A3	4.5	0.875		3.26	7.09	50.00	7,057
A4	4.5	0.875		3.23	7.10	49.00	6,904
A5	7.0	0.875		3.21	7.11	50.50	7,104
A6	7.0	0.875	5	3.18	7.10	42.00	5,916
A7	7.0	0.875		3.25	7.10	54.50	7,679
A8	7.0	0.875		3.24	7.12	58.00	8,151
B1	7.0	1.000		3.15	7.07	43.25	6,117
B2	7.0	1.000	3	3.13	7.10	48.00	6,761
B3	7.0	1.000		3.15	7.10	44.00	6,198
B4	7.0	1.000		3.14	7.10	41.50	5,842
B5	9.0	1.000		3.15	7.10	49.00	6,900
B6	9.0	1.000	1	3.14	7.06	45.50	6,443
B7	9.0	1.000		3.16	7.11	35.50	4,996
B8	9.0	1.000		3.12	7.10	34.00	4,788
B9	13.0	1.000		3.09	7.14	51.50	7,216
B10	13.0	1.000	2	3.18	7.07	56.00	7,917
B11	13.0	1.000		3.10	7.11	50.50	7,102
B12	13.0	1.000		3.17	7.09	43.00	6,065
C1	7.0	1.125		3.13	7.08	33.50	4,731
C2	7.0	1.125	7	3.13	7.10	41.00	5,777
C3	7.0	1.125		3.12	7.09	45.00	6,349
C4	7.0	1.125		3.13	7.11	45.00	6,330
C5	9.0	1.125		3.10	7.10	41.00	5,771
C6	9.0	1.125	6	3.11	7.09	48.00	6,775
C7	9.0	1.125		3.12	7.09	35.00	4,933
C8	9.0	1.125		3.12	7.09	47.00	6,625

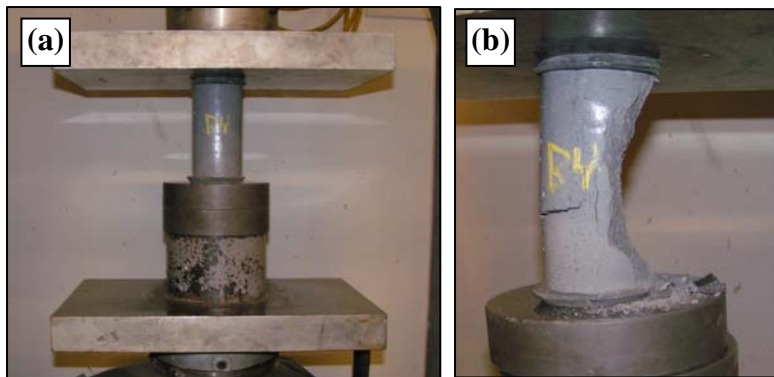[1]Nominal cylinder size = 3" diameter, 6" height

Figure A.3 – Photographs showing representative grout cylinder test (a) before and (b) after failure

BASF
The Chemical Company

PRODUCT DATA

3 03 62 13   **Non-Metallic Non-Shink Grouting**

CONSTRUCTION GROUT
General construction, mineral-aggregate nonshrink grout

Description

Construction Grout is a noncatalyzed, multi-purpose construction grout containing mineral aggregate.

Yield

One 50 lb (22.7 kg) bag of Construction Grout mixed with 1.15 gallons (4.35 L) of water (flowable mix) provides approximately 0.45 ft³ (0.013 m³) of mixed grout.

Packaging

50 lb (22.7 kg) multi-wall paper bags

Color

Concrete gray when cured

Shelf Life

1 year when properly stored

Storage

Store in unopened bags under clean, dry conditions.

Features

- Concrete gray color (after curing)
- No organic accelerators, including chlorides or other salts
- Can be extended with clean, well-graded coarse aggregate
- Hardens free of bleeding when properly placed

Where to Use

APPLICATION

- Normal loads for columns and baseplates
- Bedding grout for precast panels
- Repairing of cavities resulting from ineffective concrete consolidation
- Caulking concrete pipe
- Backfilling, underpinning foundations, and pressure grouting of slabs needing alignment
- General construction applications
- Damp pack applications

LOCATION

- Interior or exterior

How to Apply

Application

For aggregate extension guidelines refer to Appendix MB-10: Guide to Cementitious Grouting.

Mixing

By using the minimum amount of water to provide the desired workability, maximum strength will be achieved. Whenever possible, mix the grout with a mechanical mixer. Either a mortar mixer or an electric drill with a paddle device is acceptable. Put the measured amount of water into the mixer, add grout, then mix till a uniform consistency is attained. Do not use water in an amount or a temperature that will cause bleeding or segregation.

Benefits

Blends in with surrounding concrete

Will not corrode reinforcing steel

Fills large voids without additional mix water

Provides high effective bearing area for proper support and load transfer

Curing

Cure all exposed grout shoulders by wet curing for 24 hours and by applying a recommended curing compound compliant with ASTM C 309 or preferably ASTM C 1315.

For Best Performance

- Contact your local representative for a pre-job conference to plan the installation.
- Construction Grout is designed for the 50 to 90° F (10 to 32° C) application temperature range. Consult your BASF representative when applying outside this range. Use cold and hot weather concreting practices (ACI 305 and ACI 306) when grouting within 10° F (6° C) of these minimum and maximum temperature ranges.
- To ensure optimum performance of Construction Grout, place at a plastic or flowable consistency and at ambient temperatures of 50° F (10° C) and above.
- For best results, allow a minimum of 1" (25 mm) vertical clearance under baseplates when placing Construction Grout.
- Do not use Construction Grout where it will come in contact with steel designed for stresses above 80,000 psi (552 MPa). Use Masterflow® 816, Masterflow® 1205, or Masterflow® 1341 post-tensioning cable grouts.

Figure A.4 – Grout product data from manufacturer (first page)

MBT PROTECTION & REPAIR PRODUCT DATA
CONSTRUCTION GROUT

Technical Data

Composition

Construction Grout is a noncatalyzed hydraulic cement-based grout containing mineral aggregate.

Compliances

- CRD C 621 and ASTM C 1107, Grade C, at flowable or plastic consistency
- City of Los Angeles Research Report Number RR 23137

Typical Properties

Mixed Grout Data* (Flowable Mix)

PROPERTY	VALUE
Approximate Water, gal (L)	1.15 (4.35)
Initial set, hrs, at 70° F (21° C)	6
Final set, hrs, at 70° F (21° C)	8

*At a constant percent of water, consistency will vary with temperature. Final set takes place in approximately 8 hours at a flowable consistency and 70° F (21° C).

Test Data

PROPERTY	RESULTS	TEST METHODS
Flow, %, 5 drops	126 – 145	ASTM C 230
Volume change, %, flowable consistency, after 28 days	0.08	ASTM C 1090
Compressive strength, psi (MPa)		ASTM C 942, according to ASTM C 1107

	Flowable[1]	Consistency Plastic[2]	Stiff[3] (damp pack)
1 day	1,500 (10)	—	—
3 days	5,000 (34.5)	6,000 (41.4)	8,000 (55.2)
7 days	6,000 (41.3)	7,000 (48.3)	9,500 (65.5)
28 days	7,000 (48.0)	8,500 (58.6)	10,000 (69.0)

[1] 140% flow on flow table, ASTM C 230, 5 drops in 3 seconds
[2] 100% flow on flow table, ASTM C 230, 5 drops in 3 seconds
[3] 40% flow on flow table, ASTM C 230, 5 drops in 3 seconds
Test results are averages obtained under laboratory conditions. Reasonable variations can be expected.

- Do not add plasticizers, accelerators, retarders, or other additives unless advised in writing by BASF Technical Services.
- The surface to be grouted should be clean, strong, and roughened to CSP 5 – 9 according to ICRI Guideline 03732 to permit proper bond. For freshly placed concrete, consider using Liquid Surface Etchant (see Form No. 1020198).
- Do not place Construction Grout in lifts greater than 6" (152 mm) unless the product is extended with aggregate to dissipate hydration heat.
- Where precision alignment and severe service, such as heavy loading, rolling, or impact resistance are required, use metallic-reinforced, noncatalyzed Embeco® 885 grout. If the amount of impact resistance needed is not great enough to require metallic reinforcement, use natural-aggregate, Masterflow® 928.
- The water requirement may vary with mixing efficiency, temperature, and other variables.
- The concrete surfaces should be saturated (ponded) with clean water for 24 hours before grouting. Remove water immediately before application.
- Make certain the most current versions of product data sheet and MSDS are being used; call Customer Service (1-800-433-9517) to verify the most current versions.

- Proper application is the responsibility of the user. Field visits by BASF personnel are for the purpose of making technical recommendations only and not for supervising or providing quality control on the jobsite.

Health and Safety

CONSTRUCTION GROUT

WARNING!

Construction Grout contains silica, crystalline quartz; portland cement; limestone; calcium oxide; gypsum; silica, amorphous.

Risks

Product is alkaline on contact with water and may cause injury to skin or eyes. Ingestion or inhalation of dust may cause irritation. Contains small amount of free respirable quartz which has been listed as a suspected human carcinogen by NTP and IARC. Repeated or prolonged overexposure to free respirable quartz may cause silicosis or other serious and delayed lung injury.

Precautions

Avoid contact with skin, eyes and clothing. Prevent inhalation of dust. Wash thoroughly after handling. Keep container closed when not in use. DO NOT take internally. Use only with adequate ventilation. Use impervious gloves, eye protection and if the TLV is exceeded or used in a poorly ventilated area, use NIOSH/MSHA approved respiratory protection in accordance with applicable Federal, state and local regulations.

First Aid

In case of eye contact, flush thoroughly with water for at least 15 minutes. In case of skin contact, wash affected areas with soap and water. If irritation persists, SEEK MEDICAL ATTENTION. Remove and wash contaminated clothing. If inhalation causes physical discomfort, remove to fresh air. If discomfort persists or any breathing difficulty occurs or if swallowed, SEEK IMMEDIATE MEDICAL ATTENTION.

Waste Disposal Method

This product when discarded or disposed of is not listed as a hazardous waste in federal regulations. Dispose of in a landfill in accordance with local regulations. For additional information on personal protective equipment, first aid, and emergency procedures, refer to the product Material Safety Data Sheet (MSDS) on the job site or contact the company at the address or phone numbers given below.

Proposition 65

This product contains material listed by the State of California as known to cause cancer, birth defects or other reproductive harm.

VOC Content

0 g/L or 0 lbs/gal less water and exempt solvents.

For medical emergencies only, call ChemTrec (1-800-424-9300).

Figure A.5 – Grout product data from manufacturer (second page)

Appendix B

Base Plate Test Data

GUIDE TO BASE PLATE TEST DATA

Frictional force – absolute value of the load recorded by lateral (horizontal) actuators for the surface friction tests

Lateral displacement – lateral displacement of the base plate measured from the displacement of the lateral (horizontal) actuators minus lateral displacement of concrete pedestal

Axial force – axial load recorded by vertical (axial) actuators minus the self weight of test assembly

"Time" – a representation of the progression of the test; since lateral displacement rate is approximately constant for most tests, this may be considered as the approximate cumulative lateral displacement

Effective coefficient of friction - frictional force normalized by the axial compression load

Lateral load – load recorded by lateral (horizontal) actuators

Vertical uplift – vertical (axial) displacement of the base plate averaged from four locations

Lateral slip – lateral displacement of the base plate for the shear key tests
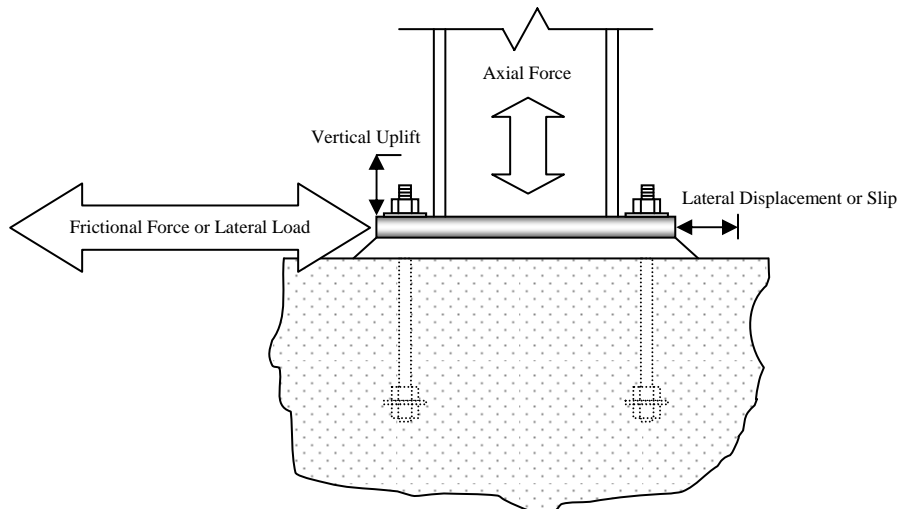

Figure B.1 – Schematic illustrating definitions of base plate test data

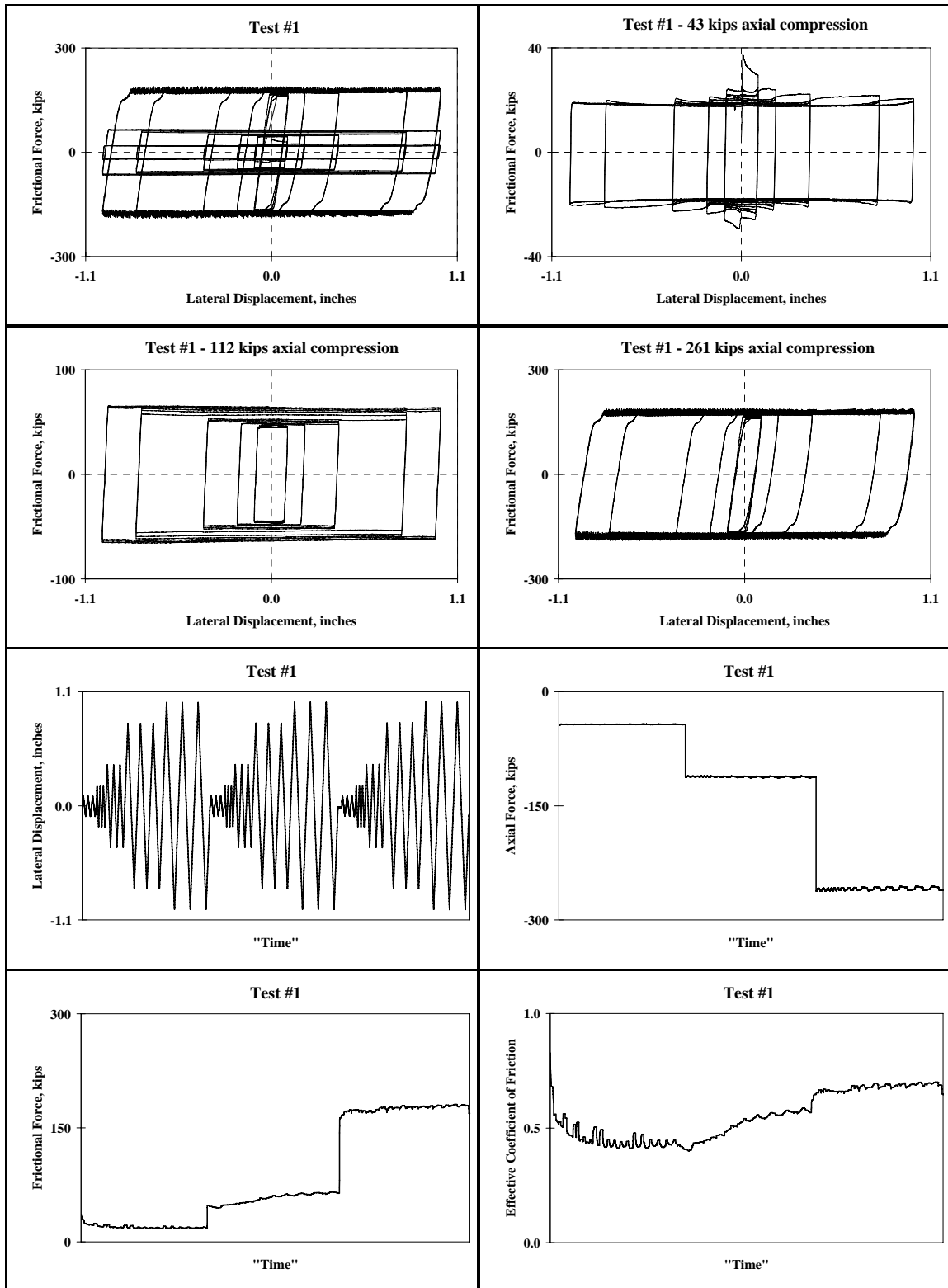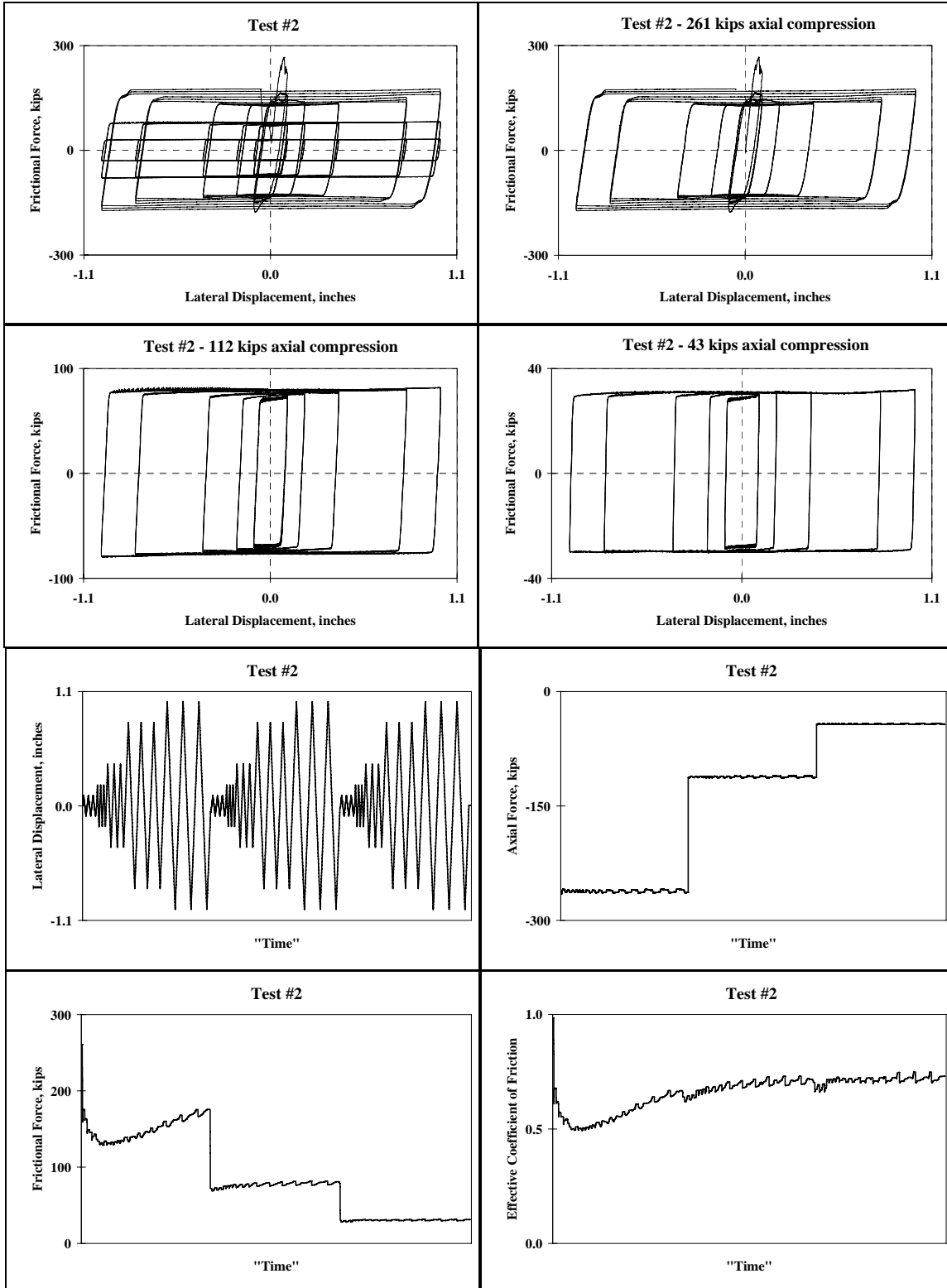**Figure B.2** – Data for Test #1 – Surface friction with shim stacks

Figure B.3 – Date for Test #2 – Surface friction with shim stacks
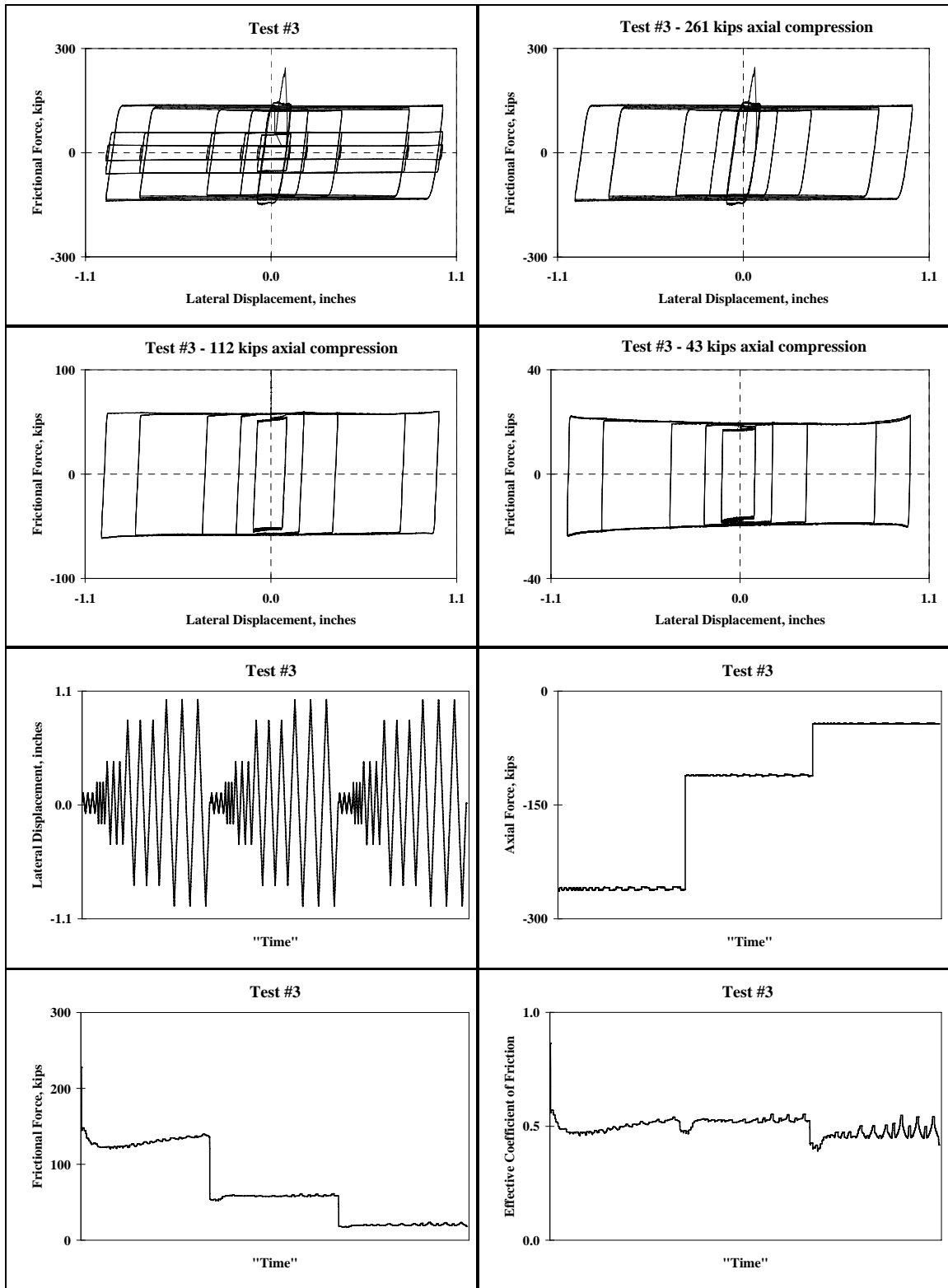
Figure B.4 – Data for Test #3 – Surface friction without shim stacks
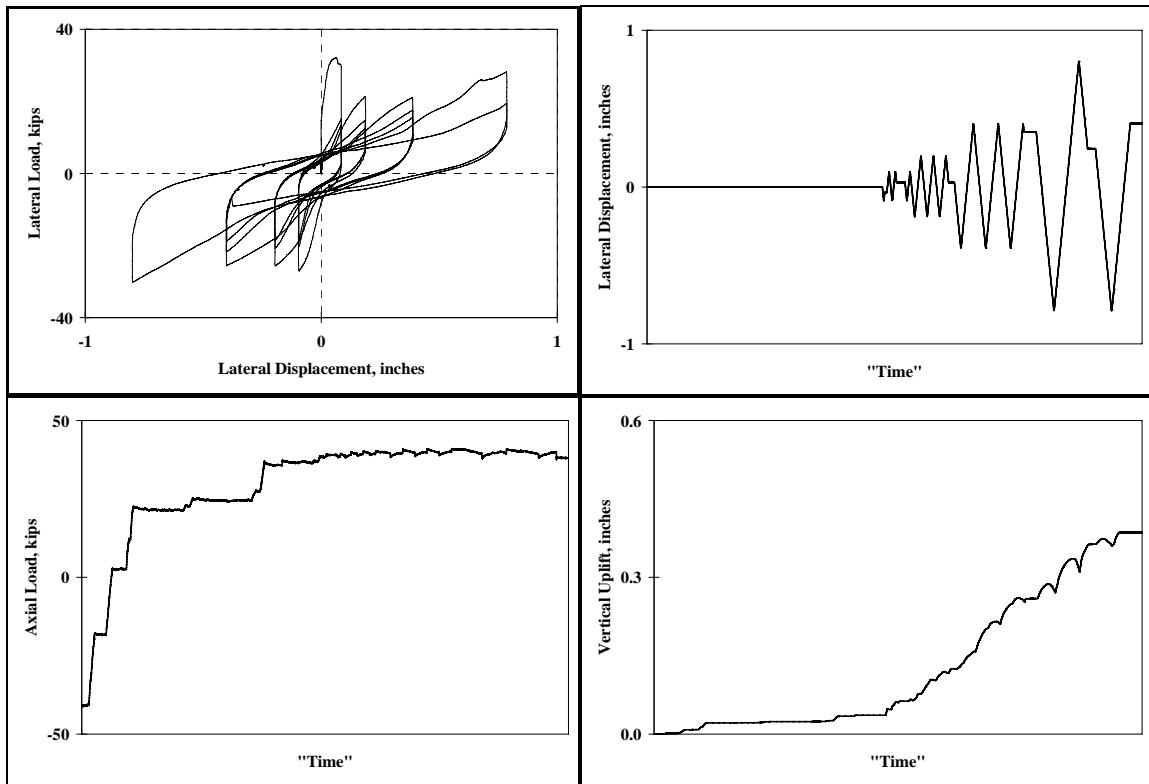
Figure B.5 – Data for Test #4 – 3/4" diameter anchor rod bearing
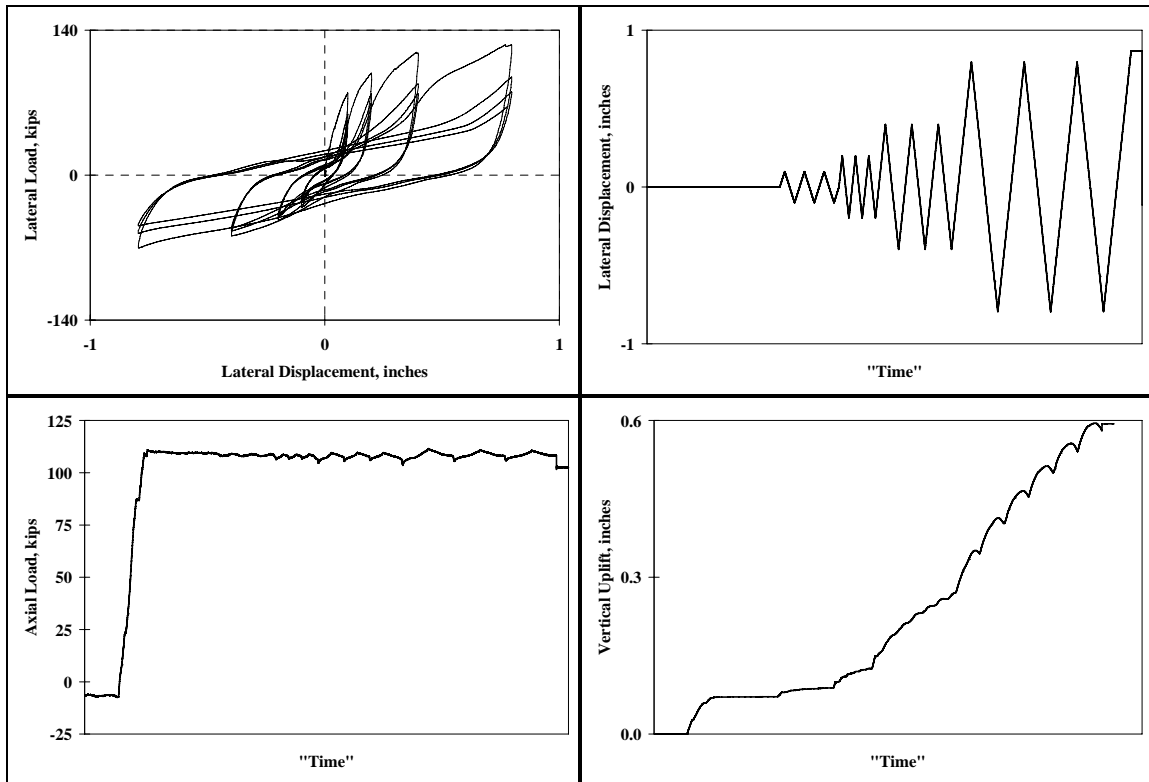
Figure B.6 – Data for Test #5 – 1-1/4" diameter anchor rod bearing

Figure B.7 – Data for Test #6 – shear key bearing – 5.5" embedment – positive loading direction
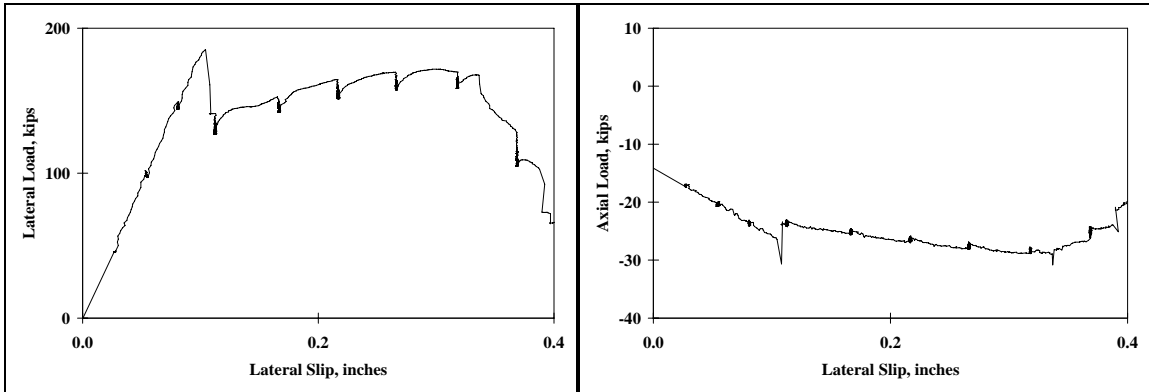
Figure B.8 – Data for Test #6 – shear key bearing – 5.5" embedment – negative loading direction
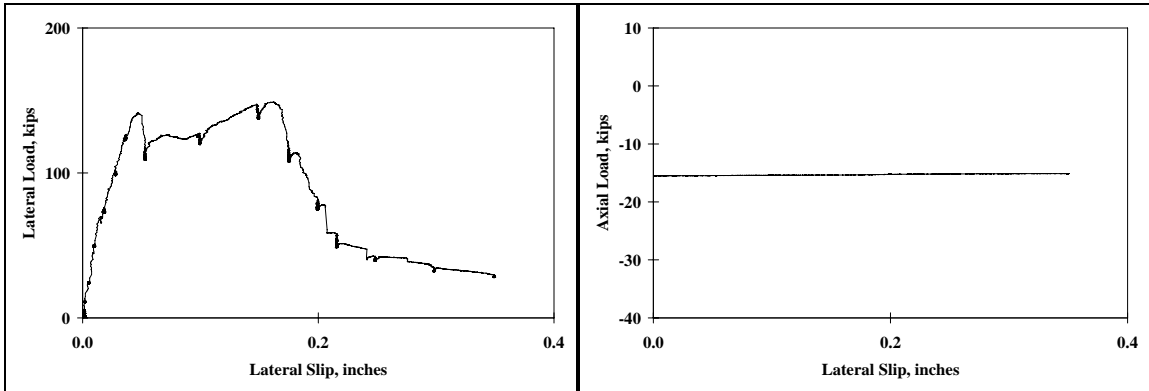
Figure B.9 – Data for Test #7 – shear key bearing – 3.0" embedment – positive loading direction
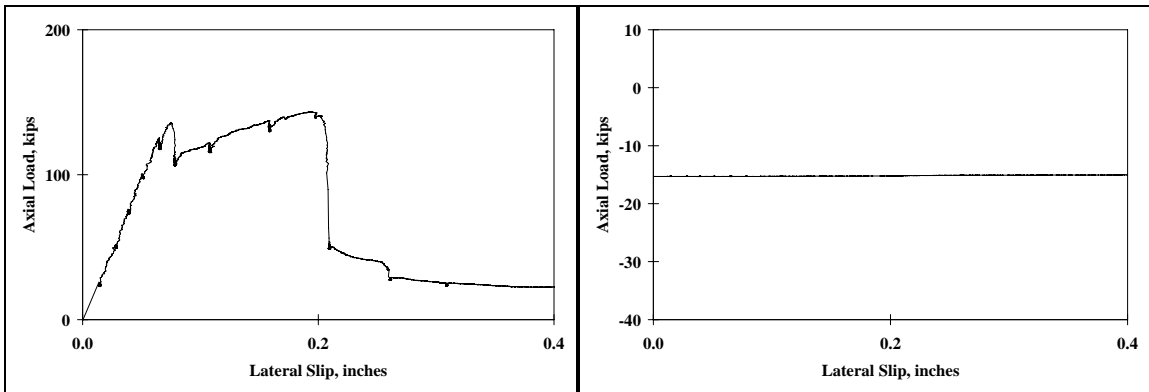
Figure B.10 – Data for Test #7 – shear key bearing – 3.0" embedment – negative loading direction
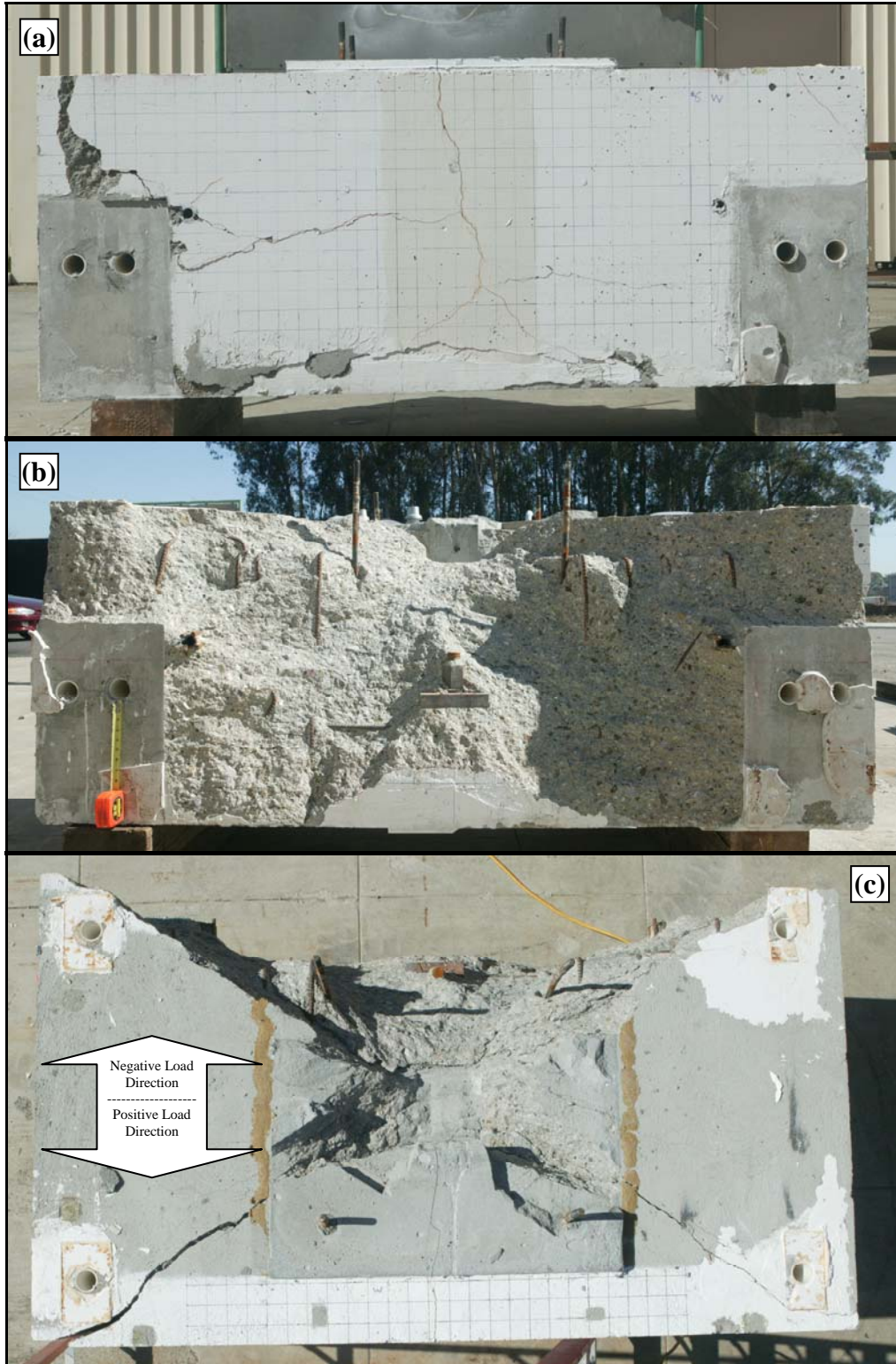
Figure B.11 – Photograph showing post test condition (negative load direction side extracted) of pedestal from Test #6 – 5.5" shear key embedment depth (a) elevation view of positive load direction side (b) elevation view of negative load direction side (c) plan view
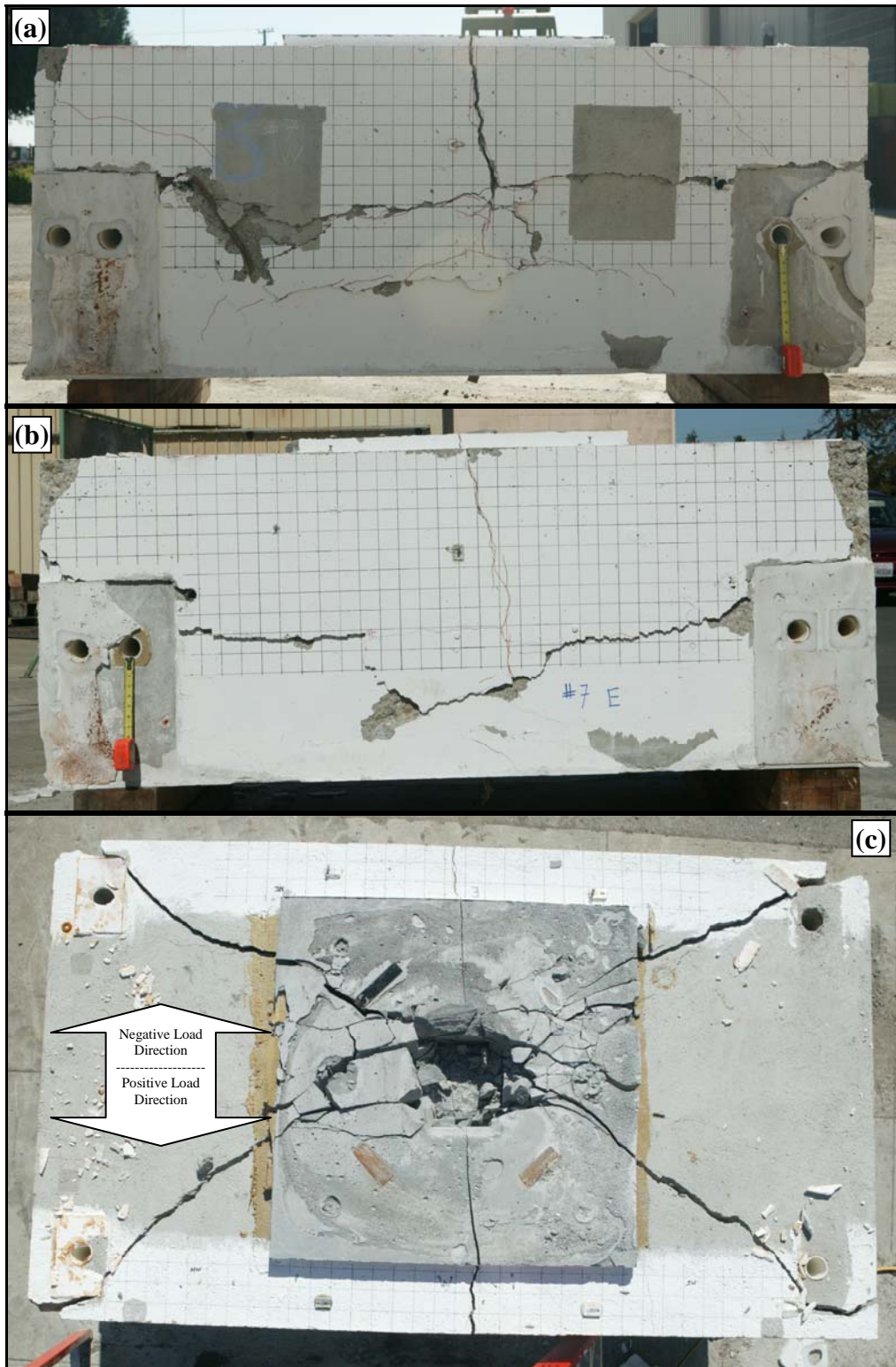
Figure B.12 – Photograph showing post test condition of pedestal from Test #7 – 3.0" shear key embedment depth (a) elevation view of positive load direction side (b) elevation view of negative load direction side (c) plan view
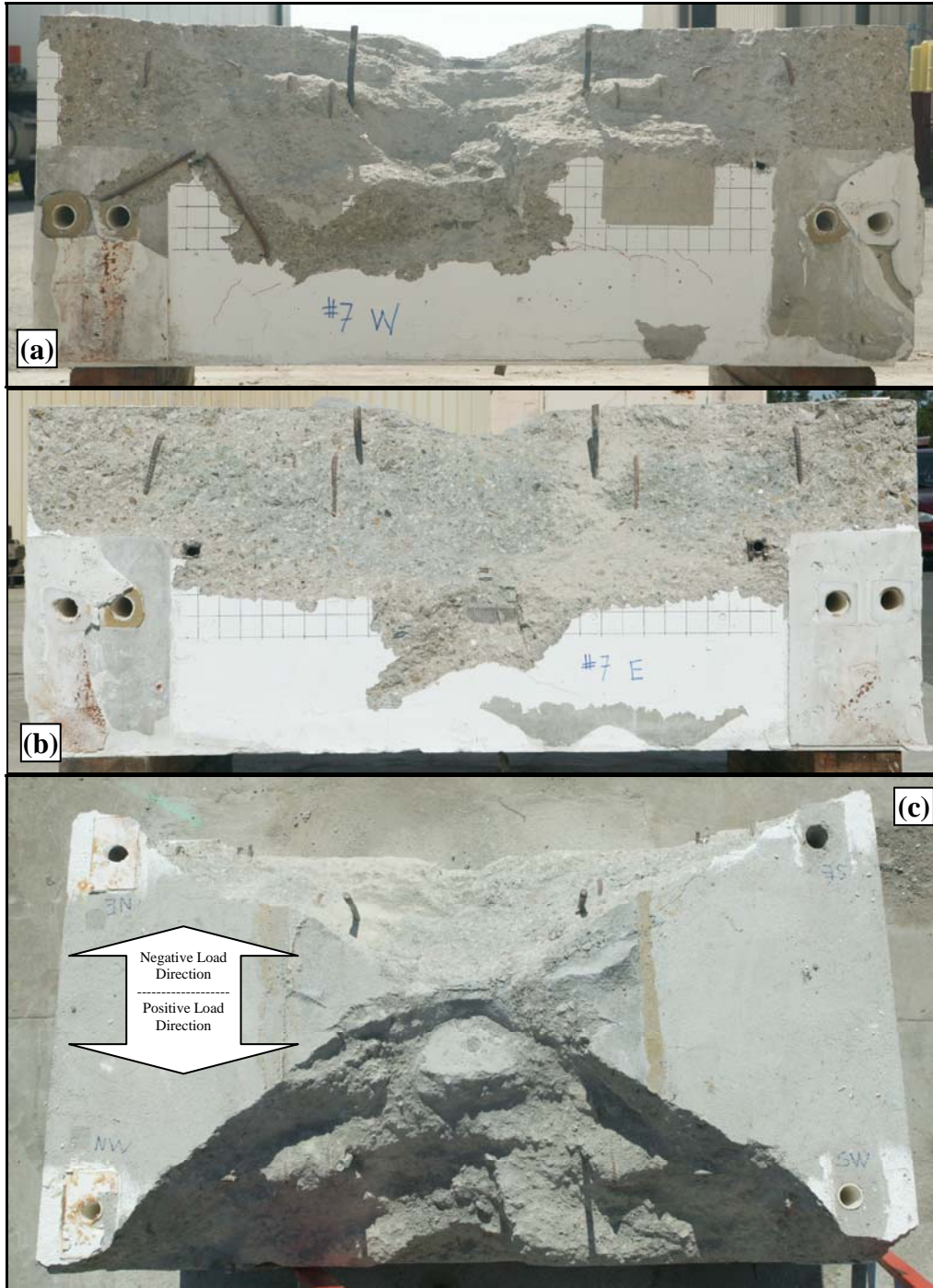
Figure B.13 – Photograph showing post test condition (failure surfaces extracted) of pedestal from Test #7 – 3.0" shear key embedment depth (a) elevation view of positive load direction side (b) elevation view of negative load direction side (c) plan view
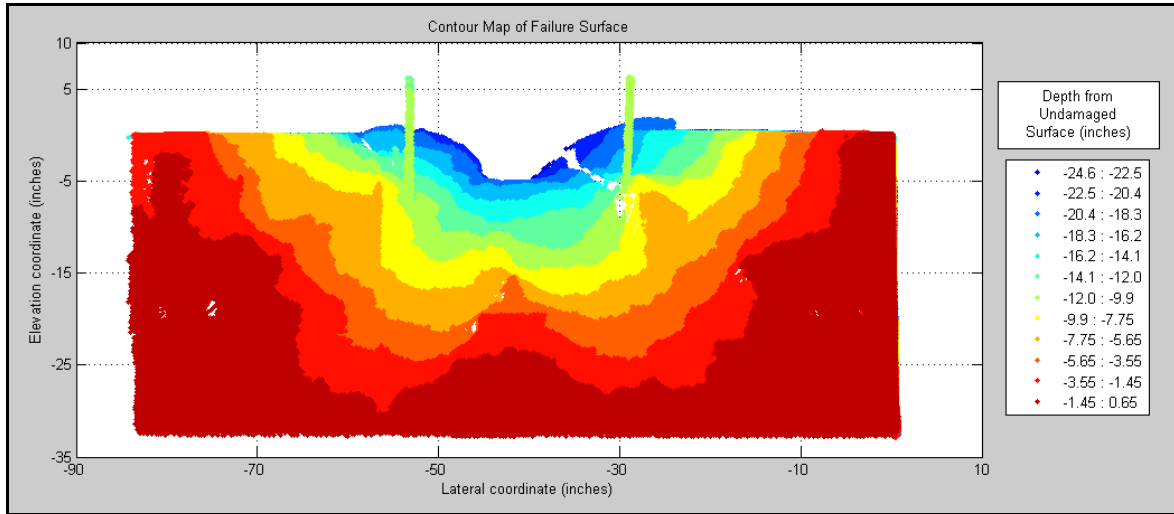
Figure B.14 – Contour map of Test #6 (5.5" shear key embedment depth - negative load direction) failure surface recorded by HD laser scanner

Appendix C

Anchor Rod Capacity Theory and Examples

C.1 DEVELOPMENT OF ANCHOR ROD CAPACITY EQUATION CONSIDERING SHEAR AND TENSION LOADING

According to the American Institute of Steel Construction (AISC, 2005), tests have shown that the strength of bearing fasteners subject to combined shear and tension resulting from externally applied forces can be closely defined by an ellipse (Kulak *et al.*, 1987). The relationship, based on AISC (2005) Equation [C-J3-5a], is expressed as

$$\left(\frac{f_t}{F_{nt}} \right)^2 + \left(\frac{f_v}{F_{nv}} \right)^2 = 1 \qquad \text{[C.1]}$$

Where: F_{nt}, F_{nv} = nominal tensile stress and shear stress, respectively

                 f_t, f_v = required tensile and shear stress, respectively

From AISC (2005) Equation [C-J3-2], the nominal tensile stress of a bolt is expressed as

$$F_{nt} = 0.75 F_u \qquad \text{[C.2]}$$

Where: F_u = ultimate tensile stress of bolt

            0.75 = a factor accounting for the approximate ratio of the effective area of the threaded portion of the rod to the area of the shank of the bolt for common rod sizes

From AISC (2005) Equation [C-J3-3], the nominal shear stress, when the threads are included in the shear plane, is expressed as

$$F_{nv} = 0.40 F_u \qquad \text{[C.3]}$$

Where: 0.40 = a factor accounting for the effect of shear and for the reduced area of the threaded portion of the fastener when the threads are not excluded from the shear plane; AISC (2005) makes this value conservative for the threaded portion by 11.1% (e.g. the typical shear factor considering the reduced area is $0.75 * 0.6 = 0.45$).

The required shear stress is expressed as

$$f_v = \frac{V}{nA} \qquad \text{[C.4]}$$

Where: V = applied shear load

n = number of rods

A = unthreaded area of rod = $0.25\,\pi\,d^2$

d = unthreaded diameter of anchor rod

The required tensile stress, based solely on tensile forces in the rod, is expressed as

$$f_t = \frac{P}{nA} \qquad \text{[C.5]}$$

Where: P = applied axial load

Solving Equations [C.1] - [C.5] for shear load provides

$$V = 0.4 \sqrt{\left(0.25 \pi d^2 n F_u\right)^2 - \left(\frac{16}{9}\right) P^2}$$

[C.6]

C.2 DEVELOPMENT OF ANCHOR ROD CAPACITY EQUATION CONSIDERING SHEAR AND TENSION PLUS FLEXURAL LOADING

The strength of bearing fasteners subject to combined shear, tension and flexure loading is identical to Equations [C.1] – [C.4] except that the required tensile stress is based on tensile loading plus bending. Thus, the required tensile stress is expressed as

$$f_t = f_{ta} + f_{tb}$$

[C.7]

Where: f_{ta} = the required axial stress from axial loading

f_{tb} = the required axial stress from bending

The required axial stress from the axial load is expressed as

$$f_{ta} = \frac{P}{nA}$$

[C.8]

The required axial stress from bending is expressed as

$$f_{tb} = \frac{M_l}{nZ}$$

[C.9]

Where: M_l = resisting moment of the rod

Z = plastic section modulus of circular cross section = $\dfrac{d^3}{6}$

The resisting moment of a rod, taken from beam theory, is expressed as

$$M_l = klV \tag{C.10}$$

Where: k = "effective length" factor of the rod (i.e. lever arm factor)

            l = length of rod in bending

Solving Equations [C.1] - [C.5] and [C.7] - [C.10] for shear load provides

$$V = \frac{d^2\sqrt{\left(12\pi^2 k l F_u n d\right)^2 + \left(15\pi F_u n d^2\right)^2 - \left(80P\right)^2} - 64\pi P k l d}{96\left(\pi k l\right)^2 + 150 d^2} \tag{C.11}$$

C.3 VARIATIONS ON THE ANCHOR ROD CAPACITY EQUATION

Two possible variations exist to estimate the capacity of an anchor rod. The first variation uses the measured, rather than the nominal, anchor rod diameter. Recall in Equation [C.2] the AISC Steel Construction Manual (2005) uses 75% of the nominal rod area for the tensile stress area as well as another similar reduction factor for the shear stress area (see Equation [C.3]). Table 7-18 in the AISC Manual (2005) lists the minimum root diameter for common bolts. If the minimum root diameter (measured rod diameter) is used, the rod capacity equation considering tension, shear and flexural stress can be expressed as –

$$\left(\frac{4P}{\pi d_u^2} + \frac{6klV}{d_u^3}\right)^2 + \left(\frac{V}{0.15\pi d_u^2}\right)^2 = \left(nF_u\right)^2 \tag{C.12}$$

Where: d_u = threaded diameter of anchor rod

Additionally, the AISC Steel Construction Manual (2005) states the elliptical relationship of Equation [C.1] can be replaced by a trilinear relationship as follows –

$$\left(\frac{f_t}{F_{nt}}\right) + \left(\frac{f_v}{F_{nv}}\right) = 1.3$$

$$f_t \le F_{nt}; f_v \le F_{nv}$$

[C.13]

The AISC Manual (2005) describes that this representation offers the advantage that no modification of either type of stress is required in the presence of fairly large magnitudes of the other type.

C.4 ANCHOR ROD CAPACITY EXAMPLES

Twelve methods are considered to estimate the predicted strength of the anchor rods in a grouted base plate connection (with welded plate washers) under shear and tension loading. The first four estimates of strength ($R^{PV}_{no\min al,eliptical}$, $R^{PV}_{measued,eliptical}$, $R^{PV}_{no\min al,trilinear}$, $R^{PV}_{measued,trilinear}$) disregards anchor rod bending, but instead considers only the interaction between axial force and shear; measured and nominal rod diameters, as well as ellipse and trilinear stress interaction relationships, are considered. The last eight estimates of strength reflect the interaction of axial, shear and flexure loading in which the anchor rod is assumed to deform in double curvature. Thus, the "effective length" factor of the rod (i.e. lever arm factor) "k" is assumed as 0.5. The determination of the bending strength also relies on an estimate of the length over which this reverse curvature bending occurs. The AISC *Design Guide 1* (Fisher & Kloiber, 2006) assumes that full end fixity is obtained within the grout pad and rod bolted end, such that the bending length is calculated as the distance between the top of the grout pad (i.e. bottom of the base plate) to the center of the welded plate washer. The estimate of strength corresponding to this bending length, considering measured and nominal rod diameters, as well as ellipse and trilinear stress interaction relationships, is designated as $R^{PVM}_{no\min al,eliptical}$, $R^{PVM}_{measured,eliptical}$, $R^{PVM}_{no\min al,trilinear}$ or $R^{PVM}_{measured,trilinear}$. Based on experimental observations, including evidence of extensive damage to the grout from cyclic base plate slip which may preclude full end

fixity provided by the grout, an alternate bending length is estimated as the distance between the top of the *concrete* surface to the center of the welded plate washer. The estimate of strength corresponding to this bending length (as well as considering measured and nominal rod diameters, and ellipse and trilinear stress interaction relationships), is designated as $R_{nominal,eliptical}^{PVM*}$, $R_{measured,eliptical}^{PVM*}$, $R_{nominal,trilinear}^{PVM*}$, $R_{measured,trilinear}^{PVM*}$.

Table C.1 tabulates values of the geometry of the base plate connection which details the rod length in bending for all strength estimates and large scale tests. Furthermore, Table C.2 lists variables and parameters from the two large scale tests used to calculate the twelve estimates of anchor rod strength, as well as results of these estimates.

Table C.1 – Details of rod bending length

Test Number	4	5
Average thickness of grout (inches)	1.25	1.00
Thickness of base plate (inches)	2.00	2.00
Thickness of the welded plate washer (inches)	0.25	0.5
Length of bending "l" for R^{PVM} estimate[1] (inches)	2.125	2.25
Length of bending "l" for R^{PVM*} estimate[2] (inches)	3.375	3.25

[1] Calculated as the thickness of the base plate plus half the thickness of the welded plate washer
[2] Calculated as the thickness of the grout pad plus the thickness of the base plate plus half the thickness of the welded plate washer

Table C.2 – Details of anchor rod strength estimate calculations

Test Number	4	5
Anchor rod unthreaded diameter "d" (inches)	0.75	1.25
Anchor rod threaded diameter "d_u" (inches)	0.64	1.10
Ultimate tensile stress of rod "F_u"[1] (ksi)	96.43	74.96
Number of rods "n"	4	4
Effective length factor "k"	0.5	0.5
Imposed axial load "P" (kips)	39.6	108
Rod strength "$R^{PV}_{nominal,eliptical}$" as per Equation [C.6] (kips)	64.8	135
Rod strength "$R^{PVM}_{nominal,eliptical}$" as per Equation [C.11][2] (kips)	12.9	37.5
Rod strength "$R^{PVM*}_{nominal,eliptical}$" as per Equation [C.11][3] (kips)	8.23	26.7
Rod strength "$R^{PV}_{measued,eliptical}$" as per Equation [C.12] (kips)	71.1	158
Rod strength "$R^{PVM}_{measured,eliptical}$" as per Equation [C.12][2] (kips)	10.8	35.5
Rod strength "$R^{PVM*}_{measured,eliptical}$" as per Equation [C.12][3] (kips)	6.84	25.0
Rod strength "$R^{PV}_{nominal,trilinear}$" as per Equation [C.13] (kips)	65.7	134
Rod strength "$R^{PVM}_{nominal,trilinear}$" as per Equation [C.13][2] (kips)	13.2	39.6
Rod strength "$R^{PVM*}_{nominal,trilinear}$" as per Equation [C.13][3] (kips)	8.31	27.4
Rod strength "$R^{PV}_{measued,trilinear}$" as per Equation [C.13] (kips)	73.6	157
Rod strength "$R^{PVM}_{measured,trilinear}$" as per Equation [C.13][2] (kips)	10.9	6.88
Rod strength "$R^{PVM*}_{measured,trilinear}$" as per Equation [C.13][3] (kips)	36.7	25.4
Observed anchor rod peak strength, positive direction "R_{peak}" (kips)	30.2	126
Observed anchor rod peak strength, reverse direction "$R^{reversed}_{peak}$" (kips)	28.2	70.4

[1] Determined by ancillary tension tests of the anchor rods
[2] Using a length of bending equal to 2.125" for Test #4 and 2.25" for Test #5
[3] Using a length of bending equal to 3.375" for Test #4 and 3.25" for Test #5

Appendix D

Analysis of Anchor Rod Response

D.1 INTRODUCTION

Recall from Chapter 3 that the load-deformation response of the base plate tests investigating anchor rod strength (Tests #4 and #5) is highly complex. In addition, the response does not demonstrate a well defined peak. Thus, it is somewhat challenging to characterize the strength capacity associated with anchor rod failure. The strength is influenced by the interaction of several phenomena, including (1) increased tension forces of the rods due to large deformations (i.e. geometric second order effects) (2) strength and stiffness degradation due to grout damage and (3) anchor rod contact within the base plate holes (rather than with the welded plate washers). In addition to the difficulty in measuring a peak capacity, these complex interactions necessitate a subjective (rather than a quantitative) evaluation of strength prediction approaches, since distinct failure modes are not observed. Motivated by these issues, this Appendix presents a simplified nonlinear analysis of the anchor rods, incorporating the effects of axial force, moment and shear interaction as well as geometric nonlinearities introduced by deformation of the anchor rods under large displacements. The main objectives of this analysis are to –

1. Complement experimental data and visual observations by developing an understanding of the key factors that affect the response of anchor rods under the combined actions of axial stress, bending and shear.

2. Develop insights into the relative contributions of the various phenomena that influence response.

3. Examine the influence of important parameters, such as the effective bending length on the response.

D.2 SIMPLIFIED NONLINEAR ANALYSIS OF ANCHOR ROD STRENGTH UNDER COMBINED AXIAL FORCE, BENDING AND SHEAR

Figure D.1 schematically illustrates a deformed anchor rod within a base plate under shear loading. The rod is assumed to experience double curvature bending as observed experimentally (recall prior discussion in Chapter 3). Figure D.2 presents a detailed schematic of the anchor rod free-body diagram with geometric parameters such as the lateral displacement Δ (relative to the concrete footing), the length of bending $L_{effective}$ and an effective angle of rod rotation θ, which can be approximately[1] expressed as –

$$\theta = \arctan(\Delta/L) \qquad [\text{D.1}]$$

Figure D.4 shows the free-body diagram of half of the bending length; V_1 and P_1 are the resultant shear and axial forces, respectively, at the inflection point of the rod. These resultant cross sectional shear and axial forces may be determined from the applied lateral load V and tensile load P by the following equations –

$$V_1 = V\cos\theta - P\sin\theta$$
$$P_1 = V\sin\theta + P\cos\theta \qquad [\text{D.2}]$$

Thus, the applied shear stress at the cross section may be expressed as –

$$f_v = \frac{V_1}{nA} \qquad [\text{D.3}]$$

Where: A_t = threaded area of rod = $0.25\,\pi d_t^{\,2}$

d_t = threaded diameter of anchor rod

---

[1] Assuming that a plastic hinge forms at the ends of the rods, whereby the rod is approximately aligned with its chord

The applied axial stress due to the axial force may expressed as –

$$f_{ta} = \frac{P_1}{nA_t}$$

[D.4]

The axial stress from bending may be expressed as –

$$f_{tb} = \frac{M_l}{nZ_t}$$

[D.5]

Where: M_l = moment resisted by the rod

Z_t = plastic section modulus of threaded cross section = $\dfrac{d_t^3}{6}$

Based on equilibrium on the assumed deformed anchor rod shape, the resisting moment of a rod may be expressed as -

$$M_l = \left(V \times L_{effective} - P \times \Delta\right)/2$$

[D.6]

An adaptation of the AISC (2005) interaction equation for bearing fasteners (also referenced in the AISC *Steel Design Guide Series 1* [Fisher & Kloiber, 2006]) [2] is expressed as –

$$\left(\frac{f_{ta} + f_{tb}}{F_{nt}}\right)^2 + \left(\frac{f_v}{0.6F_{nt}}\right)^2 = 1$$

[D.7]

Substituting Equations [D.1]-[D.6] into Equation [D.7] provides an equation which may be solved to generate a relationship between the applied shear force and the relative

---

[2] A trilinear relationship is often used as an approximation for the elliptical interaction equation presented here. The elliptical equation is utilized in this section.

deformation between the two ends of the anchor rod, i.e. $V = f(\Delta)$. While a closed form solution is available, it is very large and therefore is not presented. The resulting relationship represents a plastic limit state (an upper bound solution) describing the load versus displacement response of the anchor rods. Figures D.4 and D.5 illustrate these relationships overlaid on the experimental response for Tests #4 and #5, respectively. Referring to the figures, plastic limit state solutions are generated for three effective bending lengths, i.e. (1) the distance from the surface of the concrete to the middle of the plate washer, i.e. $L_{effective} = t_{plate} + t_{washer}/2$ (2) the distance from the top of the grout pad to the middle of the plate washer, i.e. $L_{effective} = t_{plate} + t_{washer}/2 + t_{grout}$ and (3) the distance from the surface of the concrete to the bottom of the base plate, i.e. $L_{effective} = t_{grout}$. The intersection of these solutions with the vertical axis (i.e. at $\Delta = 0$) represent the strength capacities calculated without the consideration of second order effects, such as described in Chapter 3 and Appendix C. Also overlaid on the plots is the initial elastic stiffness, which is expressed as –

$$k_{initial} = \frac{12EI_t}{L_{initial}^{3}} \qquad\qquad [\text{D.8}]$$

Where: E = Young's modulus

I_t = second moment of area of threaded cross section = $\dfrac{\pi d_t^{4}}{64}$

$L_{initial}$ = Effective bending length of the undeformed anchor rod, equal to the thickness of the base plate plus half the thickness of the plate washer

D.3 OBSERVATIONS FROM NONLINEAR ANALYSIS

A comparison of experimental data with respect to the plastic limit solutions generated in the previous section provides several useful insights into anchor rod response. Specific observations for each experiment are first outlined, before summarizing general

observations. Referring to Figure D.4, several observations may be made regarding the response of Test #4 –

1. The initial strength achieved by Test #4 is higher than predicted by any of the three plastic limit lines. Discussed previously in Chapter 3, all four holes in Test 4 contained some amount of grout. As expected, the presence of this grout restrains the anchor rods, resulting in very short bending lengths and correspondingly higher strengths.

2. Once this grout had broken and had been crushed by repetitive cyclic loading, the strength and stiffness of the experimental response degrades, possibly indicating that the rod loosens the grout around it and bends/yields over a progressively increasing length. It is interesting to note that the experimental hysteresis envelopes in the displacement range (-0.4 inch to +0.4 inch) are approximately coincident with the limit lines corresponding to $L_{effective} = t_{plate} + t_{washer}/2$ for the initial cycles and $L_{effective} = t_{plate} + t_{washer}/2 + t_{grout}$ for the subsequent cycles. This indicates that the strength degradation may be attributed to an increase in effective bending length of the anchor rods.

3. At larger displacements in both directions of loading (-0.5 inches and +0.5 inches), a significant increase in stiffness is observed. Several interesting observations may be made regarding this increased stiffness –

   a. This response is not captured by the second-order analysis, which considers tension stiffening in the deformed anchor rod. In fact, the second order analysis solution predicts similar abrupt stiffening at displacements of approximately 2 inches (outside the limits of Fig. D.4). The second order analysis is dominated by "$\tan\theta$" term, which appears linear for $\theta < 40^0$. For instance, the peak deformations observed in the tests are on the order of 15-20 degrees.

    b. The increase in stiffness, observed in the experiment, occurs at different displacements in the positive and negative directions. On the other hand, tension stiffening predicted by the analysis does not predict this type of unsymmetrical response.

    c. The increased stiffness is roughly equal to that predicted by the limit solution corresponding to $L_{effective} = t_{grout}$

The three points discussed above indicate that the increase in stiffness may be attributed to the base plate impinging (i.e. making contacting) upon the anchor rod, thereby reducing the bending length, rather than tension stiffening (which would become dominant at significantly larger deformations and exhibit symmetric response with respect to the displacements).

Recall that grout was completely removed from the base plate holes in Test #5. However, in Test #5, the clearance between the anchor rods and hole was smaller as compared to Test #4 (due to the larger rod diameter). Moreover, rods were placed with a larger degree of eccentricity with respect to the center of the hole, such that they were very close (almost flush) to the edge of the base plate hole in one loading direction (corresponding to the positive quadrant of Fig. D.5). Referring to Fig. D.5 and prior discussion in Chapter 3, several observations may be made regarding the response of Test #5 –

1. In the "positive" loading direction (with respect to Fig. D.5), the limit solution corresponding to $L_{effective} = t_{grout}$ results in a reasonably accurate prediction of the envelope response. This, along with measurements of the rod placement, suggests that once the base plate made contact with some (or all) rods, the rod was subjected to flexure below the surface of the base plate, i.e. within the thickness of the grout.

2. Conversely, in the opposite loading direction (where a larger clearance was available between the plate and the anchor rods) the limit solution corresponding

to $L_{effective} = t_{plate} + t_{washer}/2$ provides a good initial estimate of the observed response.

3. Progressive cyclic loading degraded the strength as well as the stiffness of the specimen, such that the degraded envelope (prior to the plate making contact with the rod) in both directions is approximated by the limit line corresponding to $L_{effective} = t_{plate} + t_{washer}/2 + t_{grout}$.

4. Similar to Test #4, stiffening behavior (at larger displacements) is observed in Test #5. However, for Test #5, the response is highly unsymmetrical – consistent with the unsymmetrical placement of the anchor rods within the holes.

5. The "negative" loading direction of Test #5 provides the best example of anchor rod bending not affected by factors such as grout (in the anchor rod holes) constraining the rod or contact with the base plate. Thus, this response is characterized by unrestrained double curvature bending contacting the welded plate washer. The response in this loading direction is represented by the limit solution corresponding to $L_{effective} = t_{plate} + t_{washer}/2$ for the initial loading cycles, and subsequently is closely followed by the limit solution corresponding to $L_{effective} = t_{plate} + t_{washer}/2 + t_{grout}$, indicating the gradual increase of effective length, possibly due to grout damage or rod elongation.

Based on the above discussion, the following general observations are presented, with a view to provide speculative insights into probable progression of events during the experiments –

1. At the start of testing, the strength of the specimen is controlled by bending of the anchor rod over the effective length $L_{effective} = t_{plate} + t_{washer}/2$, disregarding effects such as early contact between the base plate and anchor rod or presence of grout in the holes.

121

2. Under subsequent cyclic deformations, the anchor rod bending length increases until it loosens/damages all the grout around it. At this time, the envelope response may be described based on $L_{effective} = t_{plate} + t_{washer}/2 + t_{grout}$.

3. In either loading direction, if the base plate (rather than the plate washer) makes contact with the anchor rod, the bending length is abruptly reduced (resulting in $L_{effective} = t_{grout}$), accompanied by a rapid increase in force.

4. The abrupt increase in force (although consistent with tension stiffening) is attributed to contact between the base plate and anchor rod. This may be explained based on two factors. (1) Tension stiffening response will be symmetric, whereas the observed response is unsymmetrical. The increase in force due to the base plate impinging on the anchor rod depends on the placement of the anchor rod, and the corresponding response will, in general, be asymmetric. (2) The nonlinear analysis model presented in this Appendix predicts an abrupt increase in force due to tension stiffening at significantly greater displacements as compared to those observed in the experiments.
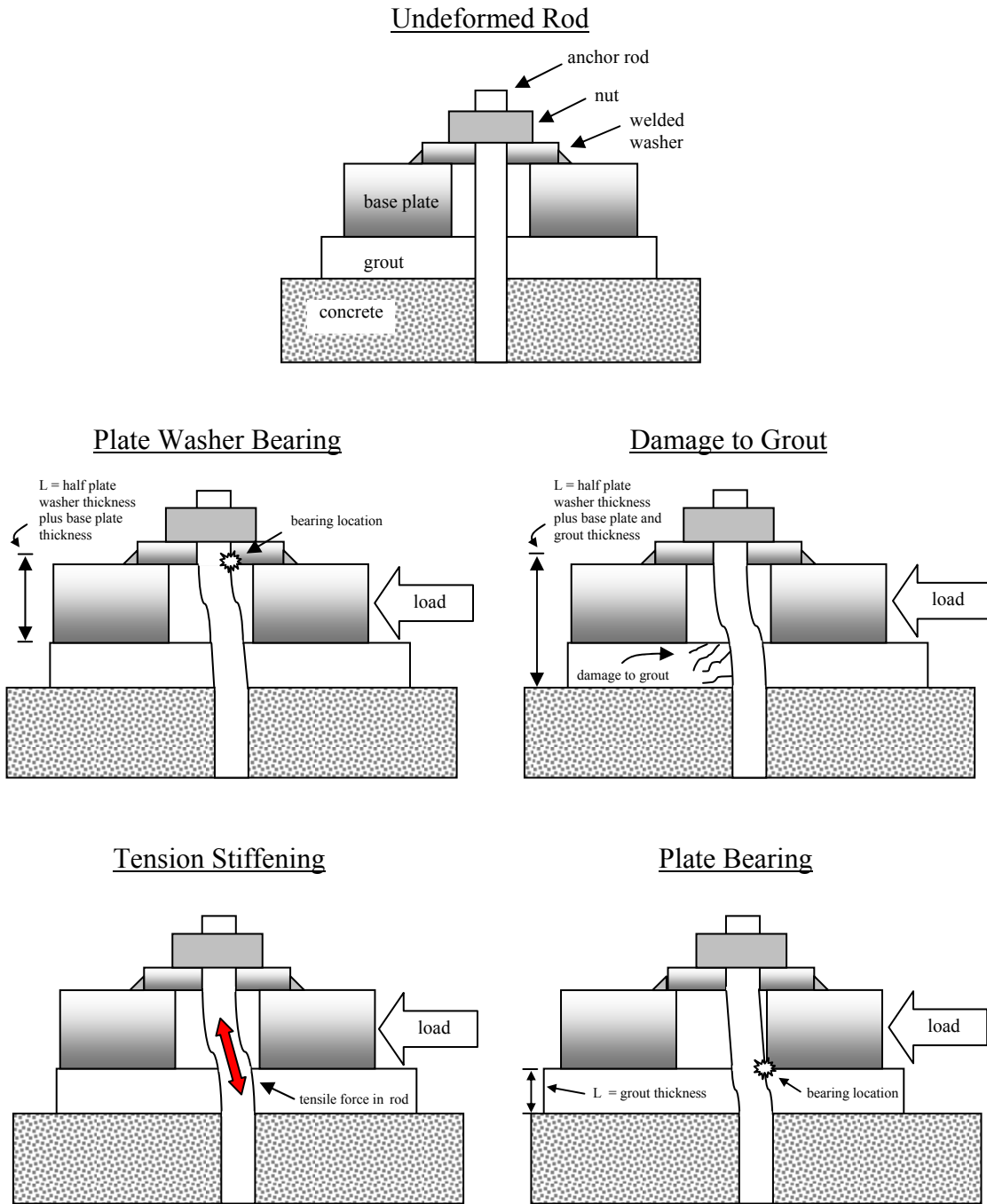
Undeformed Rod

anchor rod

nut

welded washer

base plate

grout

concrete

Plate Washer Bearing

L = half plate washer thickness plus base plate thickness

bearing location

load

Damage to Grout

L = half plate washer thickness plus base plate and grout thickness

load

damage to grout

Tension Stiffening

load

tensile force in rod

Plate Bearing

load

L = grout thickness

bearing location

Figure D.1 – Schematic illustrating various phenomenon in the anchor rod bearing mechanism
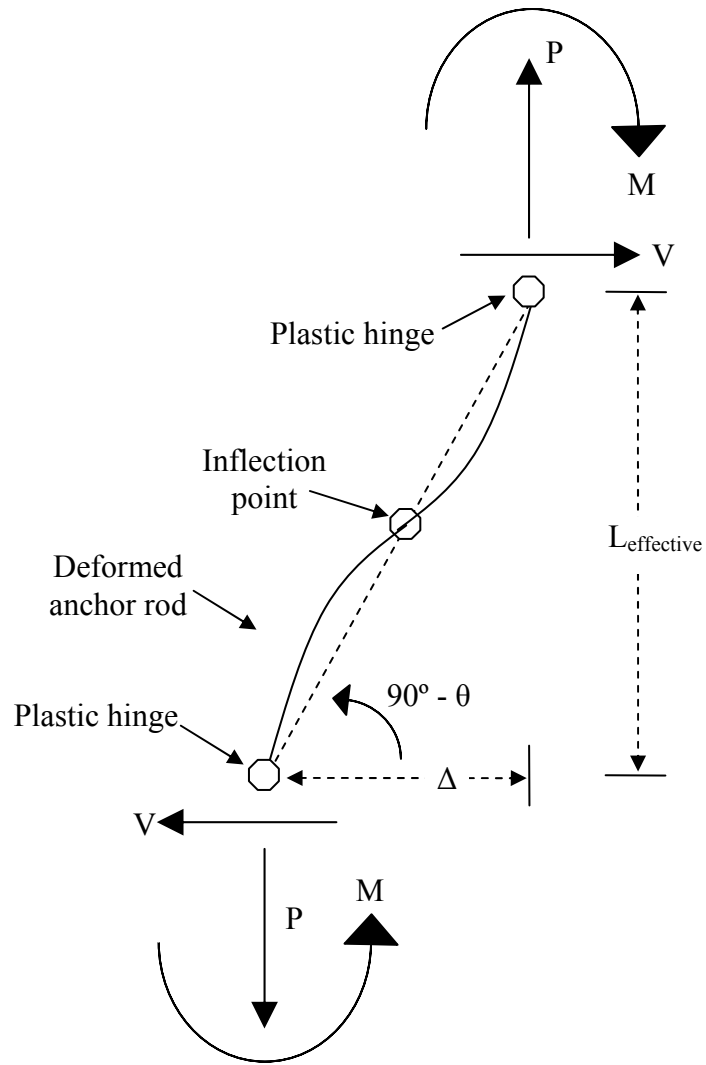
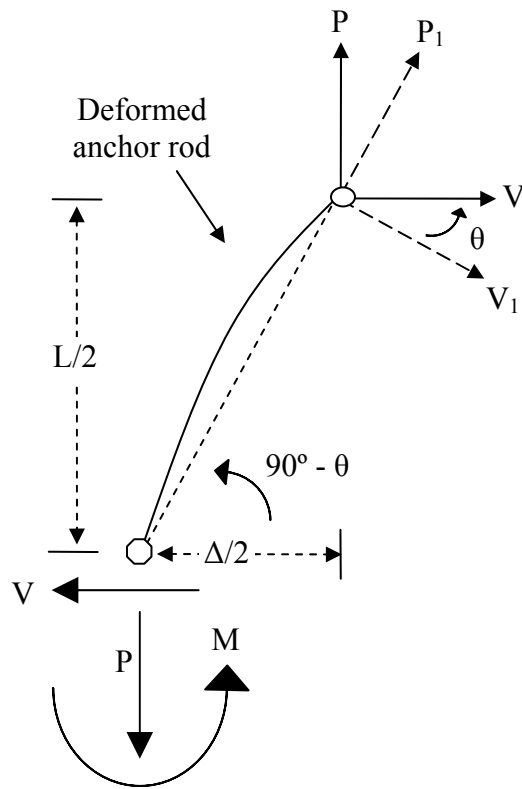**Figure D.2** – Free-body diagram of the deformed anchor rod

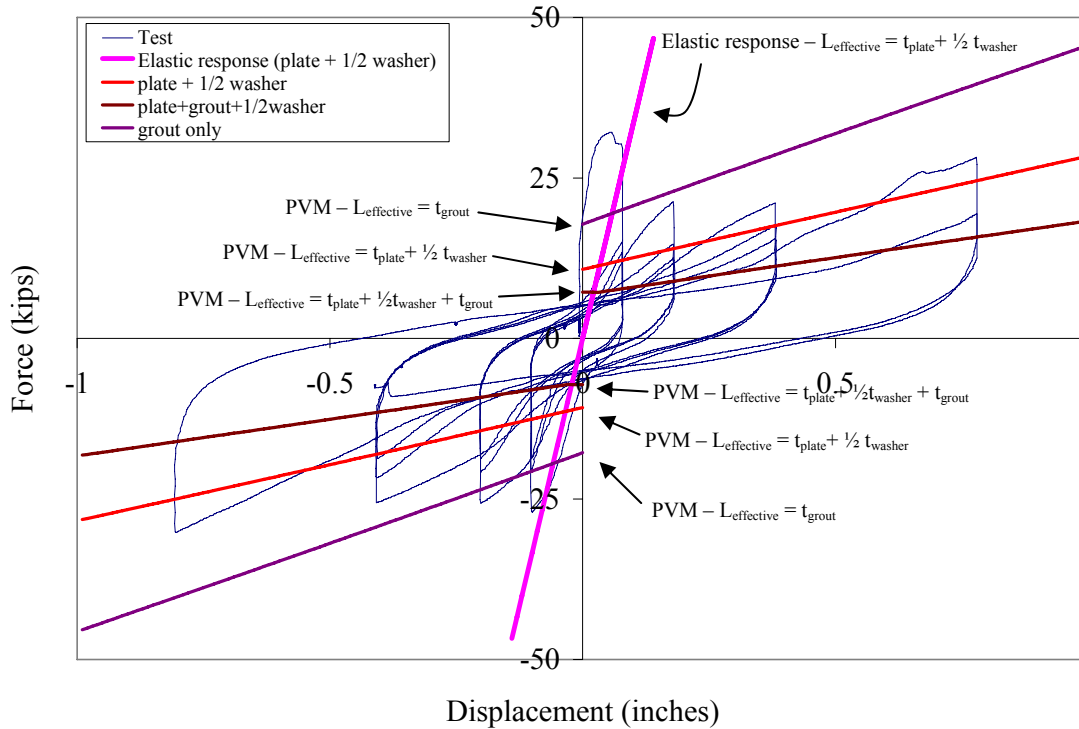**Figure D.3** – Free-body diagram of half of the deformed rod

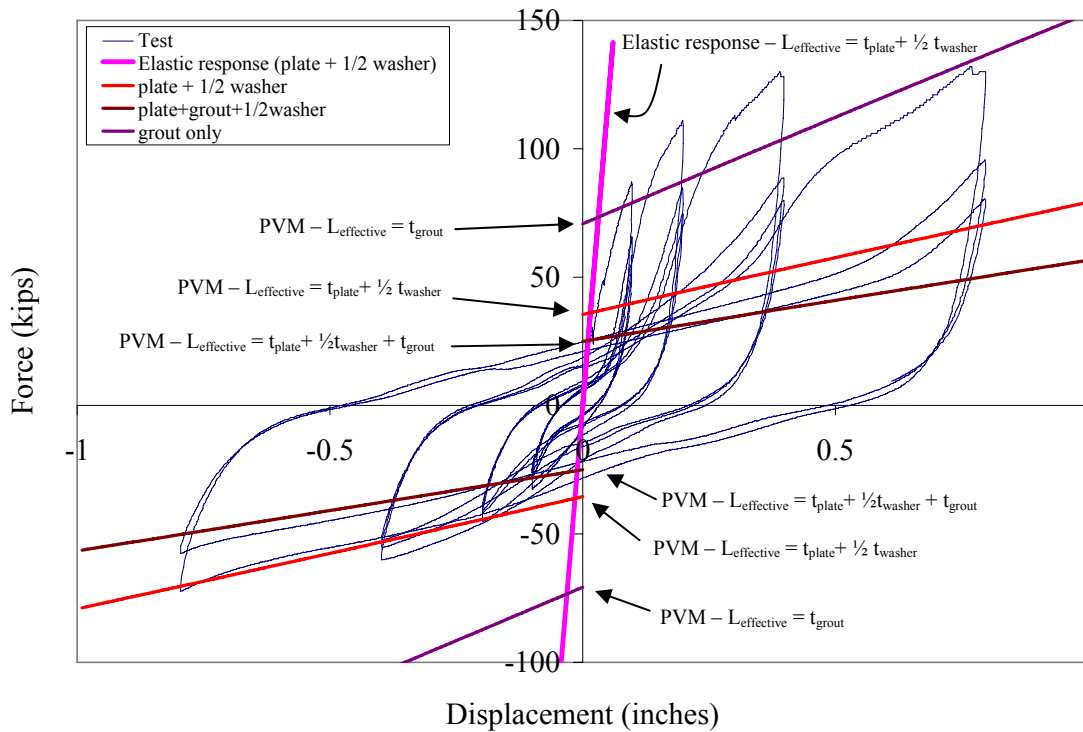**Figure D.4** – Experimental and predicted response of Test #4 (3/4" diameter anchor rods)

Figure D.5 – Experimental and predicted response of Test #5 (1-1/4" diameter anchor rods)

Appendix E

Shear Key Capacity Theory and Examples

E.1 DEVELOPMENT OF THE CCD SHEAR KEY CAPACITY EQUATION

Based on the concrete capacity design (CCD) approach for fasteners in concrete (Equation [9a] in Fuchs *et al.*, 1995), the concrete cone failure load of a single anchor loaded in tension in uncracked, unreinforced concrete unaffected by edge influences or overlapping cones of neighboring anchors is given by

$$N_{no} = k_{nc} \sqrt{f_c'}\, h_{ef}^{1.5}, \quad lb \qquad\qquad [E.1]$$

Where: k_{nc} = calibration factor = 40 for cast-in situ headed studs and headed anchor bolts

f_c' = concrete compression strength measured on 6 by 12 inch cylinders, psi

h_{ef} = effective embedment depth, inches

Assuming an idealized (i.e. pyramid shaped) concrete cone with an inclination between the failure surface and the surface of the concrete member of about 35 degrees, the concrete cone failure load can be related by

$$N_{no} = 40 \sqrt{f_c'}\, h_{ef}^{1.5} = k_{35} \left(\frac{1}{\sqrt{h_{ef}}} \right) A_{no} \sqrt{f_c'} \qquad\qquad [E.2]$$

Where: k_{35} = constant

A_{no} = projected area of one anchor at the concrete surface unaffected by edge influences or neighboring anchors, idealizing the failure cone as a pyramid with a base length of $3 h_{ef} = 9 h_{ef}^2$

127

Appendix E: Shear Key Capacity Theory and Examples

Solving Equation [E.2] for k_{35} provides a constant of $40/9 = 4.\overline{4}$. Thus, the concrete cone failure load can be expressed as

$$N_{no} = \frac{40}{9}\left(\frac{1}{\sqrt{h_{ef}}}\right)A_{no}\sqrt{f_c'}, \quad lb \qquad [E.3]$$

Shear lugs typically have a very large lateral stiffness such that the shear capacity of a shear lug in concrete loaded towards an edge may be interpreted in a similar fashion as an anchor loaded in tension. Thus, the shear load capacity of a shear key loaded towards a free edge may be expressed as

$$V_n^{CCD} = \frac{40}{9}\left(\frac{1}{\sqrt{c}}\right)A_{35}\sqrt{f_c'}, \quad lb \qquad [E.4]$$

Where: c = free edge distance from the shear key, inches

A_{35} = effective area based on a 35 degree projected plane from the bearing edges of the shear lug to the free surface, excluding the bearing area of the shear lug, inches^2

E.2 EXAMPLE CALCULATION OF SHEAR KEY CAPACITY USING THE CCD METHOD

The geometry of the concrete pedestal used to represent the foundation for the base plate tests is illustrated schematically in Figure E.1. The pedestal measures 48 inches by 84 inches in area and 32.5 inches in height. For both tests, the shear key was installed in the center of the concrete block such that an edge distance of 20.25" was provided from the shear key bearing surface to the pedestal edge. Two shear key embedment lengths, measured from below the surface of the concrete, were tested: 5.5" for Test #6 and 3.0" for Test #7. The shear key itself was 6" wide for both tests, thus providing a 33 in^2 bearing surface for Test #6 and 18 in^2 for Test #7. Note that for both tests, the projected effective failure area of the shear key is limited by the pedestal height. Schematics

128

detailing the calculation of the projected effective failure area for the CCD method are illustrated in Figure E.2.

The effective area A_{35} for Test #6 is calculated as

$$A_{35} = (height) \cdot (width) - (bearing\ area\ of\ the\ shear\ lug)$$
$$= (32.5") \cdot ((1.5 + 1.5) \cdot 20.25" + 6") - (6") \cdot (5.5") = 2{,}136\ inches^2$$

The effective area A_{35} for Test #7 is calculated as

$$A_{35} = (32.5") \cdot ((1.5 + 1.5) \cdot 20.25" + 6") - (6") \cdot (3.0") = 2{,}151\ inches^2$$

Table E.1 lists all pertinent variables and parameters from the two shear lug tests used to calculate the shear key capacity using the CCD method.

E.3 EXAMPLE CALCULATION OF SHEAR KEY CAPACITY USING THE 45 DEGREE CONE METHOD

The 45 degree cone method is prescribed by ACI 349 (2006) for the concrete shear capacity of embedded shear lugs and is featured in the AISC *Design Guide 1* (Fisher & Kloiber, 2006). As per this method, the strength capacity of the concrete corresponding to shear blowout is determined as follows –

$$V_n^{45} = \left(4\sqrt{f_c'}\right)A_{45}, \quad lb \qquad\qquad \text{[E.5]}$$

Where: f_c' = concrete compressive strength, psi

A_{45} = effective area based on a 45 degree projected plane from the bearing

edges of the shear lug to the free surface, excluding the bearing area

of the shear lug, inches^2

Thus, the method assumes a uniform tensile stress of $4\sqrt{f'_c}$ acting on an effective stress area defined by projecting a 45 degree plane from the bearing edges of the shear lug to the concrete free surface. The bearing area of the shear lug is excluded from the projected area. Note that for both tests, the projected effective failure area of the shear key is not limited by corner influences or pedestal thickness. Schematics detailing the calculation of the projected effective failure area for the 45 degree cone method are illustrated in Figure E.3.

The effective area A_{45} for Test #6 is calculated as

$$A_{35} = (height) \cdot (width) - (bearing\ area\ of\ the\ shear\ lug)$$
$$= (20.25" + 5.5") \cdot ((2) \cdot 20.25" + 6") - (6") \cdot (5.5") = 1,164\ inches^2$$

The effective area A_{45} for Test #7 is calculated as

$$A_{35} = (20.25" + 3.0") \cdot ((2) \cdot 20.25" + 6") - (6") \cdot (3.0") = 1,063\ inches^2$$

Table E.1 lists all pertinent variables and parameters from the two large scale tests used to calculate the shear key capacity using the 45 degree cone method.

Table E.1 – Details of shear key capacity calculations

Test Number	6	7
Pedestal length (inches)	84	84
Pedestal width (inches)	48	48
Pedestal height "h" (inches)	32.5	32.5
Corner distance "e" (inches)	39	39
Edge distance "c" (inches)	20.25	20.25
Shear key width "w" (inches)	6.0	6.0
Shear key embedment depth "d" (inches)	5.5	3.0
[1]Concrete compressive strength " f_c' " (ksi)	4,650	5,030
[2]Effective area based on a 35 degree projected plane " A_{35} " (inches^2)	2,136	2,151
[2]Effective area based on a 45 degree projected plane " A_{45} " (inches^2)	1,164	1,063
Shear capacity " V_n^{CCD} " calculated as per Equation [E.4] (kips)	144	151
Shear capacity " V_n^{45} " calculated as per Equation [E.5] (kips)	318	302

[1]Determined by the average of ancillary compressive tests of concrete cylinders
[2]Calculated by projecting planes from the bearing edges of the shear lug to the concrete free surface, excluding the bearing area of the shear lug and considering corner influences and pedestal thickness; see section E.2 and E.3 for details
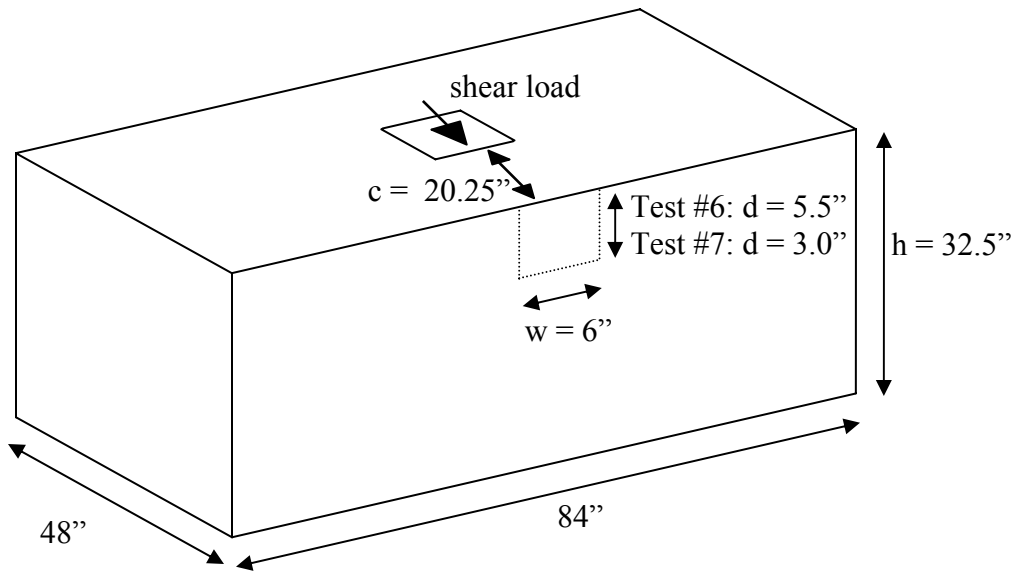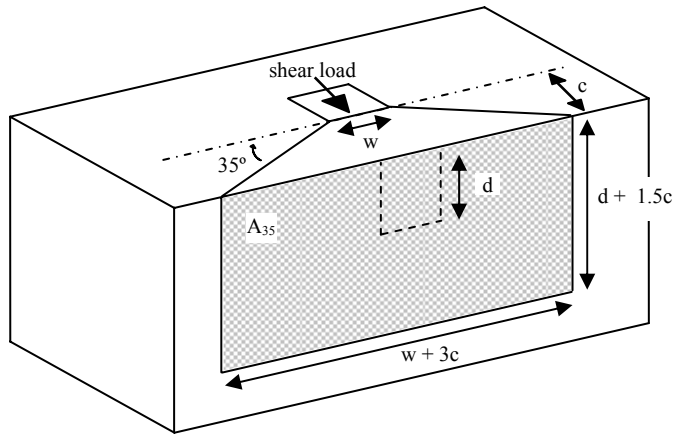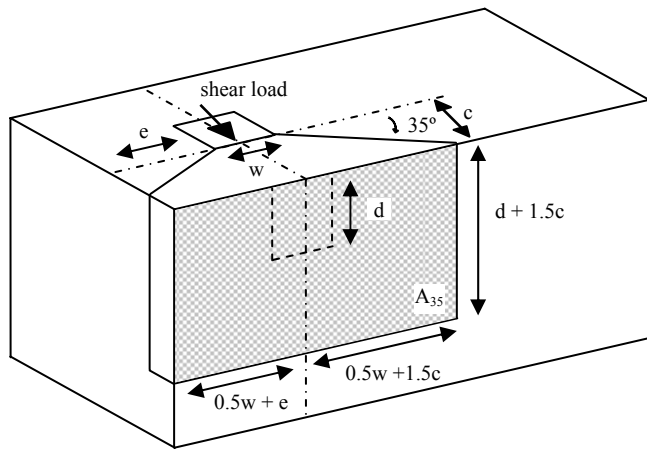
Figure E.1 – Schematic of concrete pedestal geometry

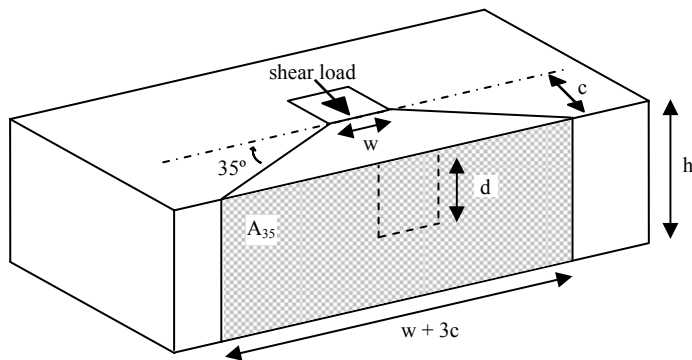$A_{35} = (d + 1.5c) * (w + 3c) - (d * w)$
$\quad = 1.5c * (w + 2d + 3c)$

$A_{35} = 0.7[(d + 1.5c) * (w + 1.5c + e) - (d * w)]$
$\quad$ if: $e \leq 1.5c$

The 0.7 factor considers the disturbance of the symmetric stress distribution caused by a corner (Fuchs *et al.*, 1995)
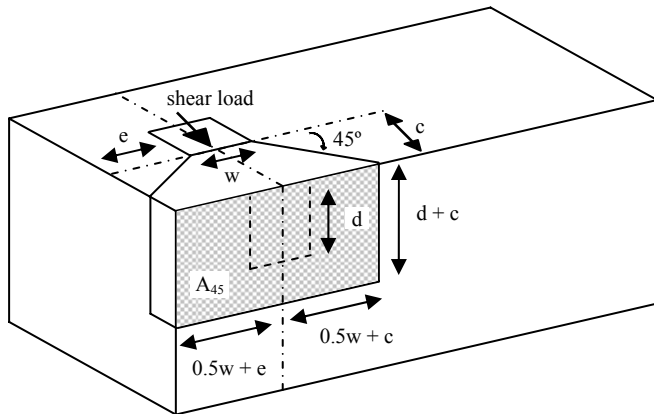
$A_{35} = (h) * (w + 3c) - (d * w)$
$\quad$ if: $h \leq 1.5c + d$

Figure E.2 – Schematic illustrating the effective stress area for the CCD method under various boundary conditions (c = edge distance; w = shear key width; d = shear key embedment depth; e = corner distance; h = foundation height)
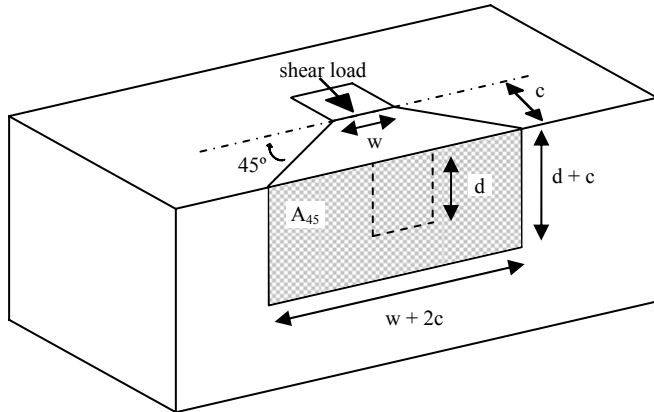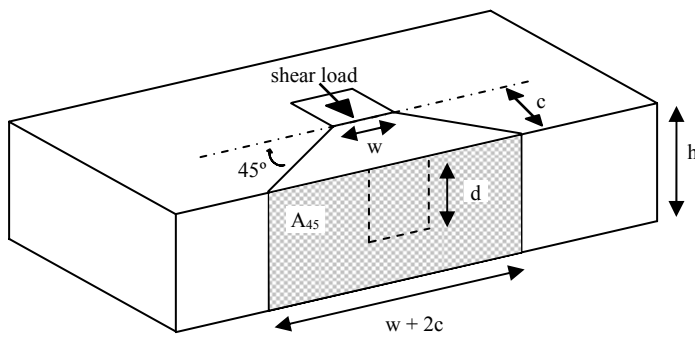
$$A_{35} = (d + c) * (w + 2c) - (d * w)$$
$$= c * (w + 2d + 2c)$$

$$A_{35} = (d + c) * (w + c + e) - (d * w)$$
$$\text{if: } e \leq c$$

$$A_{35} = (h) * (w + 2c) - (d)*(w)$$
$$\text{if: } h \leq c + d$$

Figure E.3 – Schematic illustrating the effective stress area for the 45 degree cone method under various boundary conditions (c = edge distance; w = shear key width; d = shear key embedment depth; e = corner distance; h = foundation height)